Integrated Ocean Drilling Program
Expedition 305 Preliminary Report

Oceanic Core Complex Formation, Atlantis Massif

Oceanic core complex formation, Atlantis Massif, Mid-Atlantic Ridge: drilling into the footwall and hanging wall of a tectonic exposure of deep, young oceanic lithosphere to study deformation, alteration, and melt generation

8 January–2 March 2005

Expedition Scientific Party

PUBLISHER'S NOTES

Citation:
Expedition Scientific Party, 2005. Oceanic core complex formation, Atlantis Massif—oceanic core complex formation, Atlantis Massif, Mid-Atlantic Ridge: drilling into the footwall and hanging wall of a tectonic exposure of deep, young oceanic lithosphere to study deformation, alteration, and melt generation. *IODP Prel. Rept.,* 305. http://iodp.tamu.edu/publications/PR/305PR/305PR.PDF.

Distribution:
Electronic copies of this series may be obtained from the Integrated Ocean Drilling Program (IODP) Publication Services homepage on the World Wide Web at **iodp.tamu.edu/publications.**

This publication was prepared by the Integrated Ocean Drilling Program U.S. Implementing Organization (IODP-USIO): Joint Oceanographic Institutions, Inc., Lamont-Doherty Earth Observatory of Columbia University, and Texas A&M University, as an account of work performed under the international Integrated Ocean Drilling Program, which is managed by IODP Management International (IODP-MI), Inc. Funding for the program is provided by the following agencies:

European Consortium for Ocean Research Drilling (ECORD)

Ministry of Education, Culture, Sports, Science and Technology (MEXT) of Japan

Ministry of Science and Technology (MOST), People's Republic of China

U.S. National Science Foundation (NSF)

DISCLAIMER

April 2005

The following scientists and personnel were aboard the *JOIDES Resolution* for Expeditions 304 and 305 of the Integrated Ocean Drilling Program.

Expedition Scientific Party

Donna Blackman
Co-Chief Scientist
Scripps Institution of Oceanography
University of California, San Diego
9500 Gilman Drive
La Jolla CA 92093-0225
USA
dblackman@ucsd.edu
Work: (858) 534-8813
Fax: (858) 534-5332

Benoit Ildefonse
Co-Chief Scientist
Laboratoire de Tectonophysique
Université Montpellier II
CC49
34095 Montpellier
France
benoit@dstu.univ-montp2.fr
Work: (33) 46714-3818
Fax: (33) 46714-3603

Barbara E. John
Co-Chief Scientist
Department of Geology and Geophysics
University of Wyoming
1000 East University Avenue
Department 3006
Laramie WY 82071
USA
bjohn@uwyo.edu
Work: (307) 766-4232
Fax: (307) 766-6679

Yasuhiko Ohara
Co-Chief Scientist
Ocean Research Laboratory
Hydrographic and Oceanographic Department of Japan
5-3-1 Tsukiji, Chuo-ku
Tokyo 104-0045
Japan
ohara@jodc.go.jp
Work: (81) 3-3541-4387
Fax: (81) 3-3541-3870

D. Jay Miller
Expedition Project Manager/Staff Scientist
Integrated Ocean Drilling Program
Texas A&M University
1000 Discovery Drive
College Station TX 77845-9547
USA
miller@iodp.tamu.edu
Work: (979) 845-2197
Fax: (979) 845-0876

Christopher J. MacLeod
Shore-based Contributor
School of Earth, Ocean and Planetary Sciences
Cardiff University
Main Building, Park Place
Cardiff CF10 3YE
United Kingdom
MacLeod@cardiff.ac.uk
Work: (44) 29-208-74332
Fax: (44) 29-208-74326

Expedition 305 Scientific Party

Heike Delius
Logging Staff Scientist
Department of Geology
University of Leicester
University Road
Leicester LE1 7RH
United Kingdom
hd21@le.ac.uk
Phone: (44) 116-252-3634
Fax: (44) 116-252-3918

Natsue Abe
Igneous Petrologist
Deep Sea Research Department
Japan Marine Science and Technology Center
2-15 Natsushima-cho
Yokosuka, Kanagawa 237-0061
Japan
abenatsu@jamstec.go.jp
Work: (81) 46-867-9329
Fax: (81) 46-867-9315

James S. Beard
Metamorphic Petrologist
Department of Earth Sciences
Virginia Museum of Natural History
1001 Douglas Avenue
Martinsville VA 24112
USA
jbeard@vmnh.net
Work: (276) 666-8611
Fax: (276) 632-6487

Daniele Brunelli
Igneous Petrologist
Laboratoire Pierre Süe–DRECAM
CNRS
91191 Yvette Cedex
France
brunelli@drecam.cea.fr
Work: (33) 1-6908-9522
Fax: (33) 1-6908-6923

Adélie G. Delacour
Metamorphic Petrologist
Institut für Mineralogie und Petrographie
Eidgenössische Technische Hochschule–Zentrum
Sonnegstrasse 5
Zürich 8092
Switzerland
adelie.delacour@erdw.ethz.ch
Work: (41) 1 632 7823
Fax: (41) 1 632 1088

Javier Escartin
Structural Geologist
Marine Geosciences
Université Pierre et Marie Curie
Case 89 IPGP
4 Place Jussieu
75252 Paris
France
escartin@ipgp.jussieu.fr
Work: (33) 1-4427-4601
Fax: (33) 1-4427-9969

Patricia B. Fryer
Metamorphic Petrologist
School of Ocean and Earth Science and Technology
University of Hawaii at Manoa
1680 East-West Road
Honolulu HI 96822
USA
pfryer@hawaii.edu
Work: (808) 956-3146
Fax: (808) 956-6322

Angela Halfpenny
Structural Geologist
Department of Earth and Ocean Studies
University of Liverpool
4 Brownlow Street
Liverpool, Merseyside L69 3GP
United Kingdom
a.halfpenny@liverpool.ac.uk
Work: (44) 151-794-5174
Fax: (44) 151-794-5196

Heidi-Elisabeth Hansen
Igneous Petrologist
Department of Earth Science
University of Bergen, Norway
Allegaten 41
Bergen
Norway
st08759@student.uib.no
Work: (47) 5531 3949

Amber C. Harris
Physical Properties Specialist
Graduate School of Oceanography
University of Rhode Island
Narragansett RI 02882
USA
aharris@gso.uri.edu
Work: (401) 241-6874

Akihiro Tamura Hasebe
Igneous Petrologist
Department of Earth Sciences
Kanazawa University
Kakuma, Kanazawa 920-1192
Japan
kamui@kenroku.kanazawa-u.ac.jp
Work: (81) 76 264 5723
Fax: (81) 76 264 5746

Eric Hellebrand
Igneous Petrologist
Abteilung Geochemie
Max-Planck-Institüt für Chemie
Postfach 3060
55020 Mainz
Germany
ehelle@mpch-mainz.mpg.de
Work: (49) 6131-305220
Fax: (49) 6131-371051

Satoko Ishimaru
Igneous Petrologist
Division of Environmental Science and Engineering
Kanazawa University
Graduate School of Natural Science and Technology
Kakuma, Kanazawa 920-1192
Japan
jaja@earth.s.kanazawa-u.ac.jp
Work: (81) 76-264-5723
Fax: (81) 76-264-5746

Kevin T.M. Johnson
Igneous Petrologist
Department of Geology and Geophysics/SOEST
University of Hawaii and Manoa
1680 East-West Road
Post 606B
Honolulu HI 96822
USA
kjohnso2@hawaii.edu
Work: (808) 956-3444
Fax: (808) 956-5512

Garry D. Karner
Physical Properties Specialist
Lamont-Doherty Earth Observatory of Columbia University
PO Box 1000, 61 Route 9W
Palisades NY 10964
USA
garry@ldeo.columbia.edu
Work: (845) 365-8355
Fax: (845) 365-8156

Margaret Linek
Logging Trainee
Angeandte Geophysik
Rheinisch-Westfälischen Technischen Hochschule Aachen
RW Technische Hochschule
Lochnerstrasse 4-20
52064 Aachen
Germany
m.linek@geophysik.rwth-aachen.de
Work: (49) 241-809-4832
Fax: (49) 241-809-2132

Olivia U. Mason
Microbiologist
College of Oceanography
Oregon State University
Giovannoni Laboratory
104 COAS Administration Building
Corvallis OR 97331-5503
USA
omason@coas.oregonstate.edu
Work: (503) 939-1035

Katsuyoshi Michibayashi
Structural Geologist
Institute of Geosciences
Shizuoka University
Faculty of Science
836 Oya
Shizuoka 422-8529
Japan
sekmich@ipc.shizuoka.ac.jp
Work: (81) 54-238-4788
Fax: (81) 54-238-0491

Toshio Nozaka
Metamorphic Petrologist
Department of Earth Sciences
Okayama University
3-1-1 Tsushima-naka
Okayama 700-8530
Japan
nozaka@cc.okayama-u.ac.jp
Work: (81) 86-251-7883
Fax: (81) 86-251-7895

Martin Rosner
Geochemist
Department of Marine Chemistry and Geochemistry
Woods Hole Oceanographic Institution
Clark Building, MS 23
Woods Hole MA 02543
USA
mrosner@whoi.edu
Work: (508) 289-2699
Fax: (508) 457-2193

Guenter Suhr
Structural Geologist
Mineralogisch-Petrographisches Institut
Universität Köln
Zülpicher Strasse 49b
50674 Köln
Germany
suhr@min.uni-koeln.de
Work: (49) 221-470-3196
Fax: (40) 221-470-5199

Masako Tominaga
Paleomagnetist
Department of Oceanography
Texas A&M University
3F Oceanography Building
3146 TAMU
College Station TX 77843-3146
USA
masako@ocean.tamu.edu
Work: (979) 845-7211
Fax: (979) 845-6331

Toru Yamasaki
Geochemist
Department of Earth and Planetary Sciences
Hokkaido University
Graduate School of Science
N 10, W 8
Sapporo, Hokkaido 060-0810
Japan
toru@ep.sci.hokudai.ac.jp
Work: (81) 11 716 2111, ext. 4655
Fax: (81) 11 746 0394

Xixi Zhao
Paleomagnetist
Center for Study of Imaging and Dynamics
of the Earth
Institute of Geophysics and Planetary Physics
University of California, Santa Cruz
Earth and Marine Sciences Building
1156 High Street
Santa Cruz CA 95064
USA
xzhao@es.ucsc.edu
Work: (831) 459-4847
Fax: (831) 459-3074

Expedition 304 Scientific Party

Florence Einaudi
Logging Staff Scientist
Laboratoire de Geophysique et D'hydrodynamique
Université Montpellier II, ISTEEM
Case Courrier 56
34095 Montpellier Cedex 5
France
einuaudi@dstu.univ-montp2.fr
Work: (33) 4-67-14-93-09
Fax: (33) 4-67-14-93-08

Michael W. Abratis
Metamorphic Petrologist
Institute for Geosciences
University of Jena
Burgweg 11
07749 Jena
Germany
michael.abratis@uni-jena.de
Work: (49) 3641-948-721
Fax: (49) 3641-948-602

Eric S. Andal
Igneous Petrologist
Department of Earth Sciences
Kanazawa University
Kakuma-machi
Kanazawa City, Ishikawa 920-1192
Japan
andal_es@earth.s.kanazawa-u.ac.jp
Work: (81) 076-264-5726
Fax: (81) 076-264-5746

Muriel Andreani
Metamorphic Petrologist
Laboratoire de Geosciences Marines
CNRS UMR 7097
Institut de Physique du Globe de Paris
4 Place Jussieu—Case 89
75252 Paris Cedex 5
France
Andreani@ipgp.jussieu.fr
Work: (33) 1-44-27-5193

Shunsaku Awaji
Geochemist
Department of Geosystem Engineering
The University of Tokyo
7-3-1 Hongo
Bunkyo-ku, Tokyo
Japan
Tt36508@mail.ecc.utokyo.ac.jp
Work: 81-3-5841-7019

Allison Charney
Igneous Petrologist
University of Connecticut
Geology and Geophysics Department
354 Mansfield Road, U-45
Storrs CT 06269-2045
USA
Allison.charney@uconn.edu
Work: (860) 486-0606
Fax: (860) 468-1383

David Christie
Igneous Petrologist
College of Oceanic and Atmospheric Sciences
104 Ocean Administration Building
Oregon State University
Corvalis OR 97331-5503
USA
dchristie@coas.oregonstate.edu
Work: (547) 737-5205
Fax: (547) 737-2064

Marion Drouin
Metamorphic Petrologist
Laboratoire de Tectonophysique
Université Montpellier II
Case Courrier 49
Place Eugène Bataillon
34095 Montpellier Cedex 5
France
marion.drouin@dstu.univ-montp2.fr
Work: (33) 4-67-19-39-41
Fax: (33) 4-72-44-8382

Bryce R. Frost
Metamorphic Petrologist
Department of Geology and Geophysics
University of Wyoming
1000 East University Avenue
Laramie WY 82071
USA
rfrost@uwyo.edu
Work: (307) 766-4290
Fax: (307) 766-6679

Jeffrey S. Gee
Paleomagnetist
Geosciences Research Division
Scripps Institution of Oceanography
University of California, San Diego
Mail code 0220
La Jolla CA 92093-0220
USA
jsgee@ucsd.edu
Work: (858) 534-4707
Fax: (858) 534-0784

Marguerite Godard
Geochemist
Laboratoire de Tectonophysique
Université Montpellier II
Case Courrier 49
Place Eugène Bataillon
34095 Montpellier Cedex 5
France
margot@dstu.univ-montp2.fr
Work: (33) 467-14-39-37
Fax: (33) 467-14-36-03

Craig B. Grimes
Structural Geologist
Department of Geology and Geophysics
University of Wyoming
1000 East University Avenue
Laramie WY 82071
USA
cgrimes@uwyo.edu

Nicholas W. Hayman
Structural Geologist
Division of Earth and Ocean Sciences
Duke University
103 Old Chemistry Building
Durham NC 27708-0230
USA
hayman@duke.edu
Work: (919) 681-8165
Fax: (919) 684-5833

Takehiro Hirose
Structural Geologist
Department of Geology and Mineralogy
Graduate School of Science
Kyoto University
Kyoto 606-8502
Japan
hirose@kueps.kyoto-u.ac.jp
Work: 81-75-753-4150
Fax: 81-75-753-4189

James Gregory Hirth
Structural Geologist
Department of Geology and Geophysics
Woods Hole Oceanographic Institution
MS 8
Woods Hole MA 02543
USA
ghirth@whoi.edu
Work: (508) 289-2776
Fax: (508) 457-2183

Jinichiro Maeda
Igneous Petrologist
Division of Earth and Planetary Sciences
Graduate School of Science
Hokkaido University
N10W8 Kita, Sapporo
Hokkaido 060-0810
Japan
jinmaeda@ep.sci.hokudai.ac.jp
Work: 81-11-706-4639

Andrew M. McCaig
Metamorphic Petrologist
Earth Sciences, School of Earth and Environment
University of Leeds
Leeds LS2 9JT
United Kingdom
andrew@earth.leeds.ac.uk
Work: (44) 113-3435219
Fax: (44) 113-3435259

Antony Morris
Paleomagnetist
School of Earth, Ocean, and Environmental Sciences
University of Plymouth
Drake Circus
Plymouth PL4 8AA
United Kingdom
amorris@plymouth.ac.uk
Work: (44) 1752-233120
Fax: (44) 1752-233117

Tatsunori Nakagawa
Microbiologist
Department of Mineralogy, Petrology, and Economic Geology
Tohoku University
Aoba, Aramaki-Aza
Aoba-ku, Sendai
Miyagi 980-8578
Japan
n-takko@ganko.tohoku.ac.jp
Work: (81) 22-217-6660
Fax: (81) 22-217-6660

Roger C. Searle
Physical Properties Specialist
Department of Earth Sciences
University of Durham
South Road
Durham County
Durham DH1 3LE
United Kingdom
r.c.searle@durham.ac.uk
Work: (44) 191-334-2307
Fax: (44) 191-334-2301

Anette von der Handt
Igneous Petrologist
Abeilung Geochemie
Max-Planck-Institut für Chemie
PO Box 3060
55020 Mainz
Germany
avdhandt@mpch-mainz.mpg.de

Transocean Officials

Alexander Simpson
Master of the Drilling Vessel
Overseas Drilling Ltd.
707 Texas Avenue South, Suite 213D
College Station TX 77840-1917
USA

Wayne Malone
Drilling Superintendent
Overseas Drilling Ltd.
707 Texas Avenue South, Suite 213D
College Station TX 77840-1917
USA

IODP Shipboard Personnel and Technical Representatives

Ronald M. Grout
Operations Superintendent

Roy Davis
Laboratory Officer

Lisa K. Crowder
Assistant Laboratory Officer

Chieh Peng
Assistant Laboratory Officer

Margo Cortes
Yeoperson

Charlie Endris
Marine Laboratory Specialist: Downhole Tools/ Thin Sections

Dennis Graham
Marine Laboratory Specialist: Chemistry

Michael J. Hodge
Marine Computer Specialist

Leah Shannon Housley
Imaging Specialist

Eric Jackson
Marine Laboratory Specialist: X-Ray

Jan Jurie Kotze
Marine Instrumentation Specialist

Lena Maeda
Marine Laboratory Specialist: Core

Erik Moortgat
Marine Computer Specialist

Michael Murphy
Marine Laboratory Specialist: Physical Properties

Pieter Pretorius
Marine Instrumentation Specialist

Paula Weiss
Marine Curatorial Specialist

Robert M. Wheatley
Marine Laboratory Specialist: Chemistry

Yasmin Yabyabin
Marine Laboratory Specialist: Underway Geophysics

Javier Espinosa
Schlumberger Engineer

ABSTRACT

Integrated Ocean Drilling Program Expedition 305, a joint science program with Expedition 304, was designed to investigate the processes that control formation of oceanic core complexes, as well as the exposure of ultramafic rocks in very young oceanic lithosphere. Prior studies indicated that two main drill sites on Atlantis Massif, on the western rift flank of the Mid-Atlantic Ridge (MAR) at 30°N, could provide key constraints on the structure of the detachment fault zone, rock types exposed at shallow structural levels in the footwall, and their alteration history, as well as that of the volcanic succession in the hanging wall. Expedition 305 deepened Hole U1309D in the footwall of Atlantis Massif to 1415.5 meters below seafloor, with high recovery (average = 74.8%) of dominantly gabbroic rocks. Hole U1309D was logged twice, providing the opportunity for unprecedented core–logging integration for a deep borehole in the oceanic lithosphere. The recovered rocks range from dunitic troctolite, troctolite, (olivine) gabbro, and gabbronorite to evolved oxide gabbro that locally contains abundant zircon and apatite, and diabase. The texture of the dunitic troctolite suggests a cumulate origin. The gabbroic suite from Hole U1309D is among the most primitive recovered from the MAR, with Mg# ranging from 67 to 87.

Although alteration mineral assemblages record cooling of gabbroic rocks from magmatic conditions to zeolite facies, a low-temperature phase that reflects alteration at temperatures <500°C is most significant. The overall trends in alteration and the changes in secondary mineralogy downhole suggest that there may be two separate secondary processes that have affected the footwall in the vicinity of Hole U1309D. In the upper ~840 m, seawater–rock interactions may pervade the gabbroic sequence. Below that depth, the nature of and the fluctuations in degree and style of metamorphism are related to fluids of a different composition percolating along fault/ductile deformation zones. Hence, the core records an extensive history of gabbroic rock–fluid interaction, possibly including magmatic fluids.

One of the prominent features of the rocks from Hole U1309D is the lack of extensive amphibolite facies alteration and deformation. This contrasts strongly with the gabbroic suite recovered from Ocean Drilling Program Hole 735B, at the Southwest Indian Ridge. The rocks recovered in Hole U1309D show very little deformation, and any deformation related to a major detachment fault system must have occurred at low temperature and must be strongly localized in the very upper part of the hole. This, together with very minor deformation in the amphibolite facies, is not consistent with the classical “core complex” interpretation of the corrugated, domal massifs

on the seafloor resulting from surface exposure of a detachment fault that roots deeply at the base of the lithosphere. In addition, shipboard paleomagnetic measurements indicate there has been no significant net tectonic rotation (≤15°) of the footwall. This seems to preclude a rolling hinge model for the uplift of the core of Atlantis Massif along a single concave, normal fault.

The ~1.4 km sequence of dominantly gabbroic rocks is inconsistent with the initial prediction that the footwall was composed of an uplifted mantle section where serpentinization was responsible for lower densities/seismic velocities in the upper few hundred meters. A more complex model than that put forward before Expeditions 304 and 305 will be required. The fact that we did not reach fresh mantle peridotite, together with the known exposures of serpentinized mantle along the southern ridge of the massif, supports models of complicated lateral heterogeneity in slow-spreading oceanic crust. We have, however, placed a constraint on the magnitude of this heterogeneity—gabbro bodies in this setting can exceed 1.5 km in thickness.

INTRODUCTION

Integrated Ocean Drilling Program (IODP) Expedition 305 is the second of a two-expedition program to drill and core a section of denuded lower crust, Atlantis Massif, located on the western flank of the Mid-Atlantic Ridge (MAR) at 30°N. Atlantis Massif formed within the past 1.5–2 m.y. and is the inside corner bathymeric high at the intersection between the MAR and the Atlantis Fracture Zone (Fig. **F1**). The corrugated, striated central portion of this domal massif displays morphologic and geophysical characteristics inferred to be representative of an oceanic core complex (OCC) exposed via long-lived detachment faulting (Cann et al., 1997; Blackman et al., 1998, 2004; Collins et al., 2001). The "core" of the complex is presumably composed of crust and upper mantle rocks denuded by a detachment fault exposed over an 8–10 km wide, 15 km long area that forms the elongate doubly plunging domal seafloor morphology (Fig. **F1**). An adjacent basaltic block to the east is interpreted as the hanging wall to the detachment fault. Initiation of a deep hole in the footwall of Atlantis Massif was achieved during IODP Expedition 304 at Site U1309. After drilling a pilot hole to 102 meters below seafloor (mbsf) in Hole U1309B, Hole U1309D (Fig. **F2**) was started and the upper 20 m was cased. During Expedition 304, Hole U1309D was cored to a depth of 401.3 mbsf, with overall recovery of 64%, dominantly gabbroic rocks. During Expedition 305, Hole U1309D was deepened to 1415.5 mbsf, again with high recovery (average = 74.8%) of dominantly gabbroic rocks. Hole U1309D was logged twice (~830–400 mbsf and ~1400–200 mbsf). Attempts during Expedition 304 to drill and core through the hanging wall and a detachment fault hypothesized to be present beneath it were unsuccessful (Shipboard Scientific Party, 2005).

BACKGROUND

Analysis of seismic refraction data at Atlantis Massif (Collins and Detrick, 1998) indicates that velocities of 8 km/s occur within several hundred meters of the seafloor in at least parts of the core of the massif (Figs. **F2, F3A**). The inferred gradient of seismic velocity in the central dome of Atlantis Massif is similar to that determined near Ocean Drilling Program (ODP) Site 920, where 100–200 m of serpentinized peridotite was drilled (Fig. **F3B**). This gradient is quite distinct from that characterizing gabbro-hosted Atlantis Bank (Southwest Indian Ridge) and other sections of the MAR. Multichannel seismic (MCS) reflection data show a major difference in the structure of the outside (conjugate) corner lithosphere versus that hosting Atlantis Massif (Canales et al., 2004). Although the seismic Layer 2a/2b boundary is well imaged on the eastern

flank of the ridge axis, it is not evident on the western flank where the massif is located. A strong reflector is visible at 0.2–0.5 s two-way traveltime below much of the domal surface (Fig. **F3C, F3D**). Two interpretations have been posed: (1) an alteration/serpentinization front or (2) a structurally deeper detachment fault, subparallel to the seafloor beneath the dome (Canales et al., 2004).

Modeling of sea-surface (Fig. **F4**) and sparse seafloor gravity data (Blackman et al., 1998, 2004; Nooner et al., 2003) suggests that there is a wedge-shaped body in the domal core with density 200–400 kg/m^3 greater than the surrounding rock. In the model, the footwall is overlain by tilted hanging wall blocks that are capped by material with density typical of upper crustal rock (2.5–2.7 kg/m^3). The interface between the model blocks on the east is a gently inclined (15°–25°) boundary that dips more steeply than the exposed corrugated surface (~11°) where it meets that hanging wall. It is possible that the density interface coincides with the base of the detachment fault zone, a region inferred to be highly altered and therefore of lower density.

Rock samples collected by the manned submersible *Alvin* and a dredge from the central dome are mostly angular talus and rubble of metabasalt and limestone (Fig. **F2**) (Cann et al., 2001; Blackman et al., 2004). A few samples showing cataclastic deformation fabrics or highly serpentinized and metasomatically altered peridotite were also recovered. The protolith of most of the serpentinite sampled on the south wall of the massif is harzburgite (Fig. **F2**). These rocks are commonly cut by highly altered gabbroic veins composed dominantly of talc, tremolite, and chlorite (Früh-Green et al., 2001; Schroeder et al., 2001). Low-temperature overprinting, seafloor weathering, and carbonate vein formation mark the youngest phases of alteration.

Microstructural analysis of samples from the south wall indicates shear deformation and dilational fracturing at metamorphic conditions ranging from granulite to subgreenschist facies (Schroeder et al., 2001). Ductile fabrics in peridotite samples are overprinted by semibrittle and brittle deformation (Schroeder and John, 2004). Stable mineral assemblages of tremolite, chlorite, and chrysotile indicate that the latter process occurred at <400°C. The distribution of samples and their deformation characteristics suggest that strong semibrittle and brittle deformation is concentrated at shallow structural levels (<90 m beneath the domal surface) at the southern ridge (Schroeder and John, 2004). Outcrop mapping with the *Alvin* and photomosaics constructed from *Argo* digital still camera images show that this uppermost fault extends across much of the top of the southern ridge (J. Karson, pers. comm., 2005).

Only a few expeditions in the history of scientific ocean drilling have recovered lower crust and upper mantle rocks near a mid-ocean ridge axis (Fig. **F5**). During Deep Sea Drilling Project (DSDP) Leg 45 (Melson, Rabinowitz, et al., 1979) on the western flank of the MAR south of the Kane Fracture Zone, a 587.9 m deep hole was drilled into sediments and basaltic basement. A few gabbro cobbles were recovered from the top of the core, and two serpentinized harzburgite and lherzolite cobbles were trapped between two basaltic units. During DSDP Leg 82 (Bougault, Cande, et al., 1985), with a drilling plan designed to address regional variations in basalt chemistry along the ridge axis at three sites (DSDP Sites 556, 558, and 560) between 34°43′ N and 38°56′ N, a few tens of meters of metamorphosed gabbro and pervasively serpentinized peridotite represented the first in situ recovery of these lithologies. During ODP Leg 109 (Bryan, Juteau, et al., 1988), the first intentional drilling for mantle peridotites at a mid-ocean ridge at ODP Site 670 was completed with 7% recovery of sepentinized peridotite. Figure **F5** shows all holes (recovery > 5%) in upper mantle and lower crustal rocks drilled to date at or near mid-ocean ridges during nine different ODP and IODP expeditions. ODP Leg 147 at Hess Deep (Gillis, Mével, Allan, et al., 1993) is the only one which took place in crust created at a fast-spreading ridge (Hess Deep, East Pacific Rise).

Atlantis Massif is the fourth location where drilling an inside corner high and/or a corrugated dome at a slow-spreading ridge has been attempted by ODP or IODP. A total of 11 holes (>10 m deep) were cored at 6 different sites in 3 different locations (Atlantis Bank, Southwest Indian Ridge, 57°16′ W; MAR, 15°44′ N; Kane Fracture Zone [MARK] area, MAR, 23°32′ N) during ODP Legs 118, 153, 176, and 209 (Robinson, Von Herzen, et al., 1989; Cannat, Karson, Miller, et al., 1995; Dick, Natland, Miller, et al., 1999; Kelemen, Kikawa, Miller, et al., 2004). In all of these holes, the dominant rock type recovered is gabbro and ranges from diabase to troctolitic in composition. The maximum distance between two holes in each of these regions is 2.8 km (MARK), 1.3 km (Atlantis Bank), 900 m (MAR 15°44′ N), and 20 m (Atlantis Massif). ODP Site 1270 is located on a crest of an axis-parallel ridge, inferred to be an OCC by Fujiwara et al. (2003), but with no obvious corrugation pattern on the available bathymetric data. ODP Site 1272 is located at an inside corner massif, which does not culminate higher than other hills in the 15°20′ N Fracture Zone area.

The gabbroic and ultramafic rocks recovered during previous expeditions at slow-spreading ridges show a wide range of geochemical compositions (Fig. **F6**), reflecting a strong lithologic heterogeneity, from very primitive troctolitic assemblages to evolved, oxide-rich gabbros (ODP Leg 209; Kelemen, Kikawa, Miller, et al., 2004).

SCIENTIFIC OBJECTIVES

Atlantis Massif has several key features that make it an ideal target for OCC drilling: it is <2 m.y. old, so weathering and erosion have not degraded (macro-)structural relationships; the hanging wall is interpreted to be in contact with the footwall of the detachment; and mantle seismic velocities have been reported to be present at several hundred meters depth below seafloor of the domal core, potentially affording access to fresh in situ peridotite with conventional drilling.

The scientific objectives, as outlined in the drilling proposal and the Expeditions 304 and 305 *Scientific Prospectus* (Blackman, John, Ildefonse, MacLeod, Ohara, Miller, and the Expedition 304/305 Project Team, 2004), address fundamental questions related to (1) the formation of OCCs and (2) the nature and evolution (alteration) of the oceanic lithosphere accreted at slow-spreading ridges.

The hypotheses to be tested by drilling during Expeditions 304 and 305 were:

1. A major detachment fault system controlled the evolution of Atlantis Massif.
2. Significant unroofing occurred during formation of this OCC.
3. Plate flexure (rolling hinge model) is the dominant mechanism of footwall uplift.
4. The nature of melting and/or magma supply contributes to episodes of long-lived lithospheric faulting.
5. Expansion associated with serpentinization contributes significantly to uplift of core.
6. The Mohorovicic discontinuity (Moho) at Atlantis Massif is a hydration front.
7. Positive gravity anomalies at Atlantis Massif indicate relatively fresh peridotite.

The hypothesis that the Moho at Atlantis Massif coincides with an alteration front could not be directly tested, as Hole U1309D did not penetrate into rock with seismic velocity of ~8 km/s.

If long-lived normal faulting and displacement are responsible for the evolution of the massif, uplift of the core may be the result of isostatic adjustment (Vening Meinesz, 1950) and thin-plate flexure (Spencer, 1985; Wernicke and Axen, 1988; Buck, 1988; Lavier et al., 1999). Differential rotation between the footwall and hanging wall blocks is predicted by thin-plate theory, so we can apply results from IODP Expeditions 304 and 305 to investigate whether the core–logging data show evidence of such history. Logging data provide continuous (oriented) images of fracture pat-

terns in the borehole wall. These are compared with fractures and veins measured in the cores from the same depth interval. Paleomagnetic data are incorporated to determine any history of rotation of the upper footwall. The pressure-temperature evolution of alteration reflects the tectonic and magmatic history as well, with cooling rates and water/rock ratios being controlled by intrusions, the amount of unroofing, and the degree of fracturing.

The processes responsible for the development of an OCC appear to be episodic, with one factor being the level and/or style of magmatic activity at the local spreading center. Detailed study of the igneous sequence and structural relationships therein will be used to address the evolution of melting, intrusion, and cooling during the formation of Atlantis Massif.

SITE U1309

Site U1309 (Fig. **F2**) is located on the central dome of Atlantis Massif, 15 km west of the median valley axis of the MAR, where the seafloor is interpreted to coincide with a gently sloping, corrugated detachment fault surface. Two drill holes at this site (Holes U1309B and U1309D) penetrate a multiply intruded and faulted crustal section, providing core that documents the interplay between magmatism and deformation prior to, during, and subsequent to a period of footwall displacement and denudation associated with detachment faulting. Five shallow-penetration holes (Holes U1309A and U1309E–U1309H) (Fig. **F2**) were drilled during Expedition 304 to sample the sedimentary carapace and upper few meters of the basement, test the hypothesis that the upper surface coincides with the detachment fault, and help constrain the temporal history of denudation (see Shipboard Scientific Party, 2005). In this report, we focus on results from Hole U1309D, which is where all Expedition 305 coring and logging operations were carried out.

Site selection was based on a combination of geological and geophysical data, balancing the details of seafloor character with larger-scale objectives. Centered within the gently sloping, corrugated, and striated dome (Cann et al., 1997), Site U1309 is within a positive Bouguer gravity anomaly and close to the area where high seismic velocity is inferred to indicate the presence of unaltered ultramafic rocks within several hundred meters of the seafloor (Blackman et al., 1998; Collins et al., 2001). *Argo II* imagery and *Alvin* dive mapping previously showed that the seafloor is covered by a thin layer of unconsolidated sediment, deposited on bedrock and in places interrupted by lineated rubble fields (Blackman et al., 2004). In areas without significant loose sedimen-

tary cover, a thin cover of lithified carbonate caps the underlying low-relief basement. Dredge and *Alvin* sampling indicate that loose, angular fragments on the central dome include low-grade metabasalt and serpentinite (Blackman et al., 1998, 2004).

Most of the holes composing Site U1309 are located in an area with 2–4 m of unconsolidated sedimentary deposits above basement. During Expedition 304, a 60 × 50 m survey with the vibration-isolated television camera on the drill string documented an ~2000 m^2 area free of cobble- to boulder-sized rubble. The area is ~280 m south of an *Argo II* track (run 039) and an *Alvin* dive (3642), both from cruise AT3-60 (Blackman et al., 2004), and west of EW0102 MCS Line Meg-4, at common midpoint 4100 (Canales et al., 2004). Towed ocean-bottom instrument and DSL120 side-scan sonar data show spreading-parallel striations crossing this area. A gentle northeast slope coincides with the southern flank of the corrugation the site penetrates. Drilling in Hole U1309D took place over two periods for a total of 15 days during Expedition 304; penetration reached 401.3 mbsf. The hole was spudded using a hammer drill with $13^3/_8$ inch casing, in an effort to provide stable reentry for a deep hole. No rock was recovered in the upper 20.5 m of the hole. Below 20.5 mbsf, coring was accomplished using a rotary core barrel bit. Despite rough sea conditions during some of the drilling, recovery rates were very good—64% overall. As drilling conditions in the pilot hole (Hole U1309B, Expedition 304) were very good, casing below 20 m in Hole U1309D was deemed unnecessary.

IGNEOUS STRATIGRAPHY

A total of 1043 m of mafic and ultramafic rock was recovered from Hole U1309D during Expeditions 304 and 305, ranging in composition from basalts and diabase to dunite. The following major types of rocks were recognized (Figs. **F7, F8**):

- dunitic troctolite
- troctolite
- troctolitic gabbro and olivine gabbro
- gabbro group (olivine-bearing gabbro, gabbro, microgabbro, gabbronorite, and orthopyroxene-bearing gabbro)
- oxide gabbro
- diabase/basalt

These were distinguished on the basis of primary mineral mode, igneous contacts, and variations in grain size. A total of 770 igneous units were defined in Hole U1309D, including 221 from 20.5 to 401.3 mbsf (Expedition 304) and 549 from 401.3 to 1415.5 mbsf (Expedition 305).

The most abundant rock type recovered is from the gabbro group, composing 60.8% of the core recovered during Expedition 305. This group has a wide range of modal compositions, including minor volumes (rarely exceeding 10%) of olivine, Fe-Ti oxides, and/or orthopyroxene. This group exhibits significant variations in grain size from microgabbro (<1 mm crystals) to seriate medium-grained to pegmatitic (grain size exceeding 10 cm), in places within a single section of core. Gabbronorite and orthopyroxene-bearing gabbro are included in this gabbro group. Since unambiguous identification of orthopyroxene requires careful thin section observation, the amount of orthopyroxene-bearing gabbro is a minimum estimate. Gabbronorites show the same textural relationships as the associated gabbros. In the lower part of Hole U1309D (from Cores 305-U1309D-243R to 272R), low-Ca pyroxene appears, as either orthopyroxene and/or inverted pigeonite.

Olivine gabbro is a major rock type in Hole U1309D (25.5%) (Fig. **F7**), with modal olivine ≥20%. However, the modal composition of this rock type is highly variable on a submeter scale as well as, in places, commonly grading into troctolitic gabbro. Together, olivine and troctolitic gabbro form the secondmost abundant lithology, 23.1% of the recovered rock types during Expedition 305.

Troctolite is generally spatially associated with olivine and troctolitic gabbros (Figs. **F8, F9**). The texture of troctolite is irregularly seriate, locally with poikilitic clinopyroxene. Troctolite is less common and constitutes only 2.2% of the rocks recovered during Expedition 305. Troctolite units are commonly intruded by late-stage dikes of both coarse-grained gabbro and microgabbro.

Olivine-rich rocks with relatively low modal plagioclase and clinopyroxene are grouped as "dunitic troctolite." The recovered dunitic troctolites are very olivine rich, containing >70% olivine by mode, and are commonly intercalated with olivine and troctolitic gabbro (Fig. **F10**). The downhole abundance of the dunitic troctolites is >5% of the rocks recovered during Expedition 305, with the thickest interval between 1092 and 1236 mbsf (Fig. **F8**). In contrast to troctolite, dunitic troctolite displays subhedral to rounded medium-grained olivine and interstitial to poikilitic plagioclase

and clinopyroxene in variable proportions (Fig. **F11**). This texture is commonly interpreted to suggest a cumulate origin.

Oxide gabbro, defined by the presence of >2% by mode Fe-Ti oxide minerals, is also a ubiquitous lithology, making up 7.7% of the rocks recovered during Expedition 305. The most common occurrence of oxide minerals (~80% of the oxide gabbros) is as randomly dispersed patches in undeformed, generally coarse-grained gabbros. Concentrations of oxide minerals are also present as discrete dikelets/layers cutting other rock types with either sharp or diffuse boundaries. Oxide mineral concentrations are commonly associated with intervals of ductile deformation (Fig. **F12**). Many oxide gabbros contain apatite and zircon as accessory minerals. Ubiquitous occurrences of oxide gabbros were also noted in ODP Hole 735B, Atlantis Bank (Dick, Natland, Miller, et al., 1999); in the MARK area (ODP Leg 153; Cannat, Karson, Miller, et al., 1995); and at 15°N at the MAR (ODP Leg 209; Kelemen, Kikawa, Miller, et al., 2004).

Diabase intrudes other rock types in several places throughout Hole U1309D. The deepest recovered diabase was from 1377.6 mbsf (interval 305-U1309D-287R-1, 0–48 cm).

Almost all gabbroic rock types are cut by veins/dikes of variable thickness and composition. These veins/dikes include gabbro dikelets, oxide-bearing dikelets, and trondhjemite dikelets. These dikelets may be partly magmatic in origin, partly metamorphic, partly deformation-related, or the result of a combination of all three processes.

GEOCHEMISTRY

During Expedition 305, a total of 145 discrete samples were analyzed for major and trace element concentrations by inductively coupled plasma–atomic emission spectrometry. Hole U1309D gabbroic rocks have compositions that are among the most primitive sampled along the MAR (e.g., Casey, 1997; Kelemen, Kikawa, Miller, et al., 2004), as indicated by high Mg# (67–87 excluding oxide gabbros), low TiO_2 (<0.72 wt%), and low trace element contents (Fig. **F13**). Among all other DSDP/ODP/IODP drill holes, Hole U1309D is unique in that it represents a section of primitive to slightly evolved gabbroic rocks and includes intrusive diabase intervals as well as olivine-rich rocks, which may represent primitive cumulates.

Gabbroic rocks from Hole U1309D are divided into two geochemical units based on chemical trends and range of Mg# (~10) (Fig. **F14**). Unit I includes the section from 20 to ~600 mbsf, coinciding upcore with a general decrease in the presence of olivine-rich rock types and a general increase in the thickness of relatively thick oxide gabbro, although the actual lithostratigraphy is in detail more complicated with interfingering oxide gabbros, gabbros, olivine gabbros, troctolites, and dunitic troctolites. Unit II extends from ~600 mbsf to the bottom of the hole, coinciding downcore with a general increase in the volume percent of olivine gabbro. Although four fault zones are identified in Unit II (695, 746, 785, and 1107 mbsf), systematic geochemical changes are not consistently apparent across these fault zones.

All diabase intervals have basaltic compositions (Fig. **F15**) but show significant variation in incompatible trace elements like Y and Zr. Compared to the diabases from Expedition 304 in the upper part of Hole U1309D, the samples from Expedition 305 are somewhat less evolved in composition but still overlap the compositional field defined by glasses from the MAR.

Water samples collected at the beginning of operations during Expedition 305 (~395 mbsf) and at ~1215 mbsf were both essentially indistinguishable from seawater in terms of pH (7.4–7.7) and salinity (30‰).

HYDROTHERMAL ALTERATION, METAMORPHISM, AND METASOMATISM

Alteration mineral assemblages record cooling of the plutonic rocks, from magmatic conditions to zeolite facies, during unroofing and uplift of Atlantis Massif. The alteration intensity is moderate (Fig. **F16**) and tends to decrease downcore in general. Locally, there are exceptions to this, where alteration intensity correlates with the modal abundance of olivine in the intercalated dunitic troctolites, olivine gabbros, and gabbros between ~1090 and ~1230 mbsf and in the lowermost gabbros and olivine gabbros (Fig. **F17**). The coarser grained gabbro intervals generally appear to be more altered than the medium- to coarse-grained gabbros and olivine gabbros. In dunitic troctolite intervals, alteration is mostly restricted to heterogeneous serpentine networks, with strong alteration gradients from the contact with intensely veined intercalated gabbros to the fresher cores of the dunitic troctolite units. The latter locally contain intervals of very fresh (as low as 1% serpentinization) olivine-rich (as much as ~90%) rocks. Alteration is commonly more intense in the vicinity of metamorphic

veins. The vein assemblages change with lithology (local control) and with depth, likely reflecting changes in late fluid chemistry.

The overall metamorphic history is divided into a high-temperature phase and, by far the most important, a low-temperature phase, each with multiple events that reflect alteration at temperatures <500°C. The several stages of metamorphism and alteration appear as follows.

The first high-temperature (granulite/upper amphibolite facies) event is commonly associated with the limited occurrences of high-temperature ductile deformation. It is characterized by recrystallization of plagioclase, clinopyroxene, and, more rarely, brown hornblende (which may or may not be igneous in origin).

Static replacement of pyroxene by green to brown hornblende occurs most commonly in oxide gabbros.

The main mode of alteration of the most olivine-rich rocks is serpentinization. The degree of serpentinization varies widely from >90% to <10% of the olivine. In the simplest case, serpentinization proceeds via the development of kernel texture (O'Hanley, 1996) (Fig. **F18**). In hand sample, areas of more intense serpentinization form a conspicuous, but generally irregular, foliation (Fig. **F19**). The veinlets that define the foliation appear black because of included opaque phases (Fig. **F20**), mostly magnetite and also some sulfides (pyrrhotite and, more rarely, pyrite, as identified by reflected light microscopy). Plagioclase in the serpentinized rocks ranges from virtually unaltered to partially altered (usually to prehnite) to complete replacement by hydrogarnet and/or prehnite. Hydrogarnet appears to be most common in highly serpentinized rocks. A commonly observed feature in serpentinized rocks is the development of microfracture sets that radiate or extend into plagioclase from neighboring serpentinized olivine grains (Fig. **F21**). These fractures are commonly filled with chlorite and/or amphibole.

A widespread greenschist facies event is characterized by (1) the development of corona texture in olivine-plagioclase rocks (Fig. **F22**), (2) bleaching and epidote growth that may or may not be related to late leucocratic intrusions, (3) widespread emplacement of amphibole-rich veins and accompanying halo alteration, (4) talc-carbonate metasomatic alteration of olivine-rich rocks (restricted to the upper part of the core; see Shipboard Scientific Party, 2005), and (5) relatively late emplacement of slip-fiber amphibole veins and associated metasomatism.

The most common corona texture consists of partial or complete replacement of olivine by talc/tremolite and replacement of the edges of neighboring plagioclase by chlorite. Tremolite may either entirely replace olivine or be restricted to its margins (Fig. **F23**). Talc is present, mostly in the cores of completely or nearly completely altered olivine, although, where relatively fresh olivine cores are present, an annulus of talc may separate it from the outer tremolite zone. Serpentine is generally present only as relics within fractures in olivine, as a late replacement of olivine cores, or, rarely, as a replacement of tremolite. In a few cases, carbonate is also found associated with serpentine, talc, and tremolite.

Dark green amphibole veins are the most common vein type in Hole U1309D (~48%); they are the major contributor to the overall observed alteration. Corona textures are commonly well developed near dark green amphibole veins. In hand sample, these veins are usually relatively straight, but also commonly braided, and typically associated with an alteration halo 5 mm to 2 cm wide (Fig. **F24**). In thin section, they are filled with green amphibole (probably actinolite) ± chlorite.

Late light green amphibole veins, commonly in a slip-fiber configuration, cut the dark green veins. They contain mostly tremolite and/or actinolite and, in more olivine-rich rock types, talc and/or serpentine. These veins can contain a substantial amount of isotropic and/or very fine grained material that may include hydrogarnet. The veins are commonly associated with alteration halos as thick as a few centimeters, especially in olivine-rich rocks containing talc and/or tremolite, amphibole, chlorite, albite, prehnite, zeolite, or hydrogarnet. As with the more abundant dark green veins, the signature of this alteration seems to be the transport of silica into olivine-rich lithologies.

The latest stage of alteration involves emplacement of a variety of veins, postdating greenschist facies alteration and containing variable mineralogy that, at least in part, correlates with depth. The veins contain quartz, carbonate, zeolite, prehnite (Fig. **F25**), and, in one case, anhydrite. Overprinting all of these vein types is a late, low-temperature set of clay-rich (probably saponite) veins. The clay is present along with calcite and/or zeolites (especially thomsonite) in broad, uneven fractures in the rock. The clay veins appear most commonly associated with olivine-rich rocks and are notably abundant in gabbroic rocks intercalated with dunitic troctolite between ~1090 and ~1230 mbsf.

The mineralogy of common "white" veins varies significantly with depth. Above ~400 mbsf, sulfide-, quartz-, and, possibly, zeolite-bearing veins are abundant. Quartz is rare below ~400 mbsf, and little sulfide is found in veins below ~800 mbsf. Zeolite, absent from the vein assemblage below 300 mbsf, reappears at ~700 mbsf and increases in abundance downhole to the deepest penetration of Hole U1309D (Fig. **F26**). Carbonate occurs in veins associated with ultramafic rocks throughout the hole.

Fluid flow along fracture zones, including zones of brecciation or cataclasis, or associated with late magmatic intrusions commonly results in higher degrees of alteration in the surrounding gabbro. In cores recovered during Expedition 305, it was apparent that zones of plastic and, especially, brittle deformation provide fluid pathways and thus cause greater alteration of the adjacent rocks. However, not all plastic or brittle deformation zones are highly altered.

The overall trends in alteration and the changes in secondary mineralogy suggest that two separate secondary processes affected the footwall in the vicinity of Hole U1309D. In the upper ~840 m, seawater–rock interactions pervade the sequences. Below that depth, the nature of and the fluctuations in degree and style of metamorphism are related to fluids of a different composition percolating along fault zones and zones of deformation. Hence, the rocks record an extensive history of gabbroic rock/fluid interaction, possibly including magmatic fluids.

STRUCTURAL RELATIONSHIPS

Crystal-plastic, magmatic, and brittle deformation identified in rocks recovered during Expedition 305 from ~401.3 to 1415.5 mbsf show a low overall degree of deformation (Fig. **F27**). The temporal evolution of the deformation history in Hole U1309D may be summarized as follows:

Magmatic fabric. About 22% of all recovered rocks show a generally weak magmatic foliation (Fig. **F28**). The formation of the magmatic foliation is attributed to processes related to igneous emplacement of the gabbro bodies. The growth of clinopyroxene megacrysts, commonly poikilitic, appears to have occurred late in the crystallization sequence of the gabbros, as in many samples they embed equilibrated and/or corroded plagioclase grains. Clinopyroxene growth may locally overprint early hypersolidus crystal-plastic recystallization.

High-temperature plastic deformation. Whereas core descriptions suggest an absence of plastic deformation except in local shear zones, microstructural observations frequently indicate a weak to moderate crystal-plastic strain overprint in samples (Fig. F29). Except for a few cases, there is no strong foliation development coupled to this phase of plastic strain; therefore, it is likely to have been weak.

Lower temperature and/or higher strain rate deformation. Clearly overprinting the high-temperature plastic fabric when present, and much more localized, are discrete, relatively thin (generally a few centimeters up to 1 m) porphyroclastic and mylonitic shear zones. The shear zones commonly, but not systematically, show a close spatial association with concentrations of oxide minerals (Figs. F12, F30A). Overall, crystal-plastic foliation has been identified in <3% of the core.

Magmatic veins. Magmatic veins seem to be the expression of late magmatic intrusions, and they do not show any associated high-temperature deformation. Magmatic vein types appear close to intrusive bodies of the same rock type, suggesting a local, parental relationship.

Serpentinization. Serpentinization occurred along microcracks, and the products of this process appear in all olivine-bearing rocks, most prominently and highly heterogeneously in olivine-rich rock types.

Fault zones, cataclastic deformation, and veining. All fault gouges (Fig. F31), zones of cataclasis (Fig. F32), and late, silica-rich hydrothermal veins formed under greenschist facies or lower conditions. Crosscutting relationships indicate a complex succession of events involving fluid flow and deformation. The amount of strain recorded is negligible overall, except for four fault zones (at ~695, 756, 785, and 1107 mbsf) identified by the occurrence fault gouges. These faults, however, are relatively thin (no more than a few tens of centimeters), unlikely to have accommodated large displacement, and more likely reflecting late deformation internal to the overall gabbroic body rather than major regional tectonic event(s). One of the most pervasive indicators of internal deformation is the presence of fibrous light green veins with fibers indicating the direction of vein movement (vein faults). In most cases (>75%), these fault veins display strike-slip movement, which may be associated with the deformation of structural blocks in the footwall. The relative timing of serpentinization and late brittle events is not clearly defined, although they are probably distinct events based on the difference in the fluid chemistry required for serpentinization versus the formation of talc- and tremolite-rich veins.

Open fractures. Late fracturing of the rock results in fractures that are open and have no apparent offset. Sulfides are present along these fractures only in the lower part of the drilled section (>600 mbsf).

Similar to the metamorphic record, the deformation history is essentially separated into high-temperature and low-temperature events, with no significant deformation occurring under the amphibolite facies conditions. Only very locally was syn-kinematic brown amphibole observed (in oxide gabbros). Neither the high- nor the low-temperature deformation recorded by the Expedition 305 Shipboard Scientific Party is geometrically consistent with (too steeply dipping) or directly related to a major detachment system such as the one inferred to be responsible for exposing the corrugated domal surface of Atlantis Massif. The latter is probably essentially brittle and highly localized in the uppermost part of the section at Site U1309.

GEOPHYSICAL MEASUREMENTS

Onboard physical property data in combination with downhole logging data provide an initial means to assess which aspects of the geological characteristics of the domal core of Atlantis Massif might contribute to the regional geophysical data sets. In addition, inherent rock properties can be assessed and related to rock type and alteration.

Magnetic susceptibility is highest in the dunitic troctolites recovered from Hole U1309D, and it is quite low in most of the gabbros (Fig. **F33A, F33B**). Both dunitic troctolite and oxide gabbro intervals can have very high magnetic susceptibility signal (2000–10,000 × 10^{-5} instrument units), although only the former is consistently at these levels. The dunitic troctolites are commonly highly serpentinized (Fig. **F33C**), and the susceptibility reflects magnetite produced during the alteration process.

The natural remanent magnetization (NRM) of the rocks from Hole U1309D was determined onboard following removal of a drilling-induced overprint. Alternating-field (AF) demagnetization (typically 30 mT) was used to remove the overprint, and the bulk of the archive-half sections show negative inclination direction (Fig. **F33D**), which corresponds to a reversed magnetic polarity epoch. Minicore samples, cleaned of overprint by either AF (up to 100 mT) or thermal demagnetization (to 500°–550°C), generally show very good agreement with the half-core inclination patterns downhole. The inclination for most of the hole is somewhat shallower (~32°–38°) than would be predicted for the geomagnetic field at the site location (48°). However, the

interval from ~900 to 1100 mbsf clearly has a steeper negative inclination (~42°). The standard deviation of these inclination estimates is ±9°–12°. The change to higher values is sharp, the lower boundary possibly coinciding with an inferred small fault at 1100 mbsf. Whether there is any relationship between structure or lithology and the top of this interval is not clear at this stage.

There are a number of short intervals that have positive NRM inclination. All such intervals correspond to rocks with high magnetic susceptibility and intensity—troctolite and dunitic troctolite. The steepness of some of the positive polarity determinations suggests caution, as the drilling overprint may not have been fully removed. However, many of the positive values are quite stable, so the signature must have been imparted during a normal polarity epoch. A valid working hypothesis at this point is that these intervals record the relative chronology between crystallization of the gabbro (negative polarity) and both serpentinization and intrusion of diabase intervals (positive polarity).

The physical properties that are most relevant for relating the rocks from Hole U1309D to broader scale geophysical measurements are seismic velocity and density. Onboard measurements provide an indication of the inherent properties of small samples at room temperature and pressure. Variability in the measured values can be due to a number of factors, including mineralogy, porosity and grain size, and the style and degree of alteration.

A significant change in several core sample and downhole logging properties occurs between 280 and 400 mbsf (Fig. **F34**). Density values have reduced scatter and slightly higher average values below 350 mbsf, increasing from 2.8 g/cm^3 in the interval 280–340 mbsf to 2.9 g/cm^3 in the interval 350–400 mbsf. Average compressional velocity (V_P) of minicore samples in the 280–340 mbsf interval drops to 5.3 km/s (from 5.5 km/s in the overlying 200 m) before increasing to 5.7 km/s at 340–400 mbsf. Logging V_P increases from ~5.5 to 6.0 km/s between 340 and 370 mbsf. These changes combine to produce a significant impedance contrast (Fig. **F35**), and this can be related to the seismic reflection data, as discussed below. Electrical resistivity measured by the Dual Laterolog shows a marked increase over the same interval (Fig. **F34**). The low but variable values of all these physical properties are associated with serpentinization of olivine-rich rock types (dunitic troctolites and, to a lesser extent, olivine gabbros that overly them) in the 280–340 mbsf interval (Fig. **F34A**). Overall alteration here is greater than in the overlying section, averaging 50%–75%, and it drops steadily to

20%–40% by 400 mbsf. Higher velocity and density values correspond to the underlying gabbroic interval.

Both on a local and a broader scale, the influence of crack closure with depth may contribute to the impedance contrast at 300–400 mbsf. Samples have consistently higher V_P (average = 5.6 km/s) than the downhole logging data (average = 4.5–5.5 km/s) in the ~50–300 mbsf interval, but the two data sets merge near 350 mbsf with mean sample and logging values tracking rather closely for the rest of the seismically logged interval (Fig. **F34**). The existence of open cracks in the upper few hundred meters is expected and would explain the lower logging velocities. However, the continued small downhole increase in measured sample density suggests that closure of microcracks may continue to greater depths.

If ~340 mbsf coincides with the D reflector, the average velocity of the overlying section would need to be ~5.44 km/s locally, slightly lower than the 5.54 km/s value determined by a vertical seismic profile (VSP) shot to 345 mbsf during the expedition. Both of these values are higher than the 5.0 km/s interval velocity noted by Canales et al. (2004) for the regionally applicable interval velocity above this reflector.

A second strong gradient in borehole electrical resistivity is present from 730 to 760 mbsf. Below 760 mbsf, average sample velocities steadily decrease from ~5.9 to ~5.5 km/s at 1415 mbsf. The cause of this decrease is not clear but could be related to progressive microcracking water depth, due to unloading during the coring process.

The VSP experiment extended from 275 to 840 mbsf. Tool failure and high seas combined to preclude collection of any seismic measurements during the final logging run. Initial analysis, based on automatic arrival picks of stacked seismograms, indicates an average velocity in the upper 550 m of the footwall in Hole U1309D of 5.5–5.6 km/s. An increase is indicated for greater depths by higher average velocities (5.8 km/s for stations 580–796 mbsf). The actual gradient of velocity is uncertain at this stage. More detailed processing postcruise (filtering, selection of individual seismograms that make up the stack, and repicking) should improve the estimates.

Temperature in the borehole increases with depth as expected (Fig. **F36**). Because of the significant impact of drilling in the hole, the measurements made almost certainly provide minimum estimates of what the actual formation temperature is. The Temperature/Acceleration/Pressure tool recorded a temperature of 120°C at the bottom of the hole (1415 mbsf). The temperature is somewhat lower than predictions from a simple cooling plate model of a spreading ridge flank of age near 2 Ma. How-

ever, the measured temperatures are a minimum (owing to hole cooling during coring) and much more careful measurement is required before quantitative interpretation should be made. These initial results suggest that thermally driven flow in the hole is likely to occur.

MICROBIOLOGY

Microbiological studies were conducted on whole-round core samples taken from 15 core sections from 401 to 1391 mbsf. Gabbro, olivine gabbro, and dunitic troctolite were all sampled. In an effort to establish a culture collection of endolithic microbes, four different types of media, as well as agar plates, were inoculated with portions of these core samples. Growth was observed from two samples based on a positive fluorescence test. However, due to the autofluorescence of rock particles, the presence of microorganisms can neither be confirmed nor denied until a shore-based molecular analysis of cultures is undertaken.

SUMMARY

The footwall exposed on the domal core of Atlantis Massif is heterogeneous. Site U1309 is located on the southern part of the central dome. Peridotite and the Lost City vent field (interpreted to be serpentinization-driven) crop out south of Site U1309 along the southern ridge of the massif (Kelley et al., 2001). Exposure of this apparently significant volume of peridotite 5 km south of Hole U1309D contrasts strongly with the ~1.4 km of gabbroic rock recovered at Site U1309. Analysis of the NOBEL seismic refraction data, centered ~2 km north of Hole U1309D, indicates that rock with a seismic velocity > 7.5 km/s, presumably dominantly olivine and essentially unaltered, is present at ~800 mbsf. This is in contrast with the ubiquitously lower velocities that typify gabbroic rocks such as those that dominate the recovery from Hole U1309D.

Initial work relating drilling results to possible broader scale geophysical signatures suggests some correspondence between rock type and alteration and seismic properties, but structural controls, not surprisingly, also appear to play a role. The ~1.4 km sequence of dominantly gabbroic rocks interlayered with 1–25 m thick ultramafic rocks or dunitic troctolite recovered from Hole U1309D clearly indicates that Atlantis Massif is not simply an uplifted mantle section where serpentinization is responsible for lower densities/seismic velocities (only) in the upper few hundred meters. A more

complex model than the one put forward before Expeditions 304 and 305 (Cann et al., 1997; Blackman et al., 1998; Blackman, John, Ildefonse, MacLeod, Ohara, Miller, and the Expedition 304/305 Project Team, 2004; Collins et al., 2001; Canales et al., 2004) is required. The lack of recovery of fresh mantle peridotite, or even significant sections of serpentinized mantle peridotite, is in contrast with exposures of serpentinized mantles along the southern ridge of the massif. This requires any models we develop to incorporate complex lateral and vertical heterogeneity in lithography, alteration, and structures.

Onboard synthetic seismogram modeling (Fig. **F35**) suggests that physical property changes across the 300–400 mbsf interval could give rise to the strong D reflector (Canales et al., 2004) (Fig. **F3**). In Hole U1309D, it is probably the change from less altered gabbro to more altered olivine-rich rocks that dominates the local acoustic impedance contrast in the upper few hundred meters of the massif. Given the lithologic (and related alteration) variability with depth in Hole U1309D, it would be interesting if the interface between gabbroic rocks and dunitic troctolite actually extends at a similar depth across the central dome of Atlantis Massif. Although still associated with a contrast in alteration, the increase in alteration with depth and the fact that this interval is embedded within a much larger gabbroic sequence contrast sharply with the interpretation (Canales et al., 2004) of the D reflector as the base of a regional alteration front.

The gabbroic rocks sampled from Site U1309 are among the most primitive known along the entire MAR. The most olivine-rich end-member consists in a series of dunitic troctolite intervals, on average moderately serpentinized and locally very fresh. The preferred shipboard interpretation is that they constitute the primitive cumulate of the recovered igneous sequence(s). Oxide gabbros, a common feature in slow-spreading ridge boreholes (Robinson, Von Herzen, et al., 1989; Dick, Natland, Miller, et al., 1999; Pettigrew, Casey, Miller, et al., 1999; Kelemen, Kikawa, Miller, et al., 2004) are also present at Site U1309. Commonly, mylonitic shear zones overprint these oxide-bearing intervals. However, they are most common in undeformed rocks with magmatic textures and either sharp or diffuse boundaries. The interplay between relatively late Fe-Ti oxide crystallization and deformation is probably complex, and their relative timing may be variable. The most significant unit boundary within the recovered gabbroic pluton seems to be located at ~600–800 mbsf, as indicated by a series of observations, including a rapid change in the geochemical compositions at ~600 mbsf, a series of faults with gouges between ~ 695 and 785 mbsf, and a change in the late metamorphic overprint below ~800 mbsf.

There is a striking lack of extensive amphibolite facies alteration and deformation in rocks from Site U1309 in the same way as is lacking at the 15°45′ N corrugated dome on the MAR (Escartin et al., 2003). This contrasts markedly with the nature of the gabbroic section recovered from ODP Hole 735B at the Southwest Indian Ridge (Robinson, Von Herzen, et al., 1989; Dick, Natland, Miller, et al., 1999; Dick et al., 2000). Overall, the rocks recovered from Hole U1309D show little deformation, suggesting that large-scale deformation associated with a detachment fault was either not recovered in the upper section of the borehole at Site U1309 or occurred at low temperature. The lack of extensive deformation in these footwall rocks suggests that any deformation related to a major detachment fault system must have occurred at low temperature and must be strongly localized. IODP drilling results at Atlantis Massif are consistent with the low-temperature shallow rooting detachment fault model proposed by MacLeod et al. (2002) to have controlled the evolution of the corrugated dome west of the MAR at 15°45′ N.

Hole U1309D is located approximately midway downdip along the exposed corrugated detachment fault surface. The breakaway to this system is inferred to be ~5 km west. The fault termination (where the fault dips below the basaltic hanging wall block) lies ~5 km east. The dip of the fault at its termination is ~11°, and, therefore, the minimum amount of rotation expected for this site is of the same magnitude, larger if the detachment originally steepened toward the ridge axis. The shipboard paleomagnetic measurements indicate that no significant net rotation (≤15°) of the footwall rocks with respect to the predicted geomagnetic field has occurred at this site below the Curie temperature (~520°–580°C). This lack of footwall rotation suggests that a rolling hinge model is not a viable explanation for the uplift of the core of Atlantis Massif along a single concave, normal fault. A model involving multiple faults is probably more likely correct. The low-angle detachment fault currently capping Atlantis Massif could have captured the recovered gabbroic section at a relatively shallow depth in the lithosphere. As proposed previously (e.g., Karson, 1990; Cannat et al., 1997; Lagabrielle et al., 1998; Kelemen, Kikawa, Miller, et al., 2004), the pluton may have first risen from its deeper, crystallizing depth along a series of conjugate normal faults.

PRELIMINARY SCIENTIFIC ASSESSMENT

IODP Expedition 305 was planned in conjunction with Expedition 304, with the overarching goals as noted in **"Scientific Objectives."** Our overall objectives encom-

pass investigating the nature, evolution, and geophysical signature of the oceanic lithosphere accreted at slow-spreading ridges. More specifically, the aims were (1) to address the formation of OCCs and (2) to transect a section, possibly an alteration front, corresponding to the transition to rocks with a seismic velocity of 8 km/s—commonly interpreted to represent fresh residual mantle peridotite. Objectives related to drilling the hanging wall were attempted during Expedition 304, and the footwall objectives were pursued during both Expeditions 304 and 305.

Studying the Detachment Fault Zone

Clearly, the set of working hypotheses related to drilling was only partly addressed because of logistical failures at the hanging wall site. In brief, all attempts to start/case a hole in these young basalts with the equipment on hand were unsuccessful. However, the coring results at the footwall site directly document some aspects of the detachment-controlled tectonics. The detachment system at Atlantis Massif must have developed under low-temperature (greenschist facies) conditions, and the fault zone(s) must be strongly localized. The existence of a capping fault is supported by the fragments of fault rocks and metabasalts recovered during the series of shallow cores drilled at the end of Expedition 304.

Core Complex Formation and Evolution

The initiation of the deep hole in the footwall during Expedition 304 was clearly a success, with ~400 m cored and a high-quality series of downhole geophysics logs. The 1415.5 m depth reached in Hole U1309D during Expeditions 304 and 305 provides a unique set of geological data to address fundamental questions related to the formation and evolution of core complexes (working hypotheses 2, 3, and 4) and, more generally, to the accretion of oceanic lithosphere. The most surprising finding in the 1043 m of recovered rocks from Site U1309 is the dominantly gabbroic section from a slow-spreading ridge hypothesized to be magma-starved. It is intriguing that all holes drilled in OCCs have recovered dominantly gabbroic rocks (Robinson, Von Herzen, et al., 1989; Dick, Natland, Miller, et al., 1999; Pettigrew, Casey, Miller, et al., 1999; Kelemen, Kikawa, Miller, et al., 2004; Cannat, Karson, Miller, et al., 1995). A simple lack of magma production cannot explain the development of low-angle detachment faults at slow- and ultraslow-spreading ridges. The lack of significant moderate- to low-temperature (i.e., <520°C) tectonic rotation inferred from the shipboard paleomagnetic measurements suggests that the rolling hinge model must be reconsidered.

Core from Hole U1309D offers a unique opportunity to address the evolution of intrusive sequences at slow-spreading centers. This section is unique in that it represents the most primitive interval of lower oceanic crust ever recorded, opening a window into lowermost crustal accretion processes. Among the many fresh and beautiful rocks recovered in Hole U1309D, three meter-scale intervals of dunitic troctolite were recovered below ~1000 mbsf. These ultramafic rocks, presenting cumulate textures, are locally very fresh (as low as <1% alteration) and, therefore, unique in ocean drilling records. These rocks likely represent the primitive end-member compositions of igneous oceanic crust. Alternatively, the ultramafics could be relics of mantle peridotite from a crust–mantle transition zone, where it reacted with large volumes of percolating melt. The origin of these rocks will be the focus of detailed postcruise studies. The occurrence of similar olivine-rich rocks at mid-ocean ridges is rare; in Hole U1309D their abundance reaches 5% of the core.

Drilling through a Serpentinization Front to Fresh Mantle Rocks

One rationale for drilling a deep hole in the core of Atlantis Massif was a convergent set of geophysical data (NOBEL refraction data; air gun refraction data; multichannel reflection data, and gravimetry data) that indicated the presence of fresh mantle at shallow (~800 mbsf) depth and of a gradient in V_P, presumably related to gradational serpentinization of peridotite. Site U1309, based on the available survey data (analysis of reflection and refraction seismic data, gravimetry data, swath mapping, seafloor sampling by dredges, and submersible dives), was located a few hundred meters south of one of the NOBEL experiment lines (Fig. **F2**). It was assumed that the high-velocity material extended beyond the local area of the NOBEL seismic lines. We know now that this assumption was incorrect. The olivine-rich troctolites recovered from Hole U1309D, if fresh, are potential candidates for propagating seismic compressional waves at >8 km/s. However, the intervals of fresh rock found are not thick enough to account for the NOBEL results. We did not drill through a serpentinization front, nor did we reach fresh mantle peridotite. We were, therefore, unable to directly test working hypotheses 5, 6, and 7.

Our findings dictate that more complex analysis of existing (and any future) seismic data is required. Two-dimensional variability had been considered as part of the prior refraction analysis, but inversion results were strongly dependent on starting model geometry. A first step in reanalysis of existing refraction and reflection data is to include physical property and logging information from Hole U1309D. Depending on the results of the better-constrained modeling, additional seismic acquisition may

well be quite worthwhile. The rather continuous nature of key seismic reflectors across Atlantis Massif gives the impression that broader scale seismic structure is relatively continuous. Again, now we have impetus to look in more detail than the work done by Canales et al. (2004).

Downhole Measurements

The downhole measurement program during Expeditions 304 and 305 was generally successful. For the first time, we were able to log in lower crustal rocks, to ~1400 mbsf. We obtained a complete set of very high quality triple combination (triple combo) and Formation MicroScanner (FMS) tool string data, certainly the best ever recorded in igneous rocks. This, together with the high recovery, offers a unique opportunity to establish the core–logging structural integration. Unfortunately, the failure of the sonic and VSP tools, and, eventually, the rough sea conditions, did not allow us to acquire downhole seismic data during the last logging operations (below 850 mbsf).

Accomplished versus Planned Drilling

The drilling objective of Expedition 305 was to continue drilling and coring Hole U1309D, to the targeted depth of >700 mbsf, in the presumed high seismic velocity zone. We reached 1415.5 mbsf (i.e., ~200%) of the expected final depth. The overall recovery in Hole U1309D was 75%, exceeding by far the standard average recovery (~30%) in hard rock boreholes (Fig. **F5**), with the exception of ODP Hole 735B, in which the recovery of gabbroic rocks was exceptionally high (~86%).

We fulfilled the objective of deep drilling into an OCC to study its formation and evolution. We left IODP Site U1309 with a 1415 m long crustal section from Atlantis Massif, which will be the subject of many postcruise research projects. Hole U1309D is a unique, open, deep hole into the oceanic crust, ready for drilling deeper in the future and/or for in situ experiments, and we view it as an important legacy to IODP and to the marine geosciences community.

OPERATIONS SUMMARY

Port Call

Expedition 305 began when the first line was placed ashore at Pier 12 in Ponta Delgada on the island of São Miguel, Azores Islands, Portugal, at 2120 h on 7 January

2005. The three pacing items for the port call were an American Bureau of Shipping (ABS) Annual and Statutory survey, an overhaul of the drawworks transmission, and the replacement of the active heave compensator (AHC) hydraulic hose bundle.

The ABS survey was completed by the morning of 11 January. The replacement hose for the AHC was determined to be defective, so the AHC was not operational for Expedition 305. The completion of the drawworks transmission repair was dependent upon the arrival of hardware from the Transocean warehouse in Houston, Texas (USA). Customs clearance in Lisbon, Portugal, delayed arrival of these parts until ~1530 h on 12 January. At 1715 h, 12 January, the last line was released from the dock, and, after clearing the harbor entrance, the pilot was released at 1721 h and the vessel began the journey to Site U1309. The duration of the port call was 4.8 days.

Transit to Site U1309

The transit to Site U1309 covered 1002 nmi at an average speed of 10.7 kt. During the transit, the ship's clocks were retarded two h to –3 h Universal Time Coordinated. On approach to Site U1309, we conducted a 17.8 nmi towed magnetometer survey near the site. The survey line began at 30°4.7′ N, 41°47.0′ W, and extended west-northwest to 30°07.9′ N and 42°07.1′ W.

Site U1309

Initial Deepening of Hole U1309D

The vessel was positioned over Hole U1309D at 1600 h on 16 January using the Global Positioning System and the beacon that was deployed during Expedition 304. At 0027 h on 17 January, we reentered Hole U1309D and deployed the water-sampling temperature probe (WSTP) to the bottom of the hole. To minimize contamination or disturbance of the borehole water column, the drill string was lowered to ~10 m off the bottom of the hole with minimum rotation and no circulation. After the WSTP was retrieved, ~3 m of fill was cleaned from the bottom of the hole.

Between 17 January and 30 January, we cored from 401.3 to 837.4 mbsf (Table **T1**) using four C-7 rotary core bits. The average rate of penetration steadily decreased downhole, from 2.6 to 1.6 m/h, averaging 2.2 m/h for the 14 day coring operation, with recovery averaging >80%. Based on a conservative estimate of bit life, we elected to change bits after nominally 50 h of rotation. At the end of each bit run, the bits returned worn but essentially undamaged. Mud sweeps (20 bbl) were circulated every

10 m of advance to clean the hole. Fluorescent microspheres and perfluorocarbon tracers (PFTs) were deployed episodically during cored intervals at depths where microbiology samples were requested. However, PFT use was discontinued after Core 305-U1309D-90R at the request of the shipboard microbiologist, owing to insufficient time to rapidly process samples. At the end of the fourth bit run, the hole was conditioned for logging, including displacing the borehole fluid with freshwater to improve the logging signal.

Logging Run 1, Hole U1309D

In preparation for logging, the bottom of the pipe was set at 170 mbsf. This allowed overlap with previous logging runs performed during Expedition 304 and positioned the pipe below an interval where minor obstructions were encountered in the borehole during reentry. Six logging runs were completed, including the triple combo, FMS-sonic, VSP, Ultrasonic Borehole Imager, Goettingen Borehole Magnetometer, and a test of the logging wireline heave compensation system. In accordance with IODP policy, prior to the VSP, a 1 h visual survey of the water within a 700 m radius of the vessel was undertaken to ensure that no marine mammals were present prior to the start of the VSP experiment. Also consonant with the policy, the generator injector gun was soft-started (gradually increased intensity for the first 30 min of operation) at the initiation of testing. The marine mammal watch was maintained until the VSP was secured, and no marine mammals were sighted during the experiment. Logging operations were completed at 1040 h on 2 February.

Deepening Hole U1309D

Between 2 February and 23 February, we cored from 837.4 to 1415.5 mbsf, using one C-7 and five C-9 bits. The C-9 bits are designed for harder formation coring. We elected to use C-9 bits in order to preserve the last two C-7 bits in inventory in the event we encountered softer rock or noted deteriorating performance of the C-9 bits at depth. Average rate of penetration continued at 1.6–2.4 m/h, with recovery averaging 78%. We experienced no significant difference in bit performance between the styles of coring bits employed. Our routine procedure included 20-bbl mud sweeps after every other cored interval to clean the hole. Coring was completed at 1015 h on 23 February.

During our midcruise logging run, a temperature of ~60°C was measured by one of the magnetometer tool's sensors. We used two different approaches to verify borehole temperature prior to our final logging experiment. In our first attempt, an assortment

of calibrated, heat-sensitive adhesive strips were affixed to a modified advanced piston corer (APC) brass core catcher spacer deployed in a dedicated core barrel run. The core barrel was deployed at 1162 mbsf (a few meters above the bottom of the hole at the time) and allowed to equilibrate for 17 min without circulation. Upon recovery, the temperature strips indicated a minimum temperature of ~70°C. During the ensuing bit trip, we deployed the WSTP to collect a water sample and temperature measurement. Before deploying the sampler, our technicians determined the thermistor on the WSTP was broken and no exact replacement was available. The shipboard electrical technician fabricated an ad hoc arrangement of the APC Temperature (APCT) tool on the WSTP and found an uncalibrated thermistor to install on the WSTP. In addition to these two temperature measuring devices, an assortment of the adhesive temperature recording strips were also affixed to the WSTP. Owing to a failed O-ring, the APCT failed to record a temperature. The thermistor on the WSTP recorded a maximum temperature of ~60°C. A subsequent bench test determined 60°C was the maximum recording temperature for the new WSTP thermistor/datalogger assembly. The adhesive temperature strips indicated a minimum temperature of 110°C.

Logging Run 2, Hole U1309D

After hole conditioning on 23 February, the borehole was filled with drill water to improve the logging signal in resistive rock. A logging bottom-hole assembly was deployed, and the bit was set at 194 mbsf. Two passes were completed with the triple combo tool string. The second logging run utilized the FMS-sonic tool string (two passes including overlap with our midcruise logging passes); however, the sonic tool was not deployed because of tool failure. A marine mammal watch was instituted at daybreak 24 February in preparation for a VSP experiment. The three-component VSP tool failed, and, after deployment of the single-component tool, the sea state (>5 m heave) had deteriorated to the point where we were required to terminate logging. A single station was occupied and shots recorded with the single-component well-seismic tool. Operations in Hole U1309D concluded on 26 February.

Transit to Ponta Delgada

Prior to departure from Site U1309, a towed magnetometer survey was conducted. The 950 nmi transit required 104 h at an average speed of 9.1 kt. Expedition 305 concluded with the first line ashore at Ponta Delgada at 1805 h on 2 March 2005.

REFERENCES

Blackman, D.K., Cann, J.R., Janssen, B., and Smith, D.K., 1998. Origin of extensional core complexes: evidence from the MAR at Atlantis Fracture Zone. *J. Geophys. Res.,* 103:21315–21334.

Blackman, D.K., John, B.E., Ildefonse, B., MacLeod, C.J., Ohara, Y., Miller, D.J., and the Expedition 304/305 Project Team, 2004. Oceanic core complex formation, Atlantis Massif—oceanic core complex formation, Atlantis Massif, Mid-Atlantic Ridge: drilling into the footwall and hanging wall of a tectonic exposure of deep, young oceanic lithosphere to study deformation, alteration, and melt generation. IODP Sci. Prosp., 304/305. http://iodp.tamu.edu/publications/SP/304305SP/304305SP.PDF.

Blackman, D.K., Karson, J.A., Kelley, D.S., Cann, J.R., Früh-Green, G.L., Gee, J.S., Hurst, S.D., John, B.E., Morgan, J., Nooner, S.L., Ross, D.K., Schroeder, T.J., and Williams, E.A., 2004. Geology of the Atlantis Massif (MAR 30°N): implications for the evolution of an ultramafic oceanic core complex. *Mar. Geophys. Res.,* 23:443–469.

Bougault, H., Cande, S.C., et al., 1985. *Init. Repts. DSDP,* 82: Washington (U.S. Govt. Printing Office).

Bryan, W.B., Juteau, T., et al., 1988. *Proc. ODP, Init. Repts.,* 109: College Station, TX (Ocean Drilling Program).

Buck, W.R., 1988. Flexural rotation of normal faults. *Tectonics,* 7:959–973.

Canales, J.P., Tucholke, B.E., and Collins, J.A., 2004. Seismic reflection imaging of an oceanic detachment fault: Atlantis megamullion (Mid-Atlantic Ridge, 30°10′ N). *Earth Planet. Sci. Lett.,* 222:543–560.

Cann, J.R., Blackman, D.K., Smith, D.K., McAllister, E., Janssen, B., Mello, S., Avgerinos, E., Pascoe, A.R., and Escartin, J., 1997. Corrugated slip surfaces formed at ridge-transform intersections on the Mid-Atlantic Ridge. *Nature,* 385:329–332.

Cann, J., Blackman, D., Morgan, J., and MARVEL cruise participants, 2001. Geological inferences about the Mid-Atlantic Ridge 30°N core complex from initial analysis of side-scan, bathymetry and basalt petrography. Eos, Trans. Am. Geophys. Union, 82:F1099.

Cannat, M., Karson, J.A., Miller, D.J., et al., 1995. *Proc. ODP, Init. Repts.,* 153: College Station, TX (Ocean Drilling Program).

Cannat, M., Lagabrielle, Y., Bougault, H., Casey, J., de Coutures, N., Dmitriev, L., and Fouquet, Y., 1997. Ultramafic and gabbroic exposures at the Mid-Atlantic Ridge: geological mapping in the 15 degrees N region. *Tectonophysics,* 279:193–213.

Casey, J.F., 1997. Comparison of major and trace element geochemistry of abyssal peridotites and mafic plutonic rocks with basalts from the MARK regions of the MAR. *In* Karson, J.A., Cannat, M., Miller, D.J., and Elthon, D., *Proc. ODP, Sci. Results,* 153: College Station, TX (Ocean Drilling Program), 181–241.

Collins, J.A., and Detrick, K.S., 1998. Seismic structure of the Atlantis Fracture Zone megamullion, a serpentinized ultramafic massif. *EOS, Trans. Am. Geophys. Union,* 79:800.

Collins, J.A., Tucholke, B.E., and Canales, J.-P., 2001. Structure of Mid-Atlantic Ridge megamullions from seismic refraction experiments and multichannel seismic reflection profiling. *Eos, Trans. Am. Geophys. Union,* 82:F1100. (Abstract)

Dick, H.J.B., Natland, J.H., Alt, J.C., Bach, W., Bideau, D., Gee, J.S., Haggas, S., Hertogen, J.G.H., Hirth, G., Holm, P.M., Ildefonse, B., Iturrino, G.J., John, B.E., Kelley, D.S., Kikawa, E., Kingdon, A., LeRoux, P.J., Maeda, J., Meyer, P.S., Miller, D.J., Naslund, H.R., Niu, Y.-L., Robinson, P.T., Snow, J., Stephen, R.A., Trimby, P.W., Worm, H.-U., and Yoshinobu, A., 2000. A long in situ section of the lower ocean crust: results of ODP Leg 176 drilling at the Southwest Indian Ridge. *Earth Planet. Sci. Lett.,* 179:31–51.

Dick, H.J.B., Natland, J.H., Miller, D.J., et al., 1999. *Proc. ODP, Init. Repts.,* 176 [Online]. Available from World Wide Web: <http://www-odp.tamu.edu/publications/176_IR/176TOC.HTM>.

Escartin, J., Mével, C., MacLeod, C.J., and McCaig, A., 2003. Constraints on deformation conditions and the origin of oceanic detachments, the Mid-Atlantic Ridge core complex at 15°45′ N. *Geochem., Geophys., Geosyst.,* 4:10.1029/2002GC000472.

Früh-Green, G., Kelley, D.S., Karson, J.A., Blackman, D.K., Boschi, C., John, B.E., Schroeder, T., Ross, D.K., and MARVEL cruise participants, 2001. Hydrothermal alteration, serpentinization and carbonate precipitation at the Lost City vent field (30°N MAR). Eos, Trans. Am. Geophys. Union, 82:F1101.

Fujiwara, T., Lin, J., Matsumoto, T., Keleman, P.B., Tucholke, B.E., and Casey, J.F., 2003. Crustal evolution of the MAR near the 15°20′ Fracture Zone in the last 5 Ma. *Geochem., Geophys. Geosyst.,* 4(3):10.1029/2002GC000364.

Gillis, K., Mével, C., Allan, J., et al., 1993. *Proc. ODP, Init. Repts.,* 147: College Station, TX (Ocean Drilling Program).

Irvine, T.N., and Baragar, W.R.A., 1971. A guide to the chemical classification of the common volcanic rocks. *Can. J. Earth Sci.,* 8:523–548.

Karson, J.A., 1990. Seafloor spreading on the Mid-Atlantic Ridge: implications for the structure of ophiolites and oceanic lithosphere produced in slow-spreading environments. *In* Malpas, J., Moores, E.M., Panayiotou, A., and Xenophontos, C. (Eds.), *Ophiolites: Oceanic Crustal Analogues:* Proc. Symp. "Troodos 1987": Nicosia, Cyprus (Minist. Agric. Nat. Resour.), 547–555.

Kelemen, P.B., Kikawa, E., Miller, D.J., et al., 2004. *Proc. ODP, Init. Repts.,* 209 [Online]. Available from World Wide Web: <http://www-odp.tamu.edu/publications/209_IR/209ir.htm>.

Kelley, D.S., Karson, J.A., Blackman, D.K., Früh-Green, G.L., Butterfield, D.A., Lilley, M.D., Olson, E.J., Schrenk, M.O., Roe, K.K., Lebon, G.T., and Rivizzigno, P., 2001. An off-axis hydrothermal vent field near the Mid-Atlantic Ridge at 30°N. *Nature (London, U. K.),* 412(6843):145–149.

Lagabrielle, Y., Bideau, D., Cannat, M., Karson, J.A., and Mével, C., 1998. Ultramafic-mafic plutonic rock suites exposed along the Mid-Atlantic Ridge (10°N–30°N). Symmetrical-assumetrical distribution and implications for seafloor spreading processes. *In* Buck, W.R., Delaney, P.T., Karson, J.A., and Labagrielle, Y. (Eds.), *Faulting and Magmatism and Mid-Ocean Ridges*. Monogr., Am. Geophys. Union, 106:153–176.

Lavier, L., Buck, W.R., and Poliakov, A.N.B., 1999. Self-consistent rolling-hinge model for the evolution of large-offset low-angle normal faults. *Geology,* 27:1127–1130.

Le Maitre, R.W., Bateman, P., Dudek, A., Keller, J., Lameyre Le Bas, M.J., Sabine, P.A., Schmid, R., Sorensen, H., Streckeisen, A., Woolley, A.R., and Zanettin, B., 1989. *Classification of Igneous Rocks and Glossary of Terms:* Oxford (Blackwell).

MacLeod, C.J., Escartin, J., Banerji, D., Banks, G.J., Gleeson, M., Irving, D.H.B., Lilly, R.M., McCaig, A.M., Niu, Y., Allerton, S., and Smith, D.K., 2002. Direct geological evidence for oceanic detachment faulting: the Mid-Atlantic Ridge, 15°45′ N. *Geology,* 30:10:879–882.

Melson, W.G., Rabinowitz, P.D., et al., 1979. *Init. Repts. DSDP,* 45: Washington (U.S. Govt. Printing Office).

Nooner, S.L., Sasagawa, G.S., Blackman, D.K., and Zumberge, M.A., 2003. Constraints on crustal structure at the Mid-Atlantic Ridge from seafloor gravity measurements made at the Atlantis Massif. *Geophys. Res. Lett.,* 30:1446.

O'Hanley, D.S., 1996. Serpentinites: records of tectonic and petrological history. *Oxford Monogr. Geol. Geophys.,* Vol. 34.

Pettigrew, T.L., Casey, J.F., Miller, D.J., et al., 1999. *Proc. ODP, Init. Repts.,* 179: College Station, TX (Ocean Drilling Program).

Robinson, P.T., Von Herzen, R., et al., 1989. *Proc. ODP, Init. Repts.,* 118: College Station, TX (Ocean Drilling Program).

Schroeder, T., and John, B.E., 2004. Strain localization on an oceanic detachment fault system, Atlantis Massif, 30°N, Mid-Atlantic Ridge. *Geochem., Geophys., Geosyst.,* 5:10.1029/2004GC000728.

Schroeder, T., John, B.E., Kelley, D., and MARVEL cruise participants, 2001. Microstructural observations of an 'oceanic core complex': Atlantis Massif, 30°N Mid-Atlantic Ridge, *Eos, Trans. Am. Geophys. Union,* 82:F1100.

Shipboard Scientific Party, 2005. Oceanic core complex formation, Atlantis Massif—oceanic core complex formation, Atlantis Massif, Mid-Atlantic Ridge: drilling into the footwall and hanging wall of a tectonic exposure of deep, young oceanic lithosphere to study deformation, alteration, and melt generation. *IODP Prel. Rept.,* 304. http://iodp.tamu.edu/publications/PR/304PR/304PR.PDF.

Spencer, J.E., 1985. Miocene low-angle normal faulting and dike emplacement, Homer Mountain and surrounding areas, southeastern California and southernmost Nevada. Geol. Soc. Am. Bull., 96:110–1155.

Tucholke, B.E., Lin, J., and Kleinrock, M.C., 1998. Megamullions and mullion structure defining oceanic metamorphic core complexes on the Mid-Atlantic Ridge. *J. Geophys. Res.,* 103:9857–9866.

Vening Meinesz, F.A., 1950. Les graben africains resultant de compression oe de tension dans la croute terrestres? *Kol. Inst. Bull.,* 21:539–552.

Wernicke, B.P., and Axen, G.J., 1988. On the role of isostasy in the evolution of normal fault systems. *Geology,* 16:848–451.

Table T1. Operations summary table for Site U1309 (30°10.1195′ N, 42°07.1131′ W; 1656.0 mbrf), Expedition 305.

Hole penetration	Number of cores	Interval cored (m)	Core recovered (m)	Recovery (%)	Drilled/ washed (m)	Total penetration (m)	Time on hole (h)	Time on hole (days)
U1309D-1	29	133.70	106.97	80.01	0.00	133.70	95.00	4.0
U1309D-2	23	110.40	91.77	83.13	0.00	110.40	80.50	3.4
U1309D-3	23	110.40	81.55	73.87	0.00	110.40	84.50	3.5
U1309D-4	18	81.60	71.10	87.13	0.00	81.60	83.00	3.5
Log bit			******Logging******				62.25	2.6
U1309D-5	17	81.60	69.75	85.48	0.00	81.60	79.75	3.3
U1309D-6	19	81.80	77.08	94.23	0.00	81.80	81.25	3.4
U1309D-7	21	100.80	88.60	87.90	0.00	100.80	82.50	3.4
U1309D-8	26	123.90	83.55	67.43	0.00	123.90	92.25	3.8
U1309D-9	21	100.80	62.00	61.51	0.00	100.80	90.00	3.8
U1309D-10	22	89.20	67.28	75.43	0.00	89.20	83.75	3.5
Log bit			******Logging******				55.50	2.3
Site U1309 totals:	219	1014.20	799.65	78.85	0.00	1014.20	970.25	40.4
Expedition 305 totals:	219	1014.20	799.65	78.85	0.00	1014.20	970.25	40.4

Figure F1. Tectonic and morphologic setting of Atlantis Massif. Bathymetric contours illustrate the deep median valley of the Mid-Atlantic Ridge and its intersection with the Atlantis transform fault. The shallow dome composing the core of Atlantis Massif has two structural components: the central dome, where IODP footwall drilling was focused, and the southern ridge.

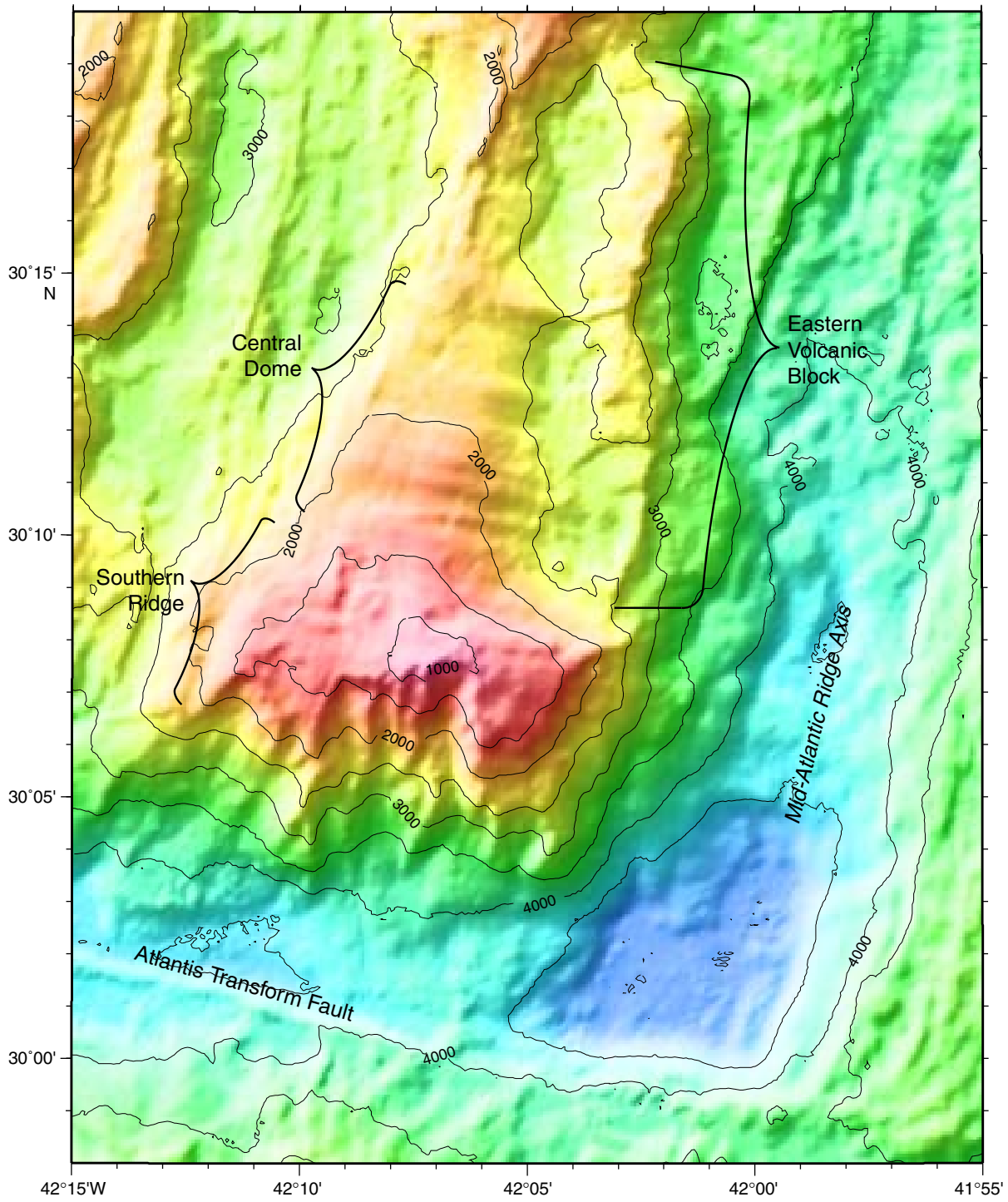

Figure F2. Basemap of Atlantis Massif showing prior geological and geophysical data coverage and the location of Integrated Ocean Drilling Program (IODP) drill sites (circles). Bathymetry is contoured at 20 m intervals, based on a 100 m grid. Seismic reflection and refraction lines and seafloor mapping/sampling sites are shown. Spreading-parallel multichannel seismic (MCS) Line Meg-9 follows the Southern Ridge; Meg-10 crosses the central dome. Line Meg-5 crosses the southeast shoulder of the massif and then subparallels the trend of the adjacent volcanic block. The corrugated detachment surface capping the central dome is inferred to extend beneath this eastern block, thereby making the upper crustal volcanics a hanging wall to the fault. OBH = ocean bottom hydrophone.

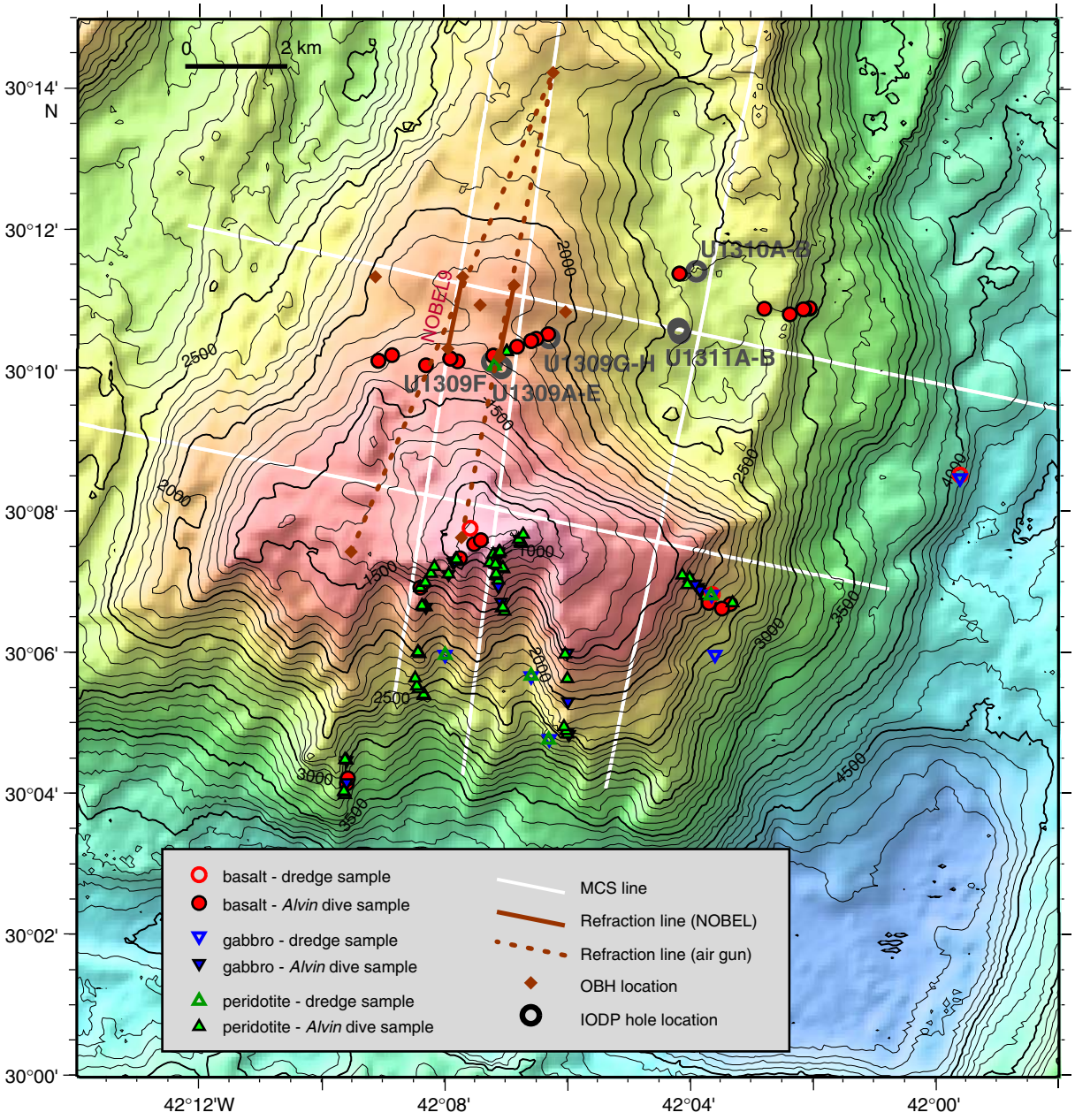

Figure F3. Seismic profiles indicate subsurface structure of the central dome of Atlantis Massif. **A.** Deep source refraction (Line NOBEL9; Fig. F2) recorded by an ocean bottom hydrophone shows arrivals from a high velocity body (8 km/s, assuming plane-layered structure) at very short range. **B.** Velocity gradient determined from refraction analysis at Atlantis Massif (from Collins et al., 2001) is similar to that determined near ODP Site 920, where serpentinized peridotite was recovered. The gradient near Hole 735B, where only gabbro has been recovered, is not as great. **C.** A portion of multichannel seismic (MCS) Line Meg-10 across the Central Dome. CMP = common midpoint. **D.** MCS Line Meg-4, along the strike of Atlantis Massif. MCS data were collected by the *Ewing* (EW-0102) in 2001 using a 10 gun array with 3100 in^3 (51 L) capacity. Shot spacing was 37.5 m. Canales et al. (2004) processed the data by common midpoint (CMP) gathers, deconvolution, normal moveout correction, dip moveout correction, and stacking. In addition, the record section in D has been time migrated. The reflector labeled "D" is recognized by Canales et al. (2004) below much of the domal surface. SWIR = Southwest Indian Ridge, MARK = Kane Fracture Zone.

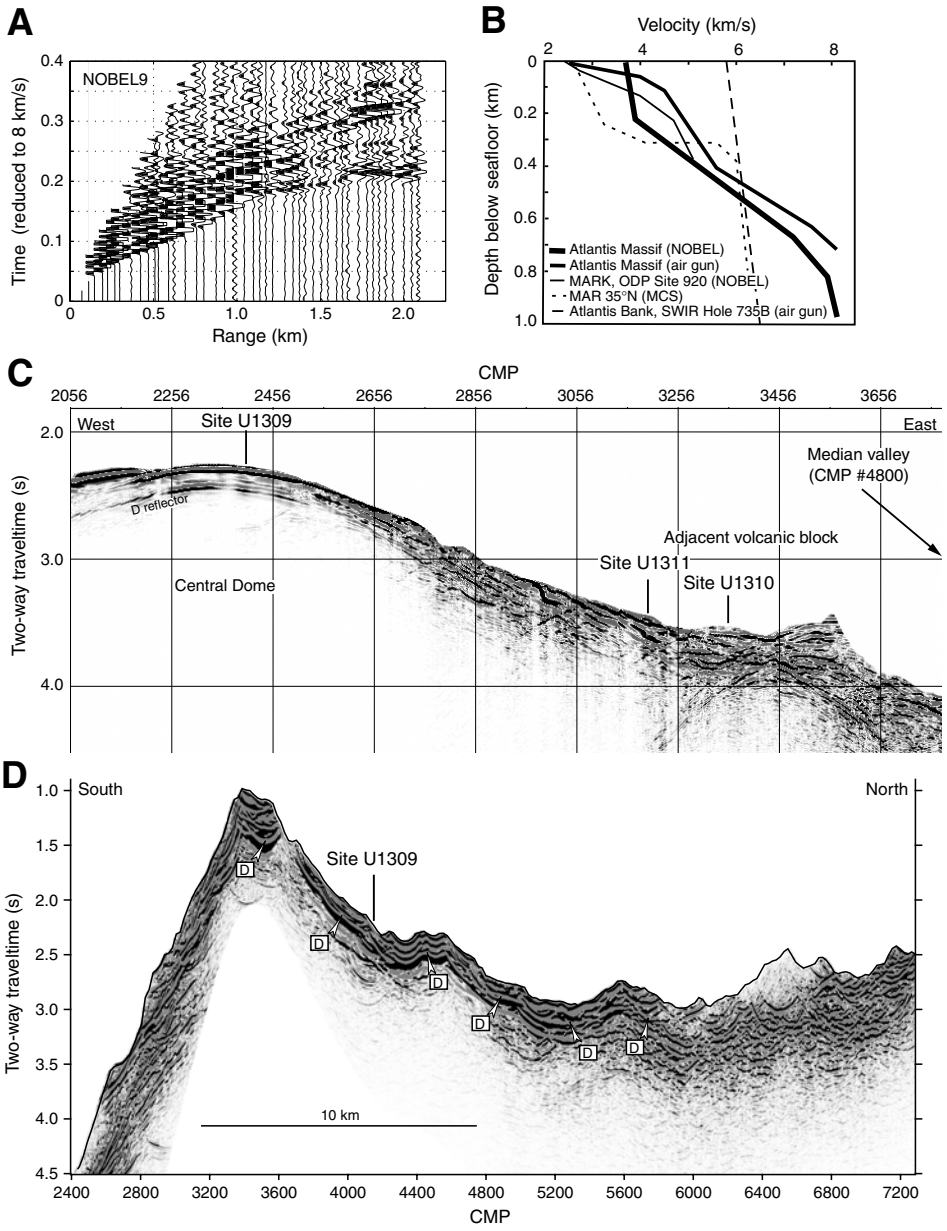

Figure F4. Bouguer gravity anomaly map at the ridge/transform intersection (30º MAR). Contribution of seafloor topography has been removed from the free-air anomaly, assuming a density contrast between seawater and ocean crust of 1700 kg/m³. Trackline data from EW0102 and EW9212 have been added to the compilation presented in Blackman et al. (1998). Anomalously high densities occur within Atlantis Massif. Lower than average density (thicker crust?) characterizes the outside corner region near the Fracture Zone. Broader scale thermal contribution of subaxial upwelling (gravity low in northern portion of rift valley) and plate cooling have not been removed.

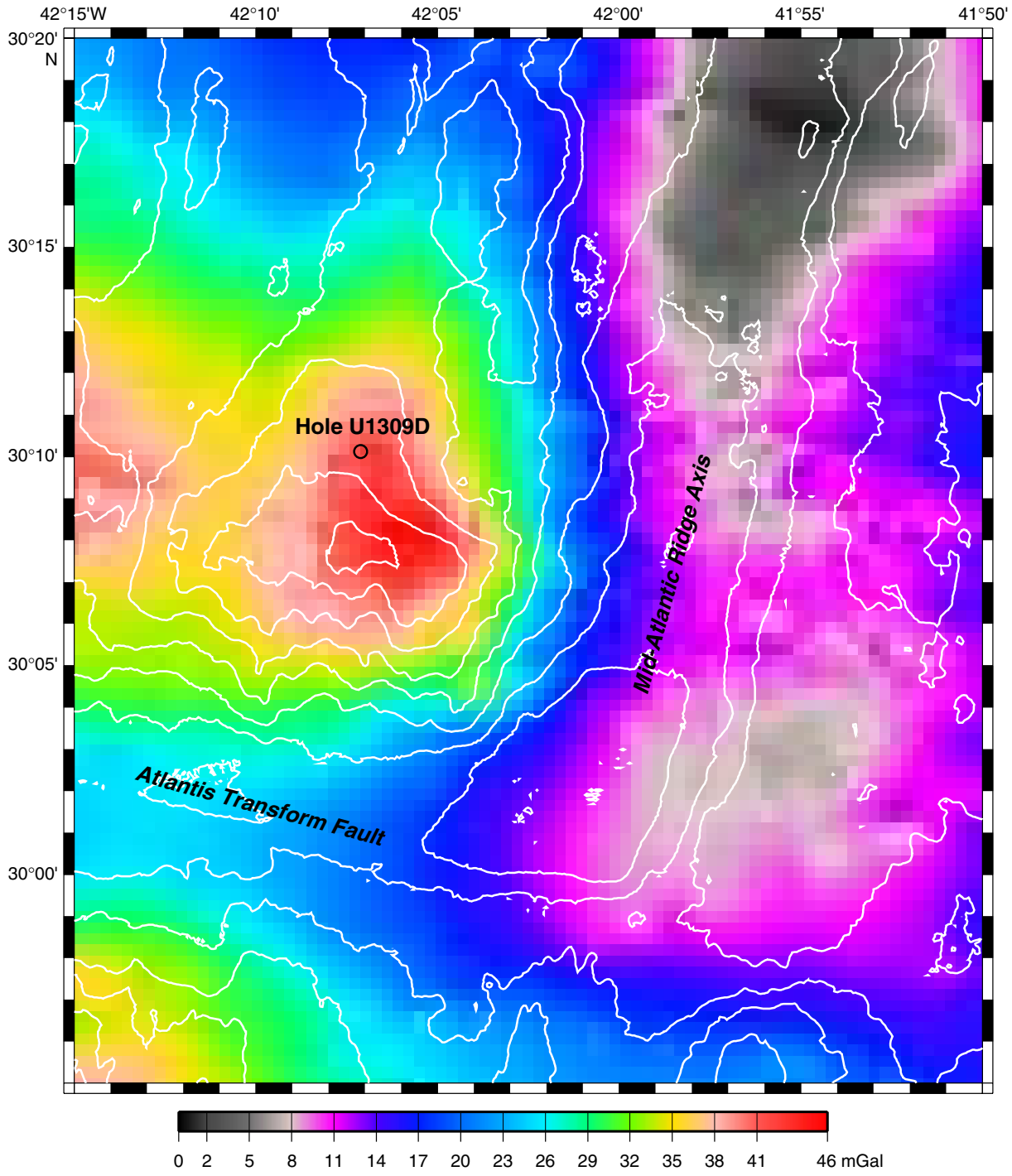

Figure F5. All holes (recovery > 5%) in upper mantle and lower crustal rocks drilled to date at or near mid-ocean ridges during nine different Ocean Drilling Program (ODP) legs and Integrated Ocean Drilling Program (IODP) expeditions. ODP Leg 147 (Gillis, Mével, Allan, et al., 1993) is the only one which took place in crust created at a fast-spreading ridge (Hess Deep, East Pacific Rise).

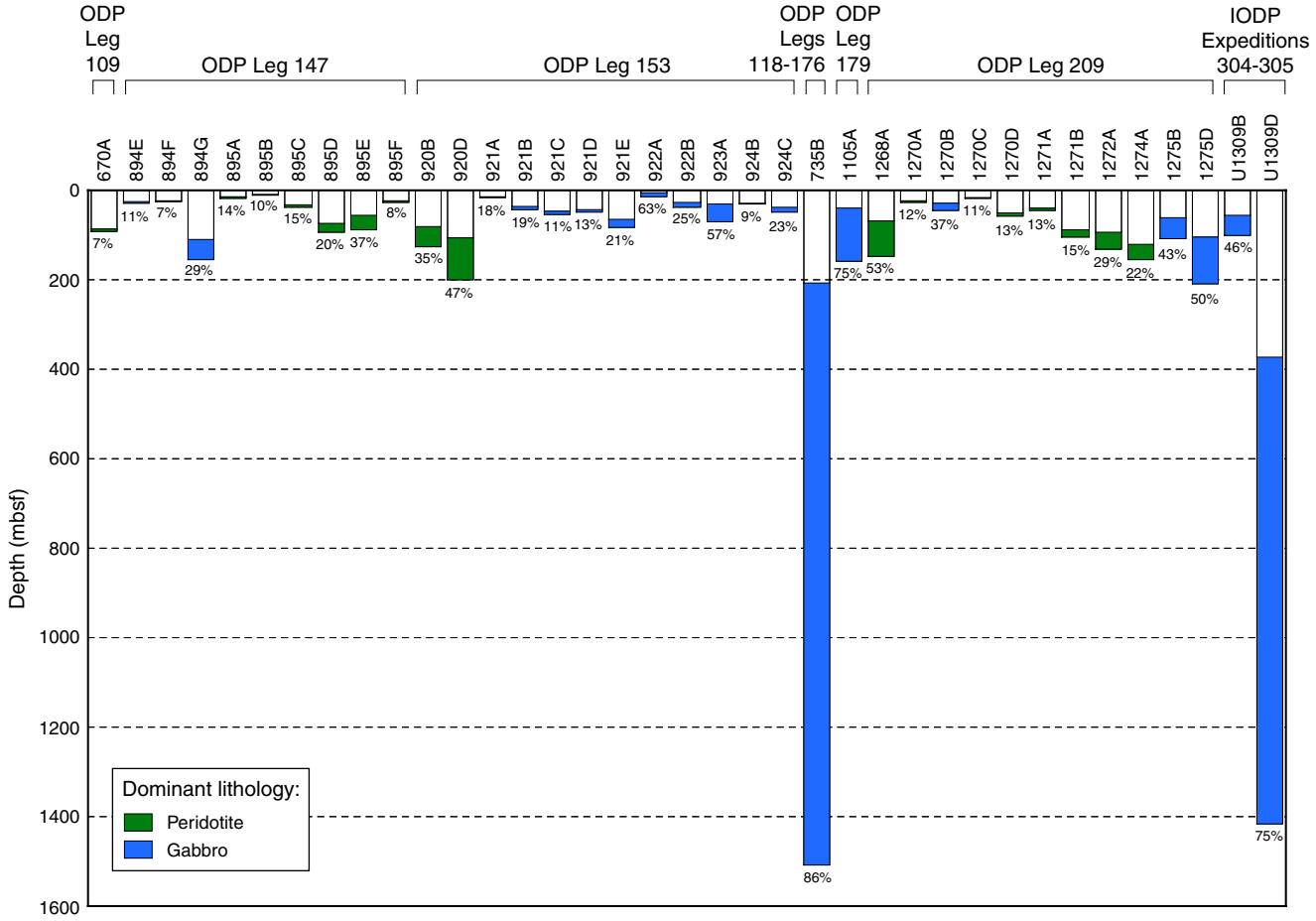

Figure F6. Geochemical composition of previously drilled gabbros and peridotites at slow-spreading ridges (note that, except for the Site 1275 troctolitic rocks, most primitive gabbroic rocks drilled so far have Mg# ~84, and there is a compositional gap between peridotitic Mg# and the gabbroic Mg#).

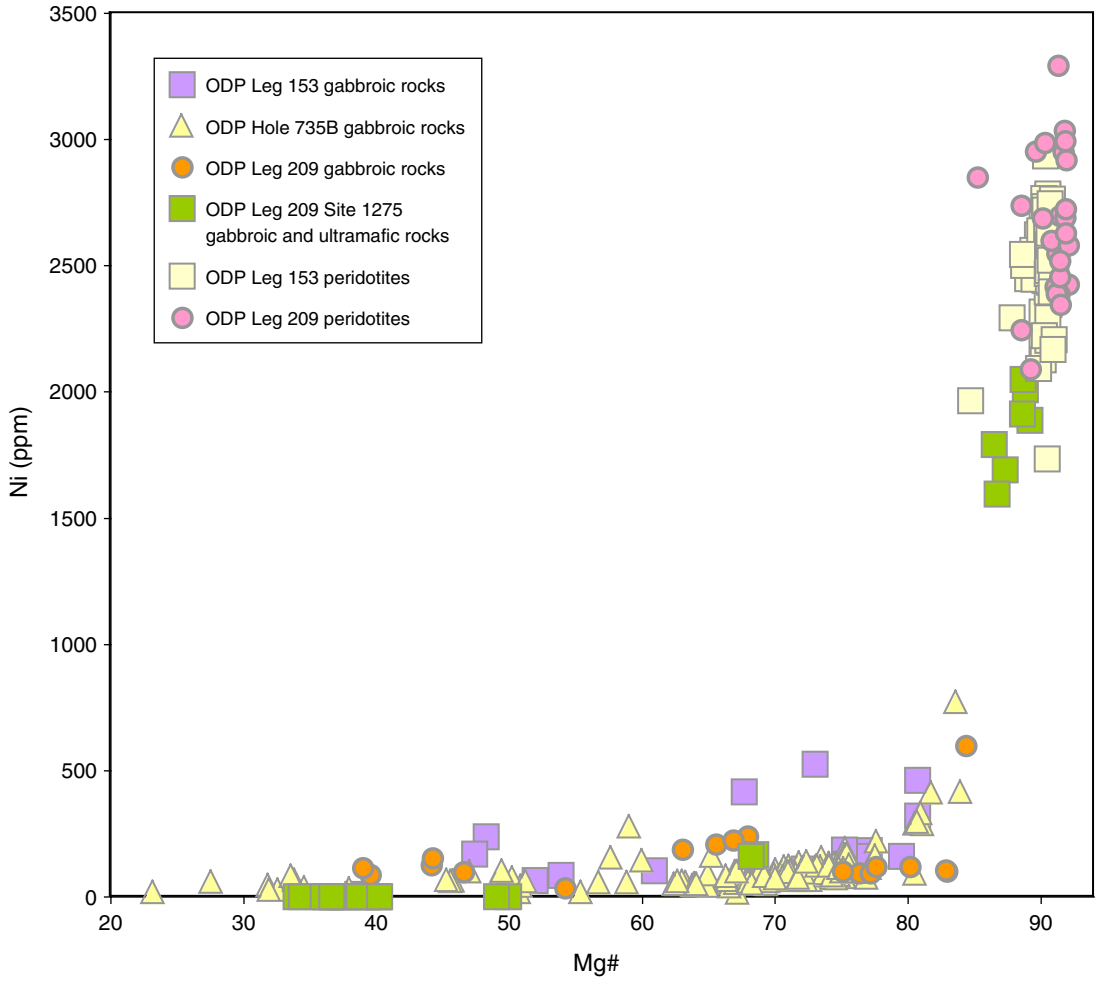

Figure F7. Pie charts of lithology proportions for (**A**) interval 0–401.3 mbsf, Cores 305-U1309D-1R through 78R, from Expedition 304; (**B**) interval 401.3–1415.5 mbsf and Cores 305-U1309D-80R through 295R from Expedition 305; and (**C**) Hole U1309D. Each number refers to the lithologic proportions in percent.

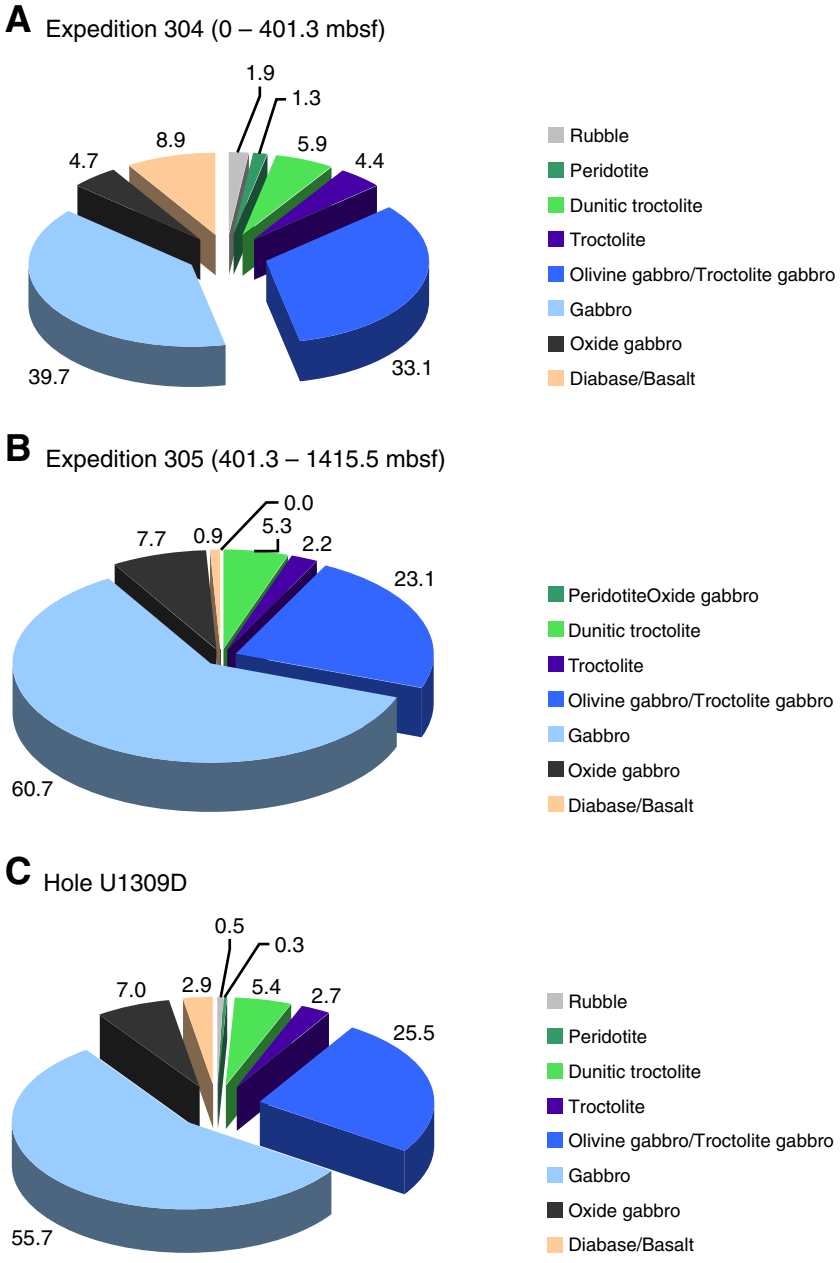

Figure F8. Stratigraphic distribution of lithologic proportions of cores recovered from Hole U1309D, including Expedition 304 data. **A.** 20 m running average of lithologic proportions (white = no recovery). **B.** Each bar represents the percentages of each lithology per core. (Continued on next page.)

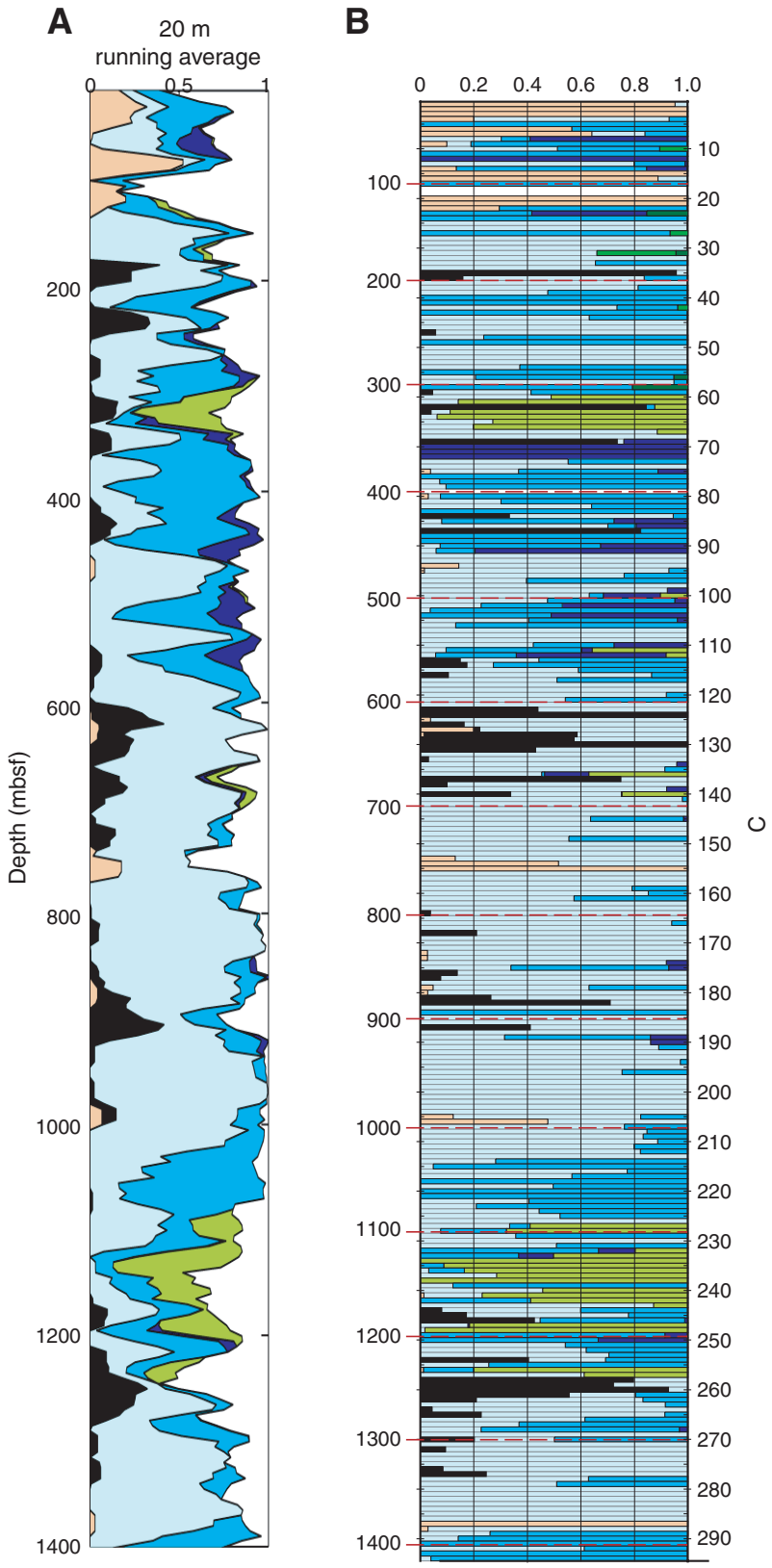

Figure F8 (continued). C. Detailed recovery and lithology summary.

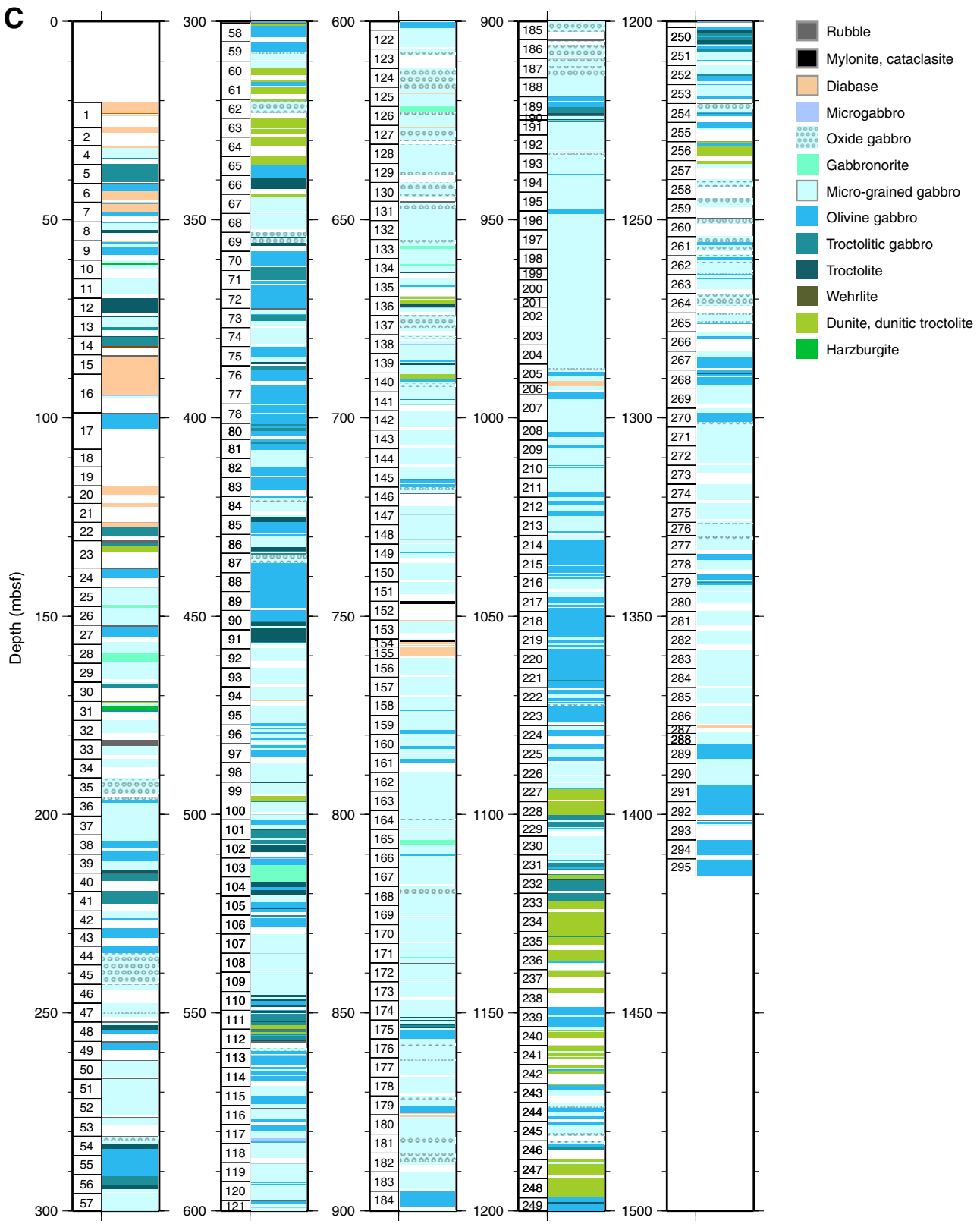

Figure F9. Contact between olivine gabbro and troctolite (interval 305-U1309D-251R-1, 44–65 cm).

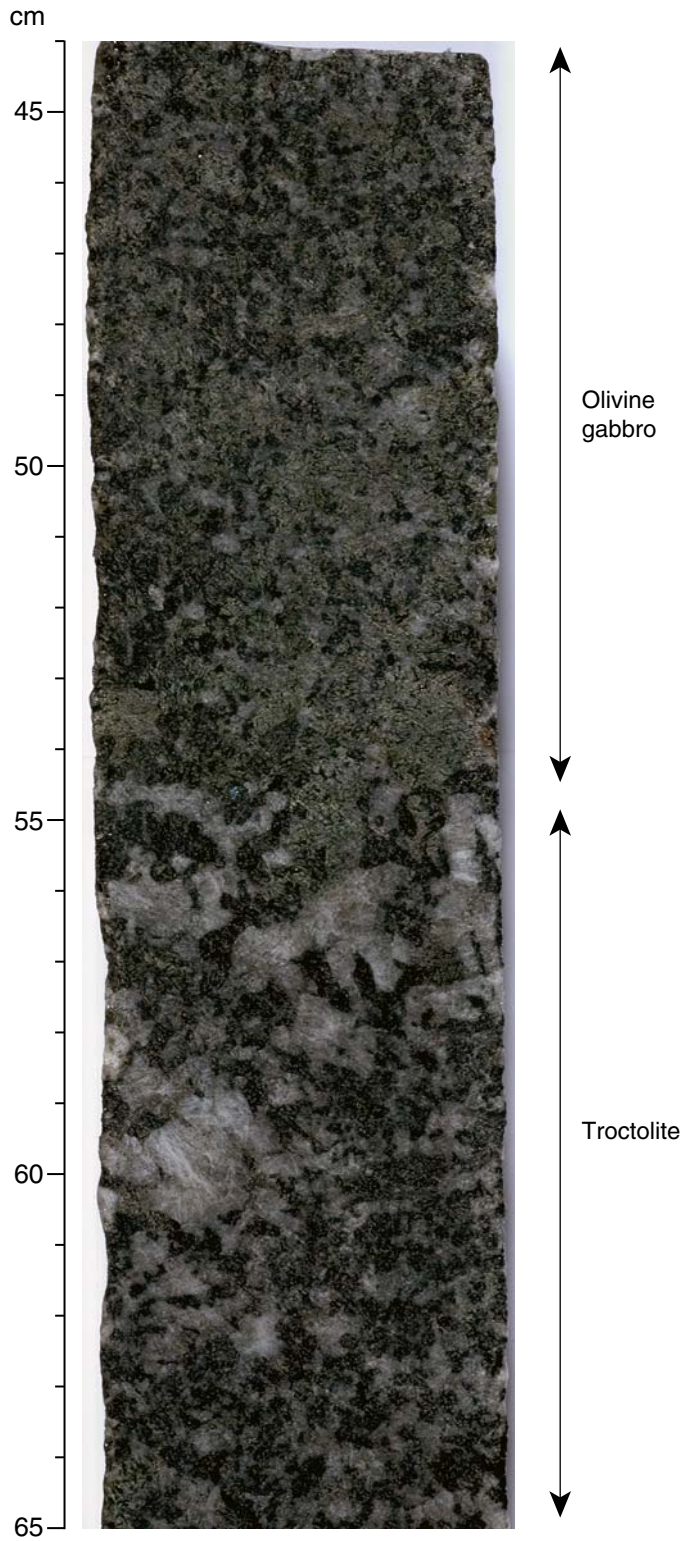

Figure F10. Mode of occurrences of dunitic troctolite in interval 305-U1309D-227R-2, 32 cm, to 228R-4, 58 cm. **A.** Interval 305-U1309D-227R-2, 22–45 cm. **B.** Interval 305-U1309D-248R-2, 0–26 cm.

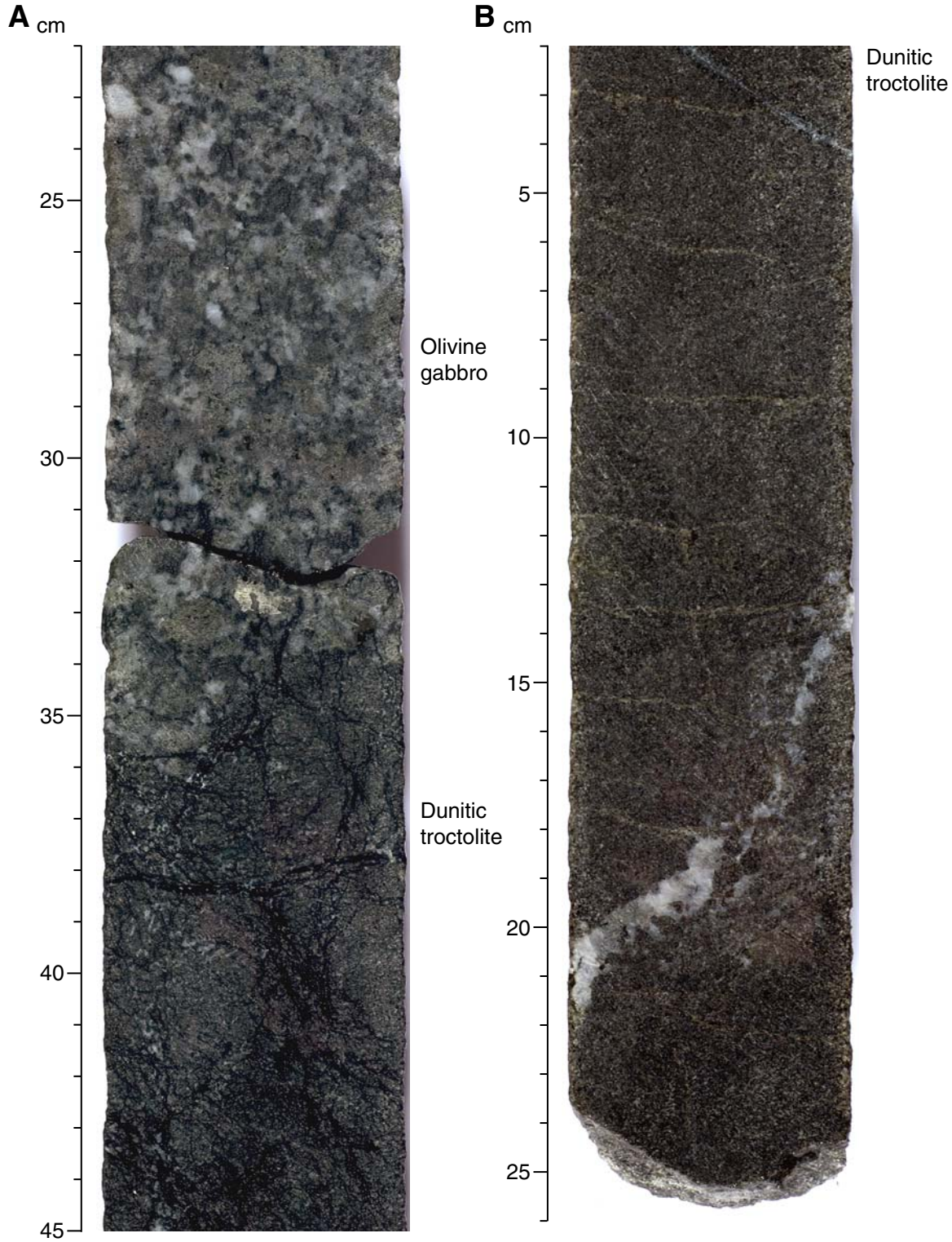

Figure F11. A–D. Photomicrographs in cross-polarized light (field of view = 22 mm); (A) plagioclase-bearing websterite (Sample 305-U1309D-100R-1, 10–13 cm), (B) dunitic troctolite (Sample 305-U1309D-227R-3, 70–72 cm), (C) dunitic troctolite (Sample 305-U1309D-248R-2, 7–9 cm), (D) dunite (Sample 305-U1309D-248R-2, 96–99 cm). **E, F.** Close-up of fresh olivine and plagioclase in a dunitic troctolite (Sample 305-U1309D-248R-2, 7–9 cm) (cross-polarized light; field of view = 11 mm).

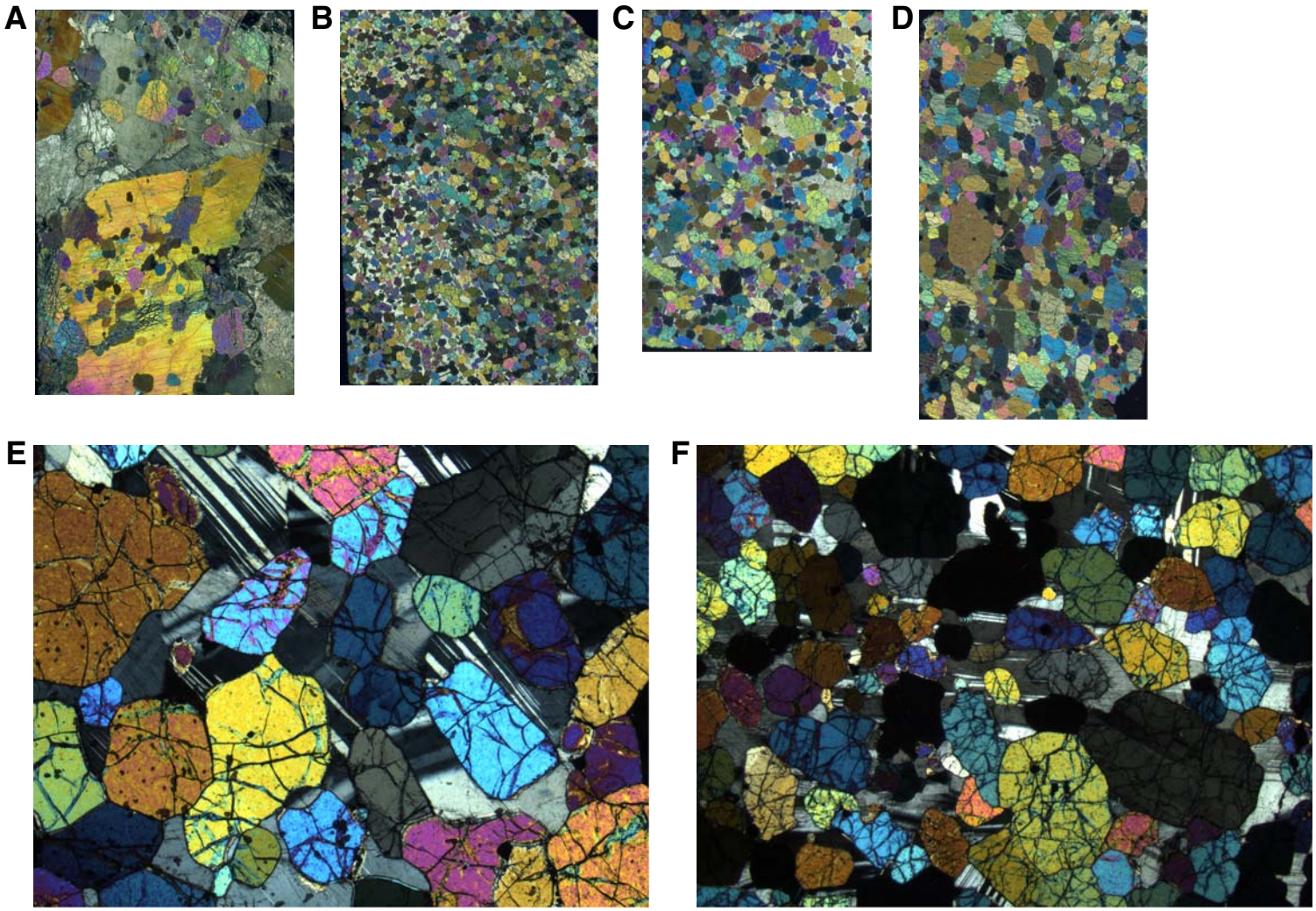

Figure F12. Oxide-rich shear zone (Sample 305-1309D-183R-2, 32–34 cm) (field of view = 25 × 35 mm). **A.** Plane-polarized light. **B.** Cross-polarized light.

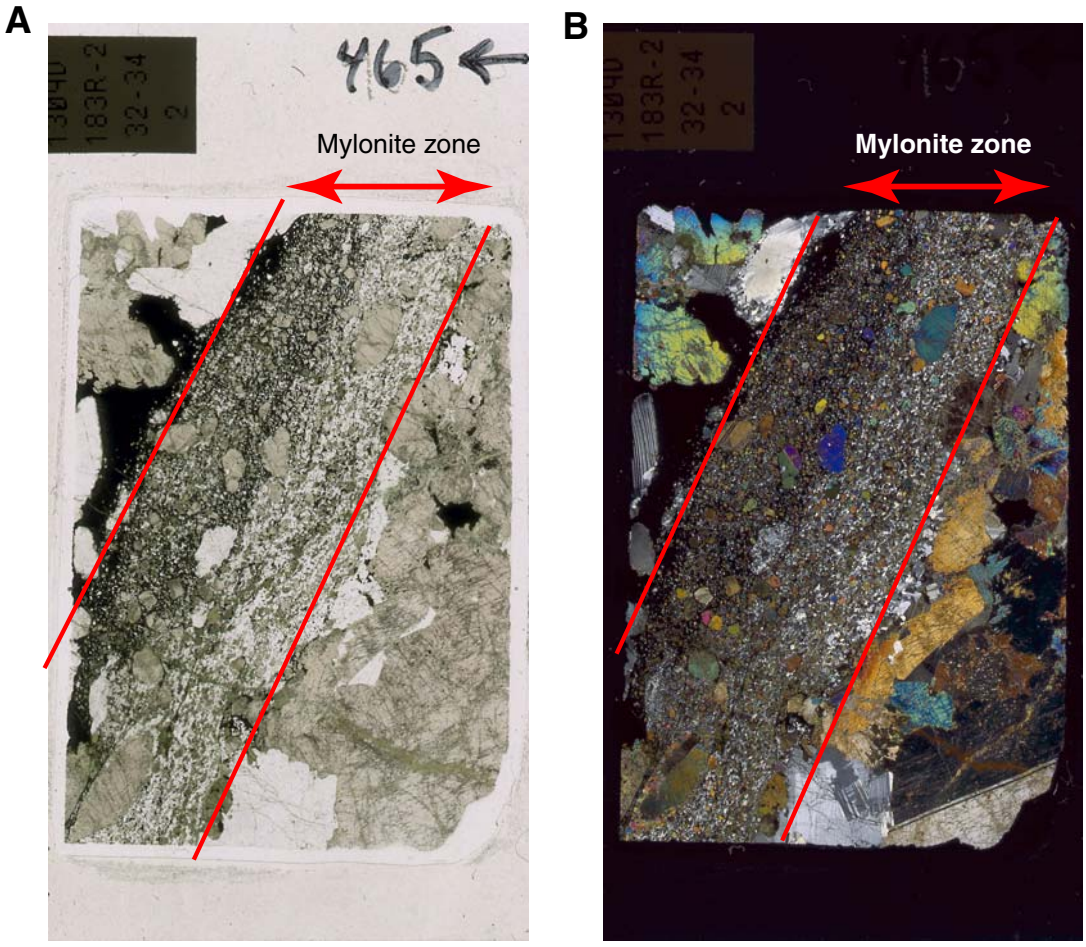

Figure F13. Ni (ppm) versus Mg# (molar Mg/Mg+Fe) for gabbros, olivine gabbros, troctolites, orthopyroxene-bearing gabbros, oxide-oxide gabbros, ultramafic rocks, and peridotites from Site U1309. Shaded fields represent data from ODP Leg 153 (peridotite and gabbro = upper and lower purple shaded fields, respectively), ODP Leg 209 (peridotite and gabbro = upper and lower yellow shaded fields, respectively), and Hole 735B (green shaded field).

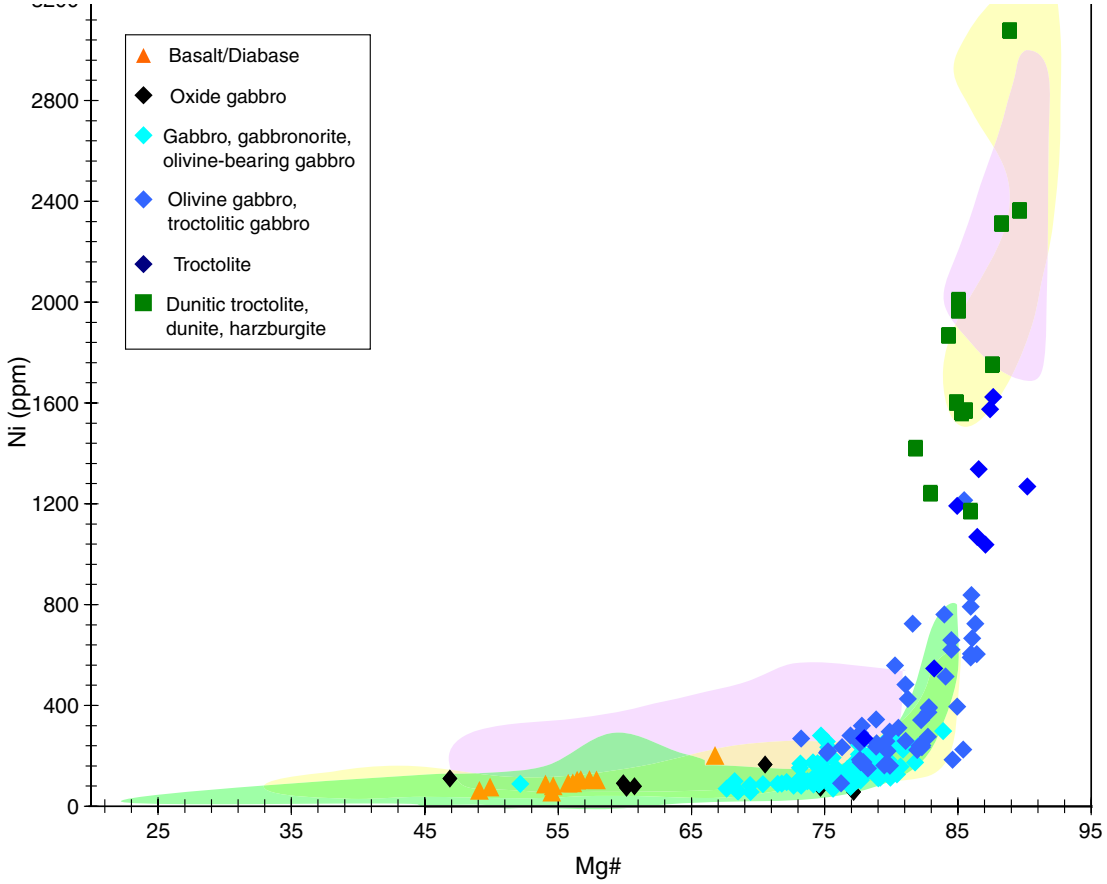

Figure F14. Downhole variations in Mg# for diabase, gabbro, and troctolitic rocks from Hole U1309D. Dashed lines = fault zones (see **"Structural Relationships"**).

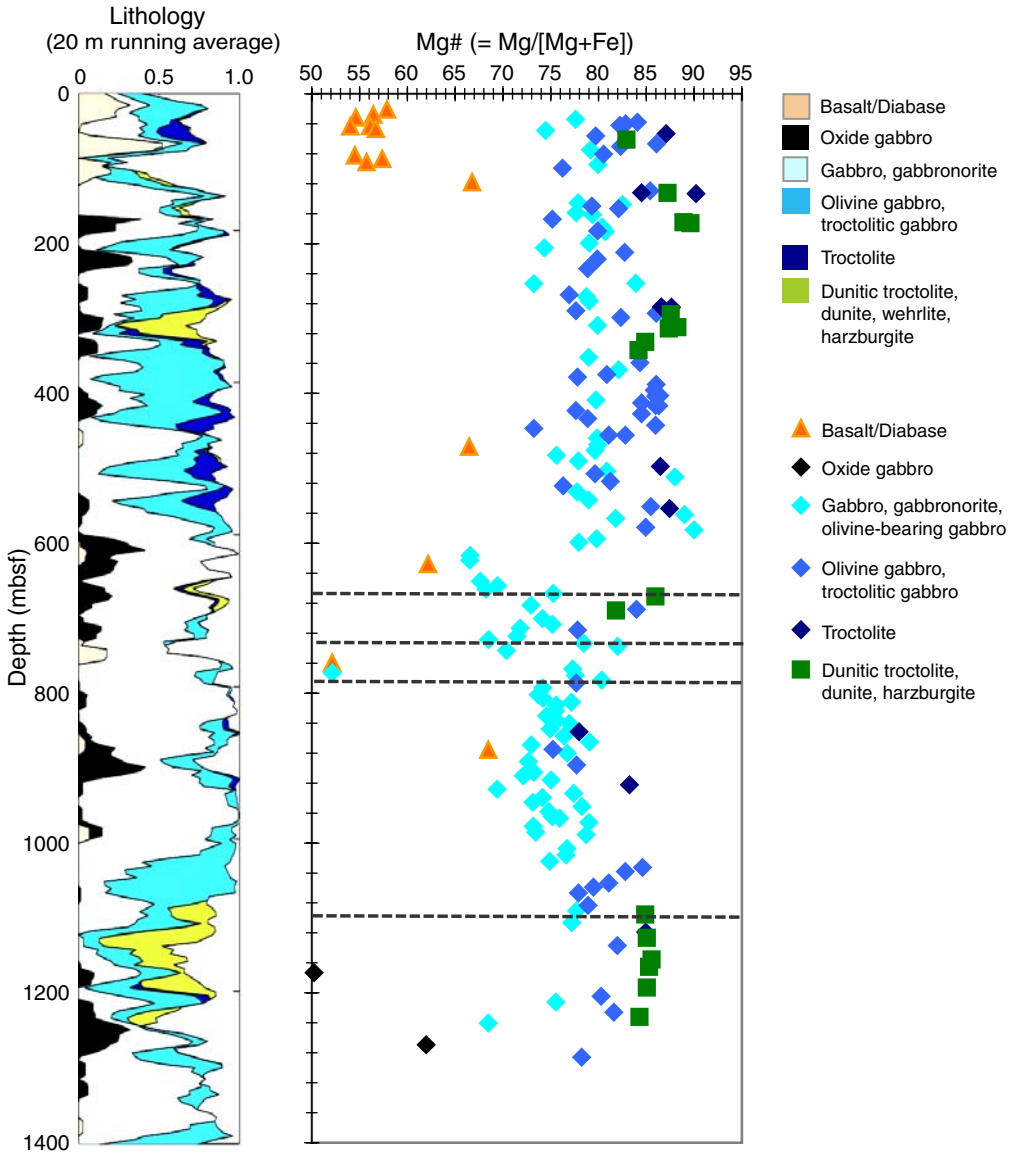

Figure F15. Total alkalis, $Na_2O + K_2O$ versus SiO_2 (after Le Maitre et al., 1989). Data are plotted on a volatile-free basis for basalts, diabases, and basalt breccia from Hole U1309B and basalts and diabases from Hole U1309D. A compilation of the compositions of Mid-Atlantic Ridge glasses (open diamonds) downloaded from PetDB in December 2004 (online at **beta.www.petdb.org**) is shown for comparison. The continuous line represents the alkalic-tholeiitic boundary of Irvine and Baragar (1971). Ol = olivine.

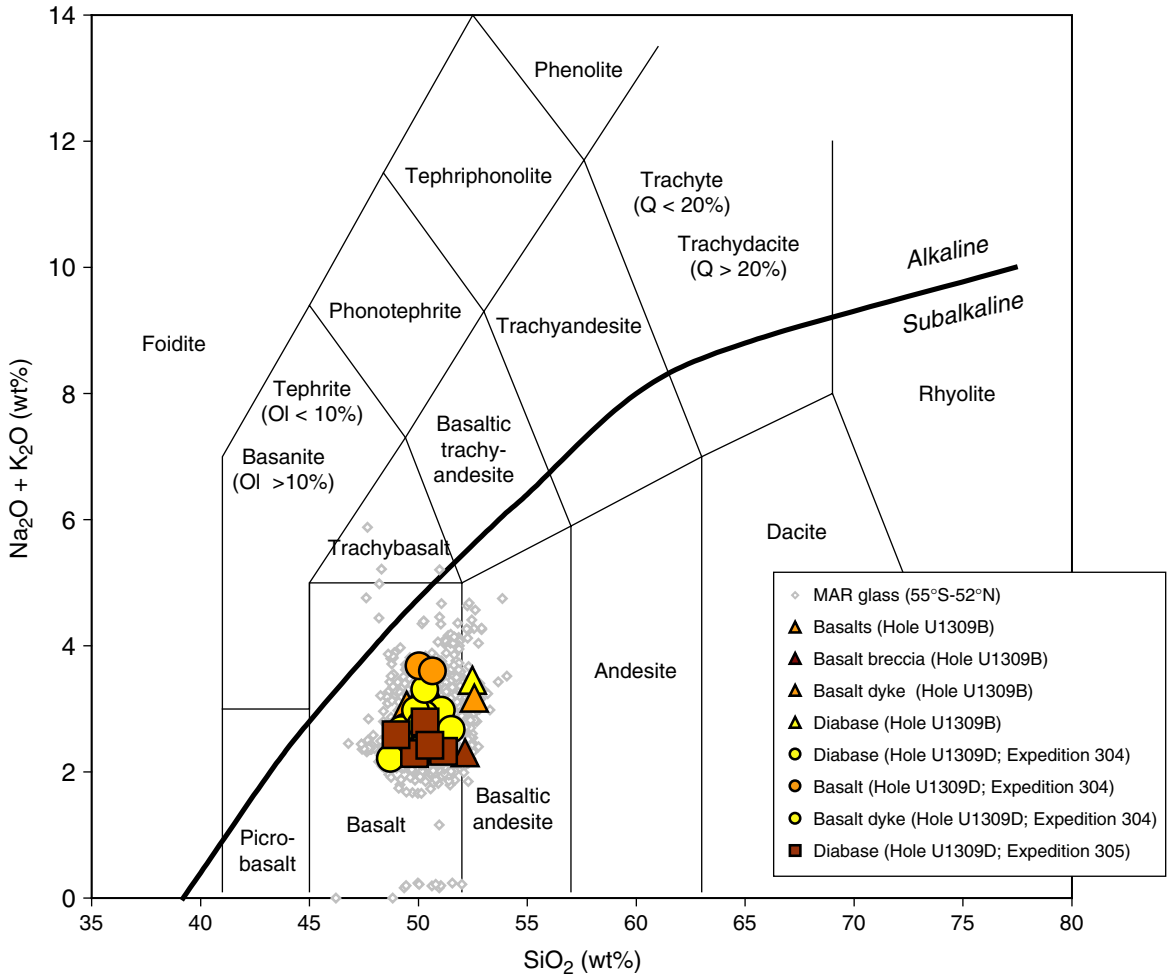

Figure F16. Proportions of the different ranges of alteration (**A**) for each lithology in meters recovered and (**B**) recalculated to 100%.

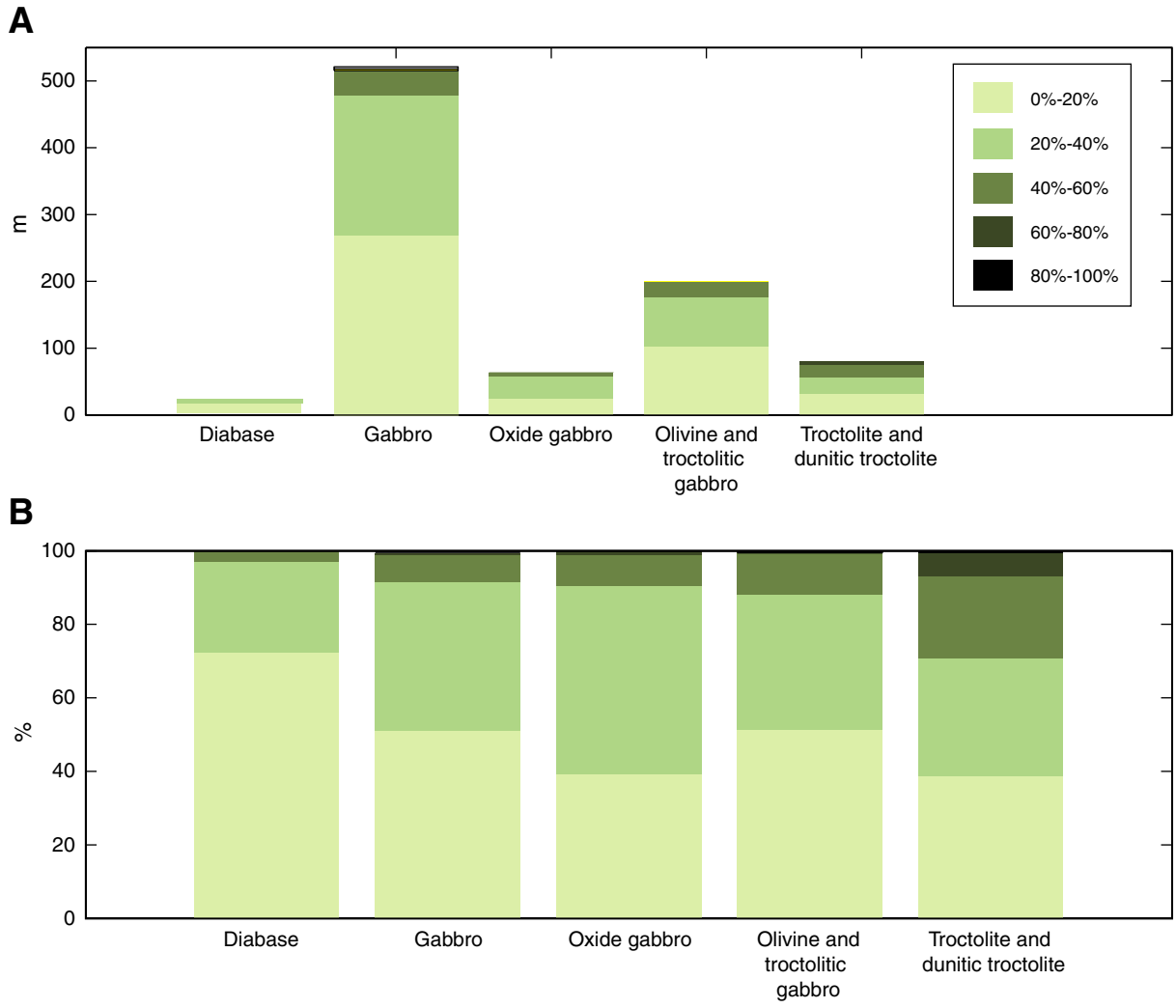

Figure F17. Plot of downhole alteration percent compared with the lithostratographic column.

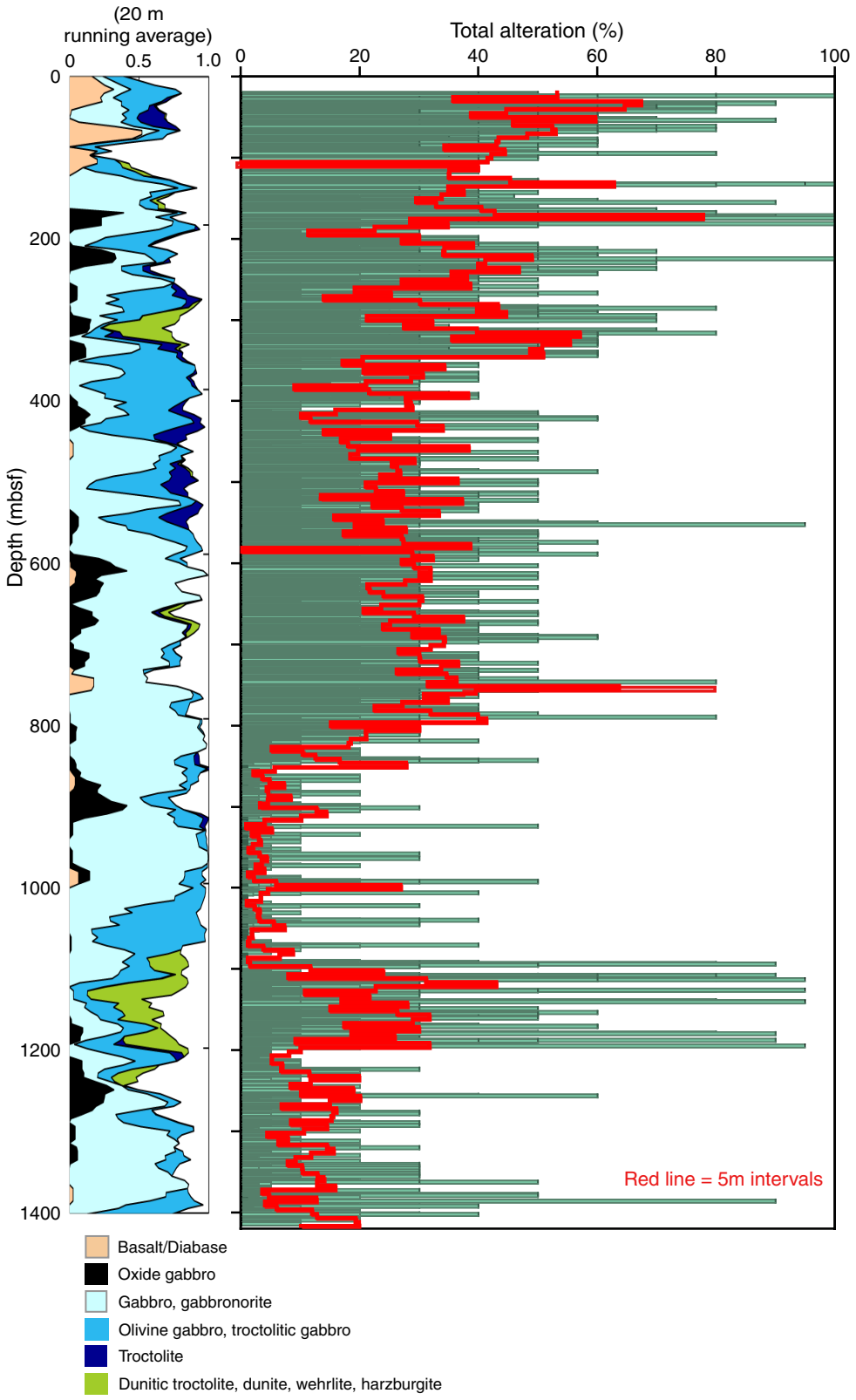

Figure F18. Serpentinized olivine with kernel texture (Sample 305-U1309-80R-1; 39–41 cm) (field of view = 5.5 mm).

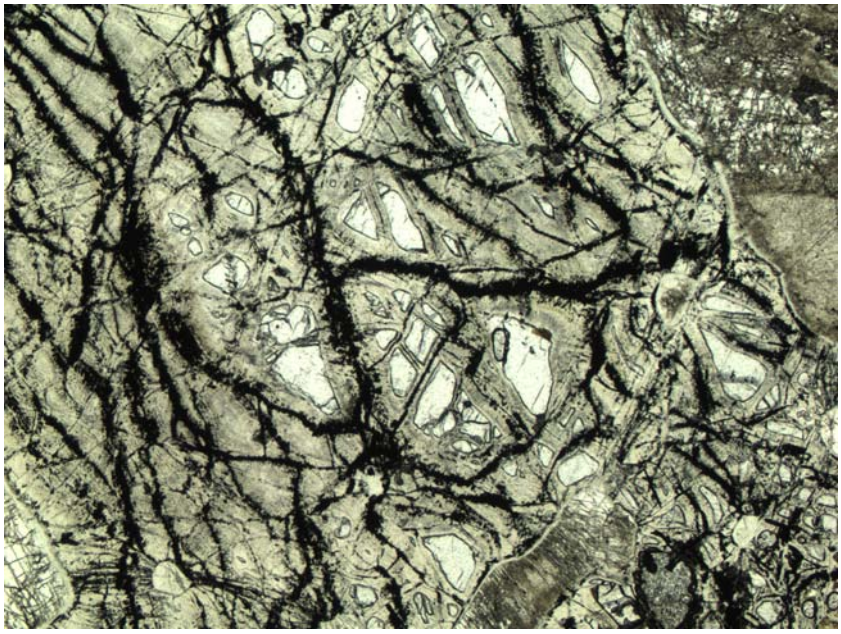

Figure F19. Serpentine foliation (interval 305-U1309D-235R-2, 98–113 cm).

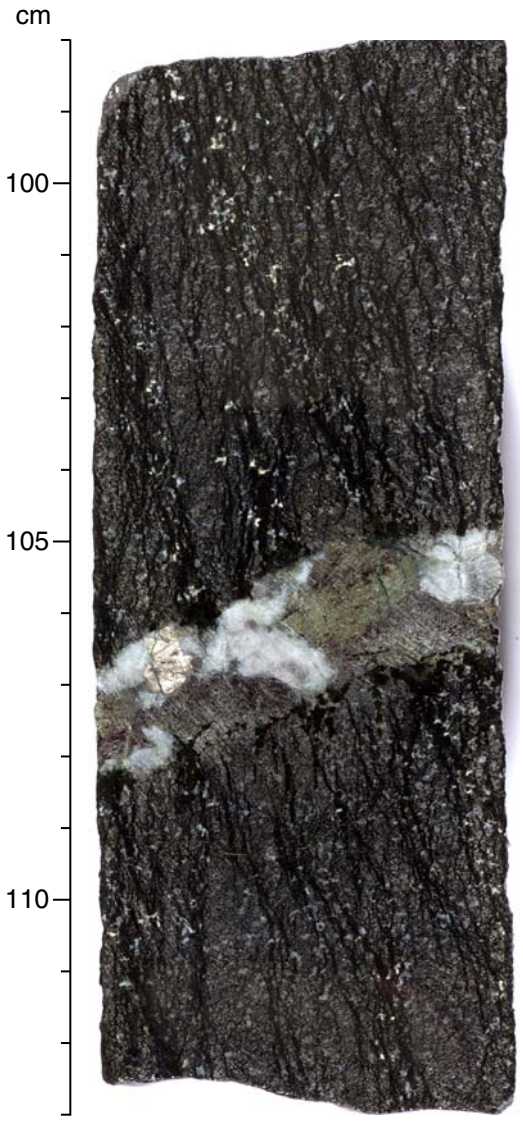

Figure F20. Serpentine vein with dusty magnetite in olivine (Sample 305-U1309-236R-2, 10–13 cm) (field of view = 700 µm).

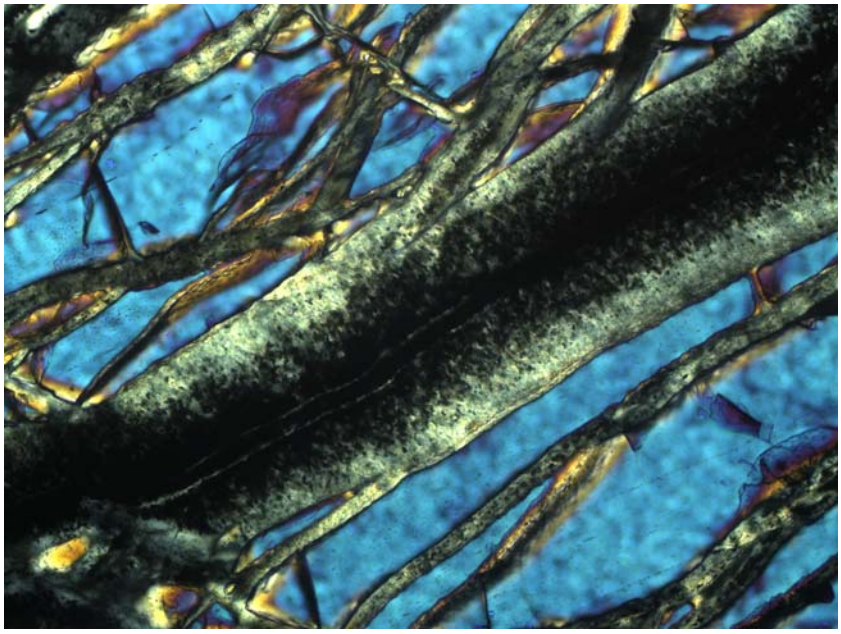

Figure F21. A. Metamorphic expansion microfractures in plagioclase adjacent to serpentinized olivine (Sample 305-U1309D-82R-2, 110–112 cm) (field of view [FOV] = 5.5 mm). **B.** Serpentinization-induced microfracturing (Sample 305-U1309D-232R-1, 102–105 cm) (FOV = 5.5 mm).

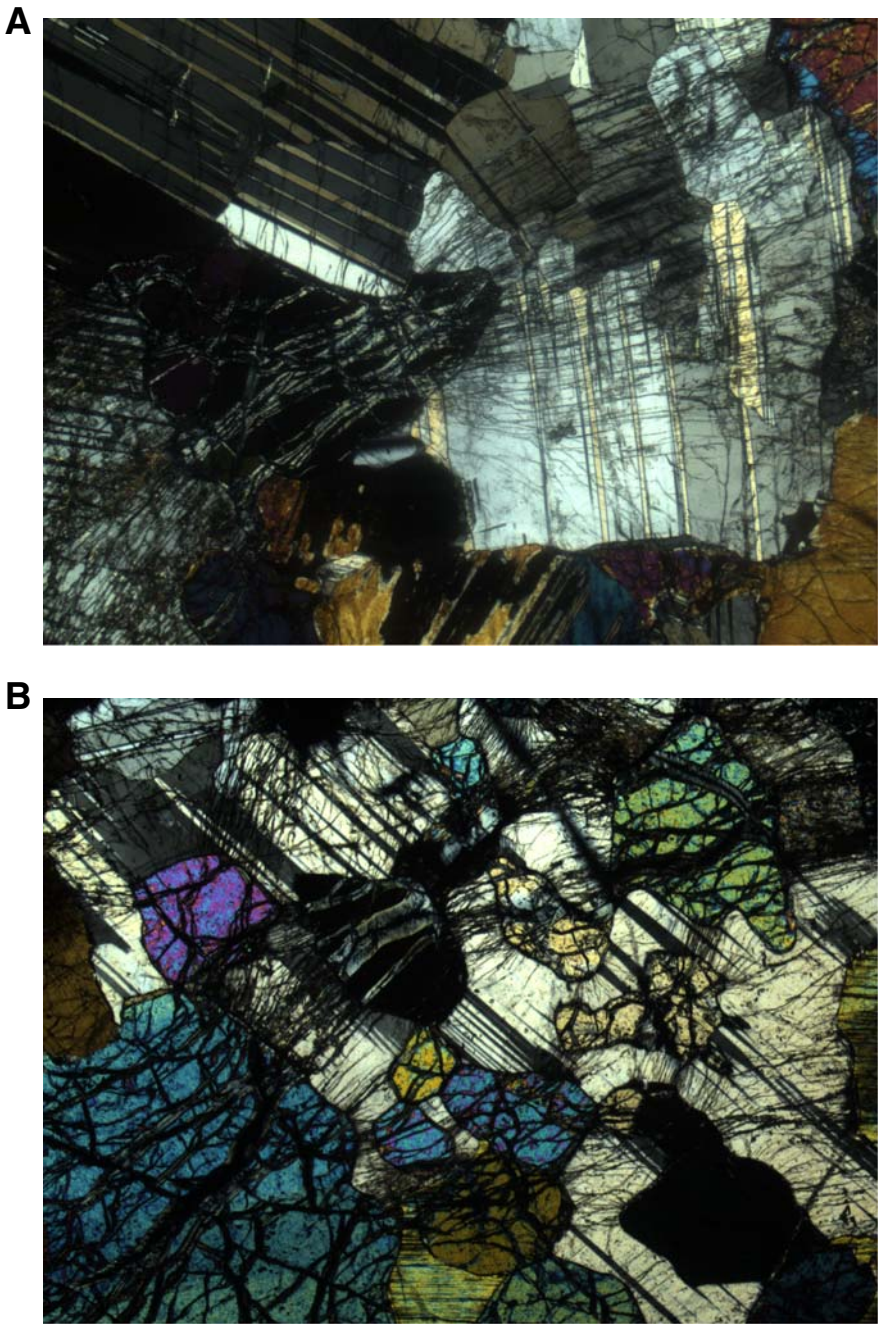

Figure F22. Corona texture in olivine gabbro (interval 305-U1309D-86R-3, 93–105 cm).

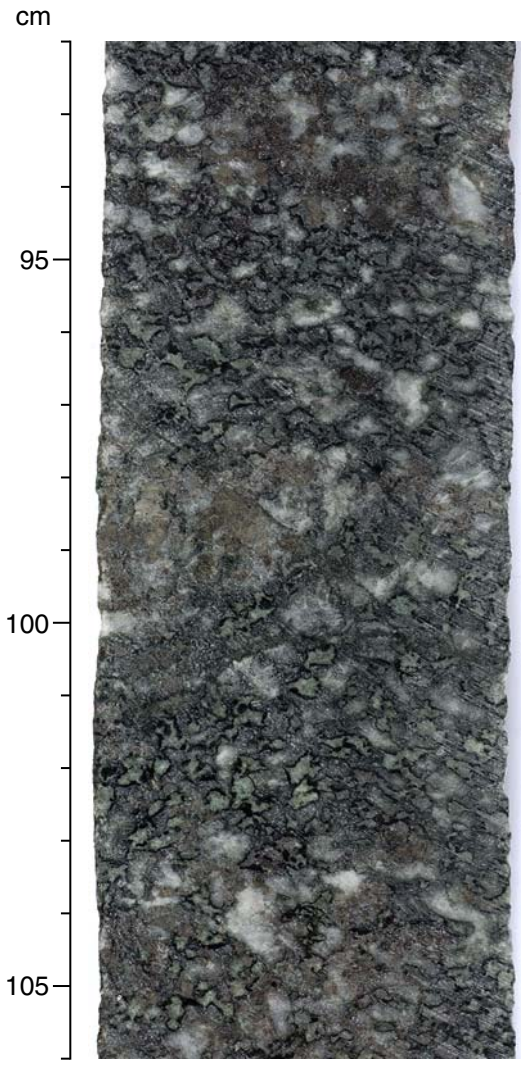

Figure F23. Corona texture in olivine gabbro consisting of talc, tremolite, and oxides after olivine and chlorite after plagioclase where the two original minerals were in contact (Sample 305-U1309D-80R-2, 16–19 cm) (cross-polarized light; field of view = 1.4 mm).

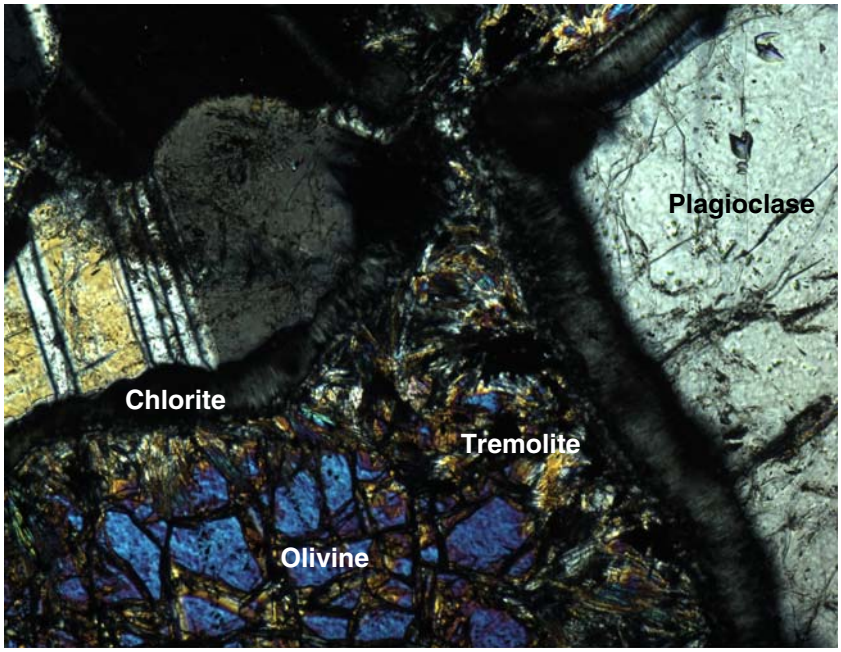

Figure F24. Dark green amphibole veins crosscutting gabbro (interval 305-U1309D-294R-2, 30–44 cm).

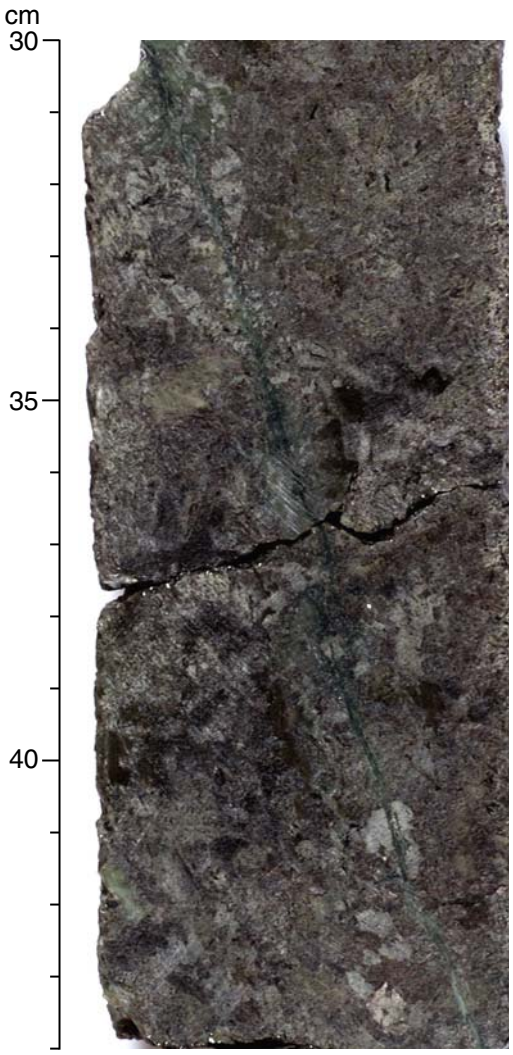

Figure F25. Prehnite vein with zeolite spherules projecting from the vein wall (Sample 305-U1309D-192R-1, 80–82 cm) (cross-polarized light; field of view = 1.4 mm).

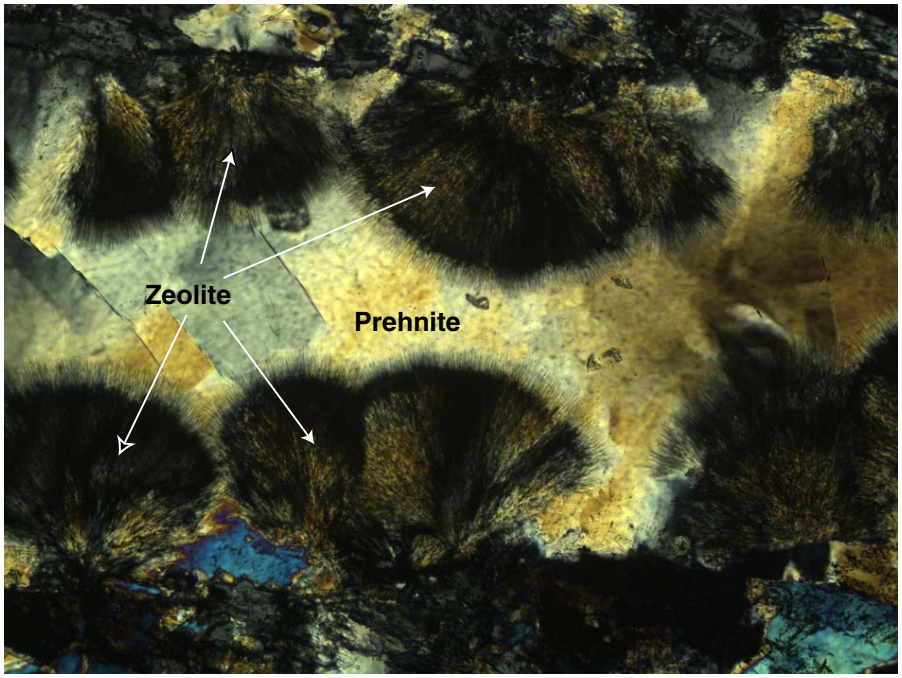

Figure F26. Downhole variation of vein mineralogy plotted with running average of lithology. The overall downcore distribution of veins is relatively homogeneous. Except for a possible occurrence shallow in the hole (not confirmed by XRD or thin section), zeolites first appear near 700 mbsf and then increase regularly to the bottom of the hole. Secondary sulfide minerals are most common in the upper 400 m of Hole U1309D.

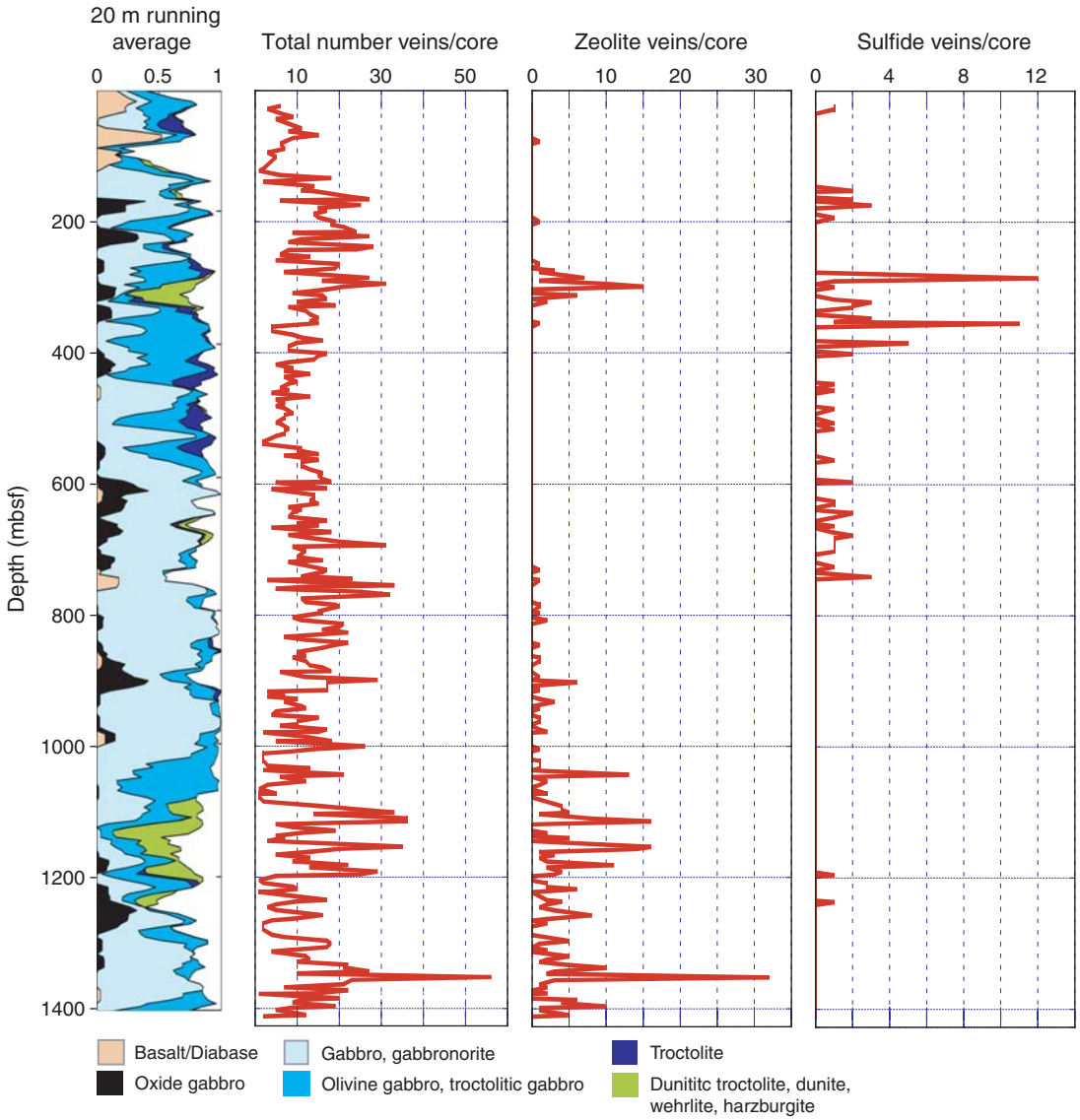

Figure F27. Downhole plots of structural features. **A.** Average intensity of magmatic and plastic foliation from core observations. **B.** Dip of magmatic and plastic foliations. Magmatic foliations above 400 mbsf show a random dip, between 400 and 600 mbsf the dip steadily increases from 20° to 60°, from 600 to 800 mbsf there is a general decrease in the dip from 60° to 40°, between 800 and 1100 mbsf there is again a steady increase in the dip from 20° to 60°, from 1100 to 1200 there is steep decline in dip from 60° to 10°, and from 1200 mbsf to the bottom of the hole there is a gradual increase in the dip up to a maximum of ~60°. Plastic foliations show a general decrease in the dip from 70° to 0° between 0 and 700 mbsf and an increase in the dip from 700 mbsf to the bottom. **C.** Dip of compositional layers, grain size layers, and oxide bands. **D.** Dip of magmatic veins, igneous contacts, and alteration fronts. The column on the right corresponds to the lithostratigraphy.

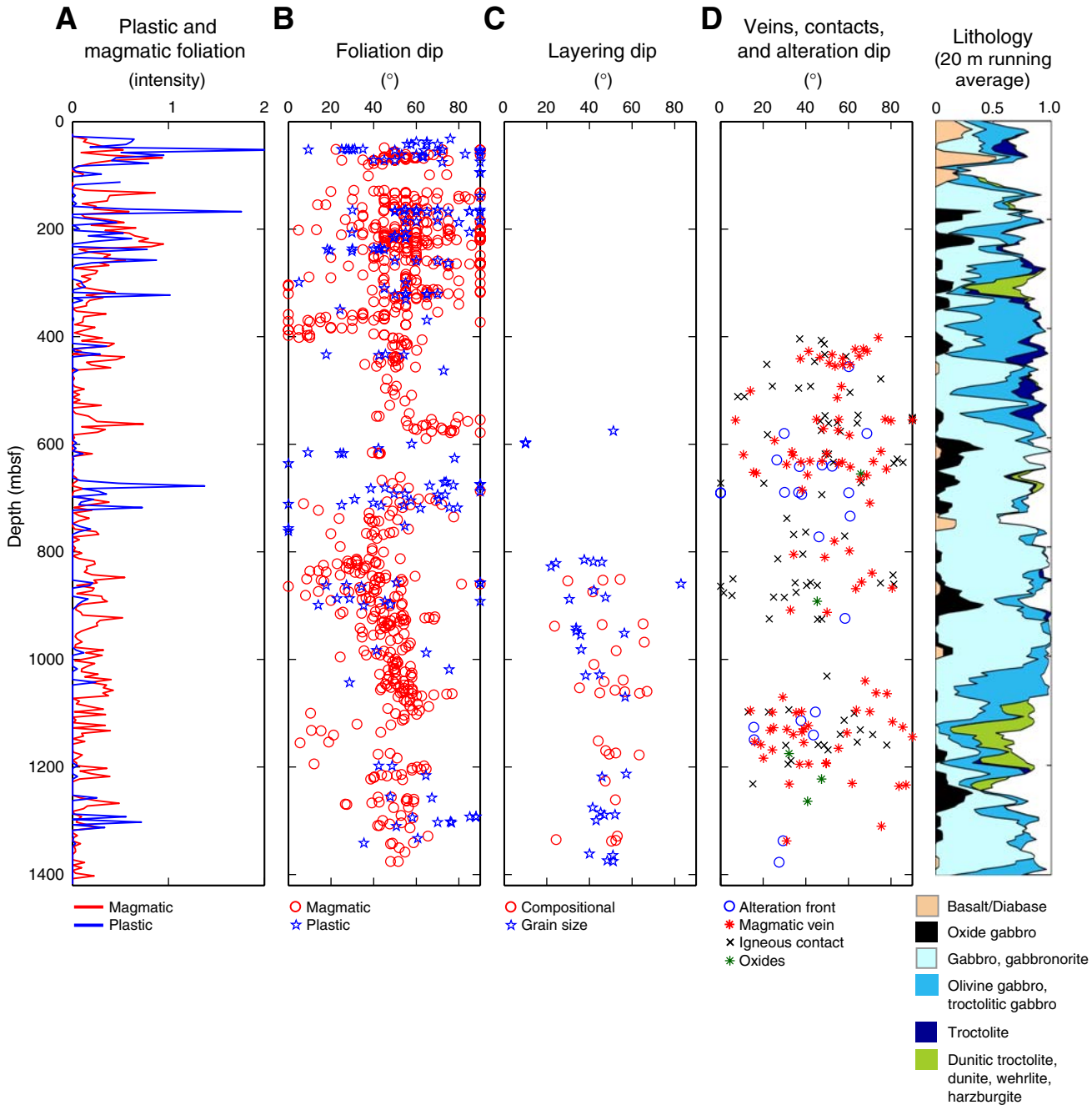

Figure F28. Magmatic foliation. About 22% of all recovered rocks show a generally weak magmatic foliation (Sample 305-U1309D-222R-2, 84–87 cm) (cross-polarized light; field of view = 22 mm).

Figure F29. High-temperature plastic deformation foliation. Although core descriptions suggest an absence of plastic deformation except for local shear zones, microstructural observations commonly indicate a weak to moderate crystal-plastic strain overprint in samples selected to be representative of primary igneous texture.

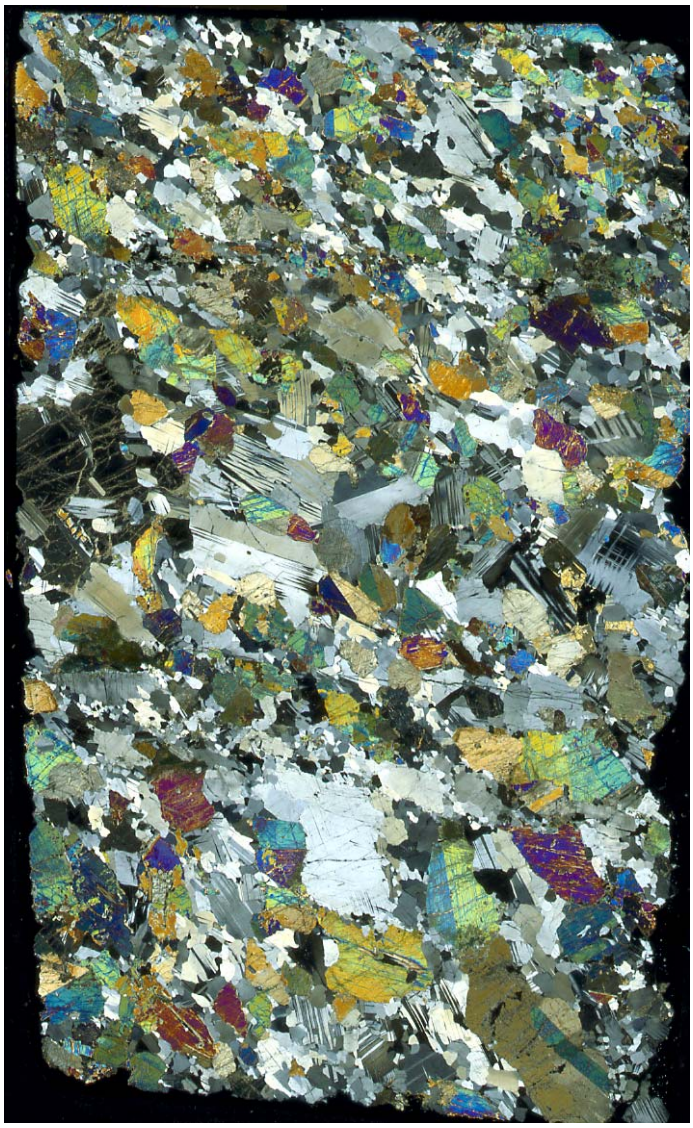

Figure F30. Lower temperature and/or higher strain rate deformation. Clearly overprinting the high-temperature plastic fabric when present and much more localized are a series of discrete, relatively thin (generally a few centimeters up to 1 m) porphyroclastic and mylonitic shear zones. They are frequently, but not systematically, closely spatially associated with oxide concentrations. **A.** Interval 305-U1309D-138R-3, 45–57 cm. (Continued on next page).

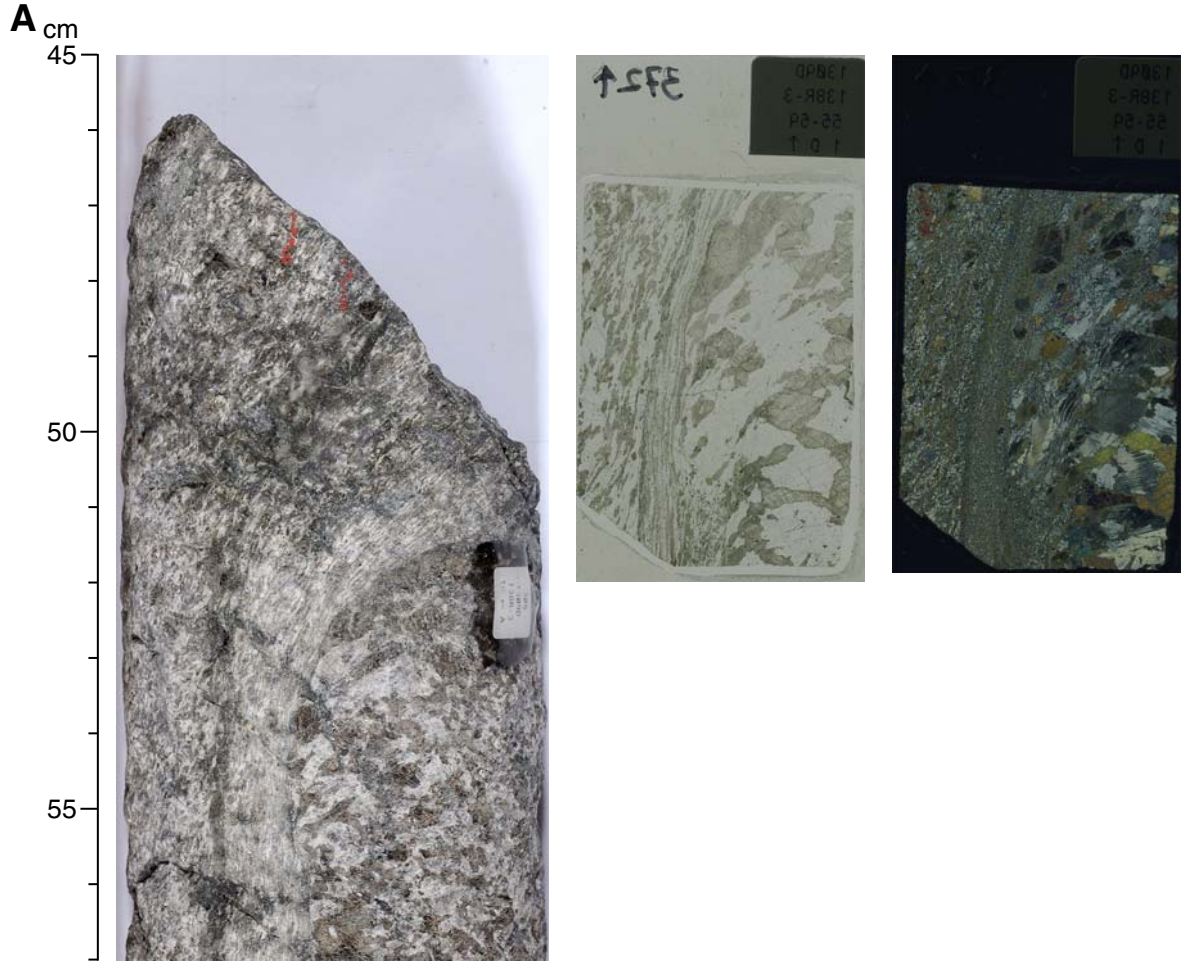

Figure F30 (continued). B. Interval 305-U1309D-137R-2, 75–93 cm. Full thin-section images in A and B are from the same interval (plane-polarized and cross-polarized light; field of view = 25 × 35 mm).

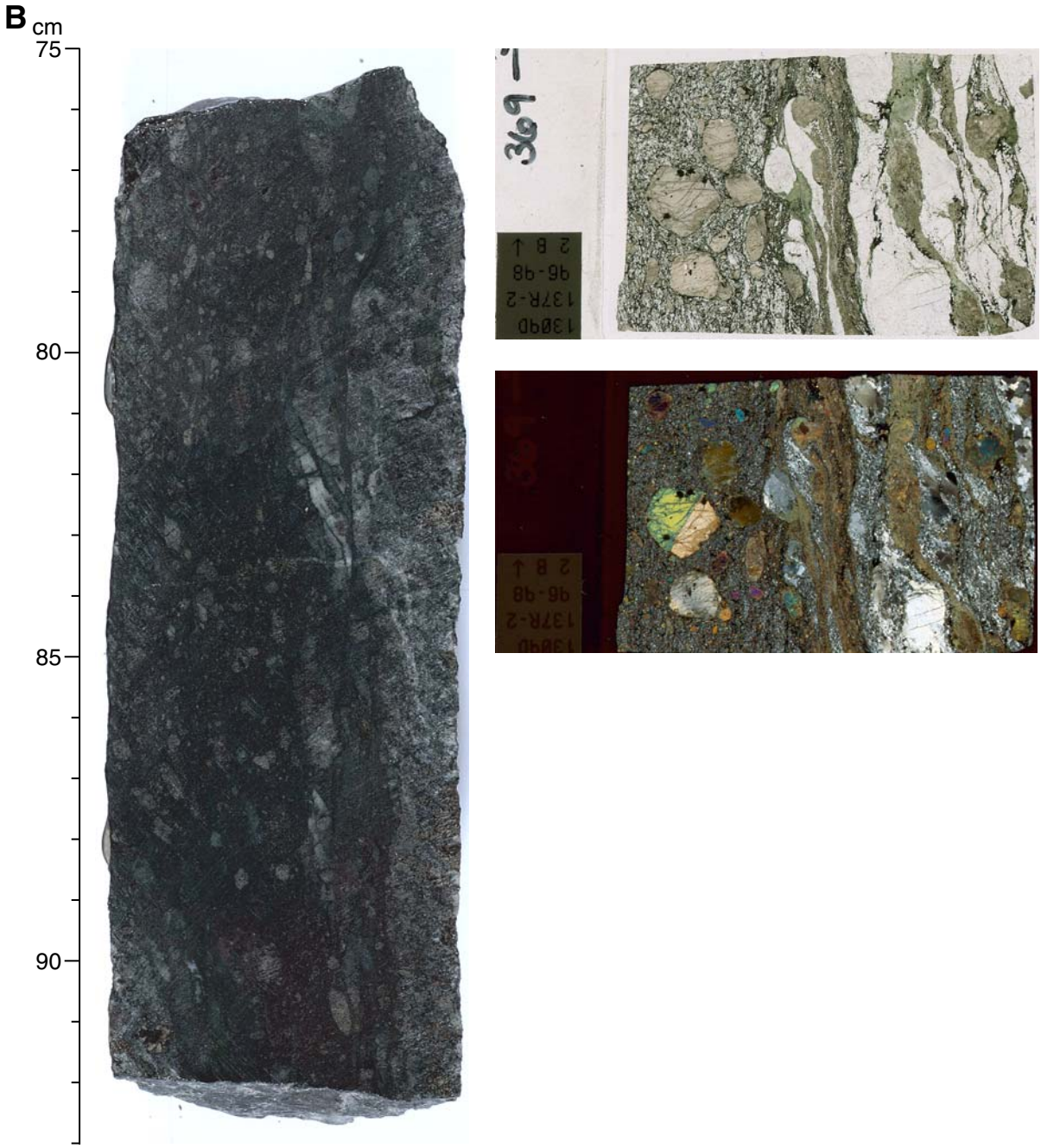

Figure F31. Fault zones, cataclastic deformation, and veining (interval 305-U1309D-152R-1, 0–22 cm).

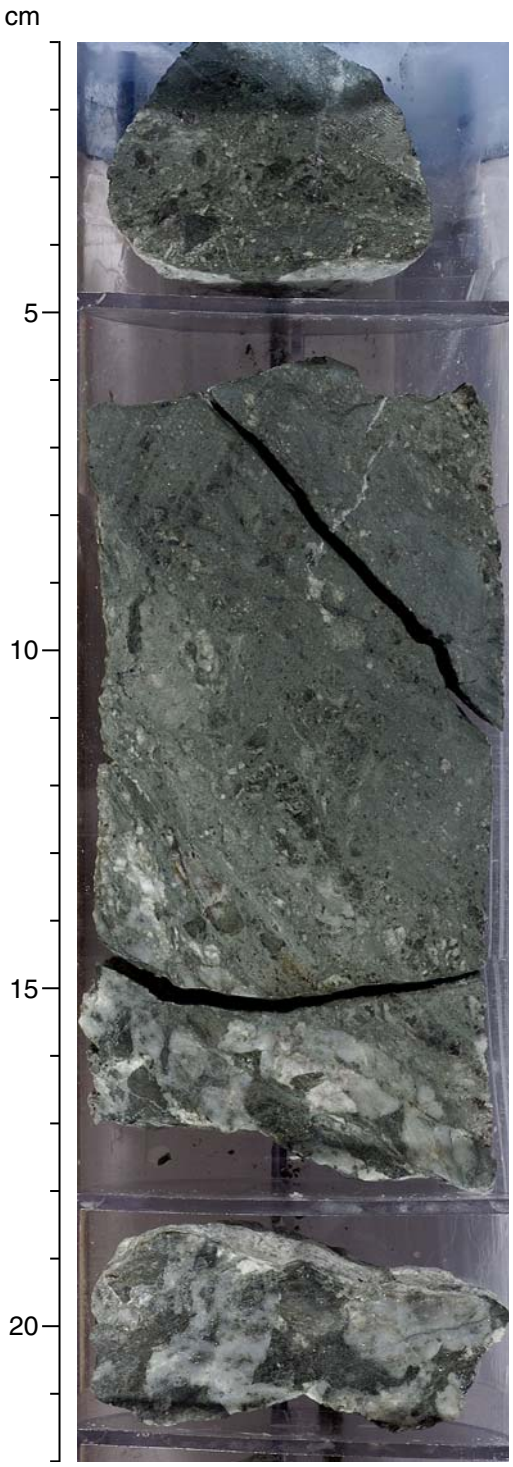

Figure F32. Cataclasis of plagioclase at the edge of a plagioclase vein (Sample 305-U1309D-80R-1, 56–59 cm) (field of view = 5.5 mm).

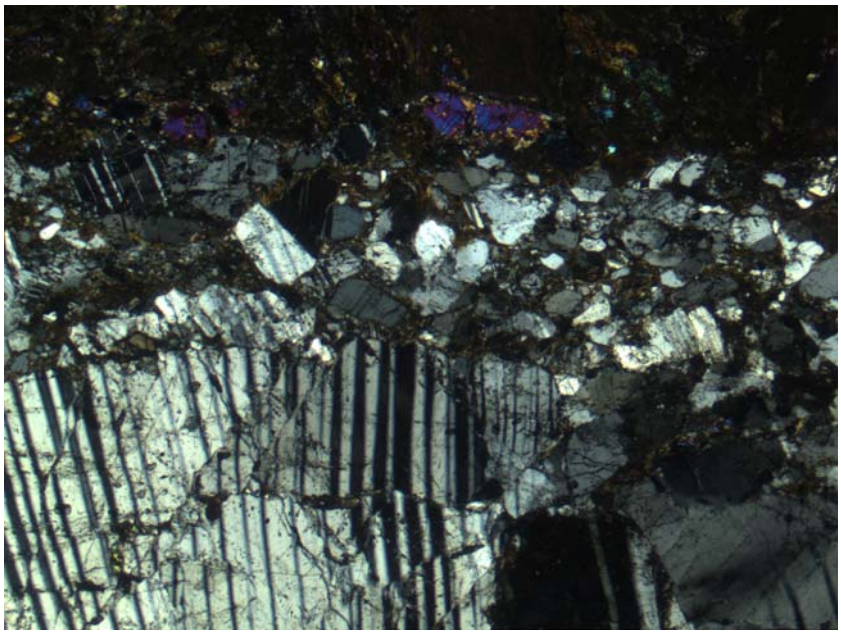

Figure F33. Downhole variation in magnetic properties and relationship to lithology and alteration. **A.** Lithology. **B.** Multisensor track (MST) magnetic susceptibility. **C.** Foliation intensity measured by the structural team illustrates regions where degree of serpentinization is high. **D.** Inclination direction of natural remanent magnetization (NRM). Red dots = value for demagnetized half core, purple circles = minicore sample values after demagnetization to remove drilling overprint, dashed lines = fault zones (see **"Structural Relationships"**).

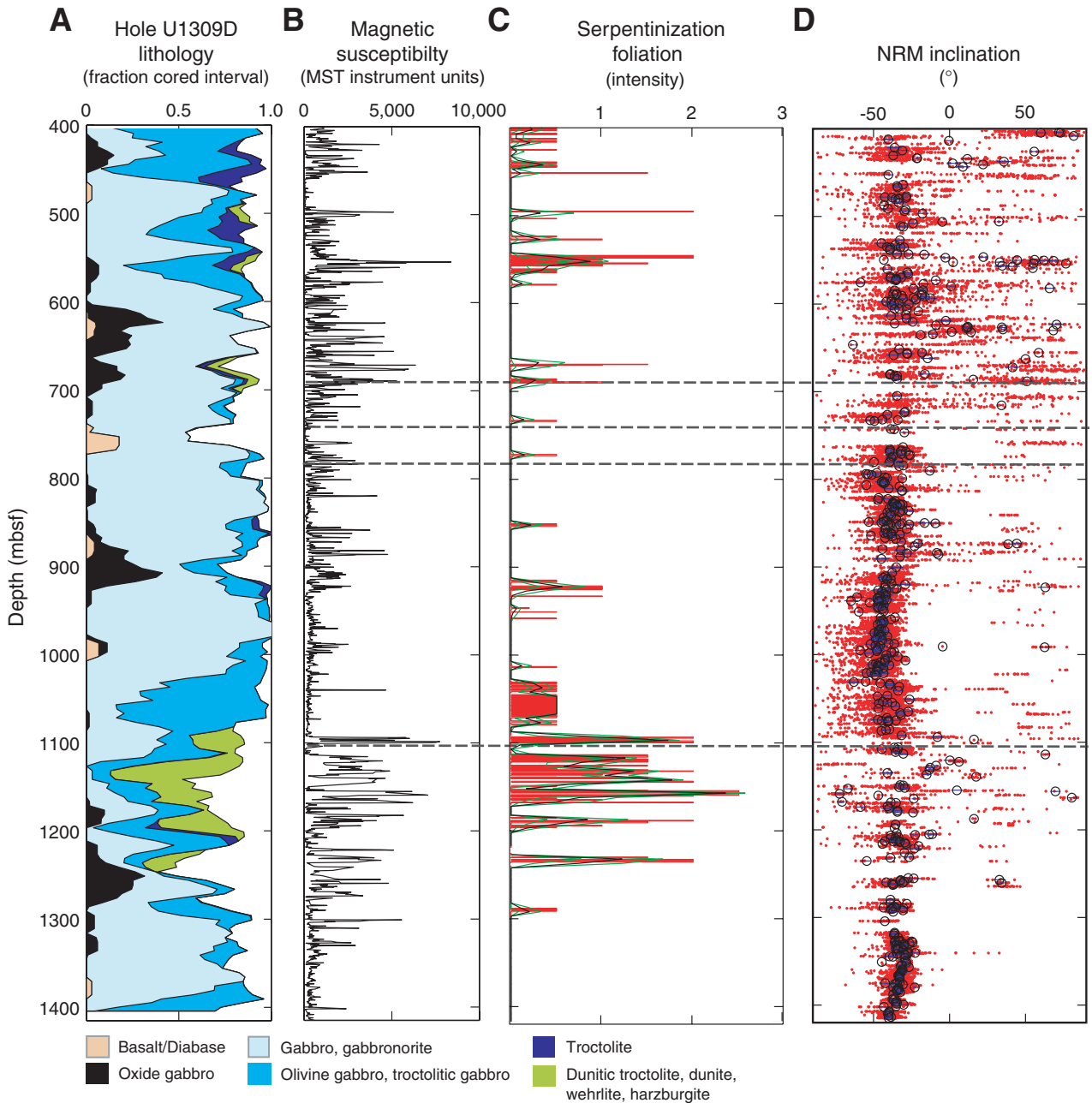

Figure F34. Downhole variations in physical properties in Hole U1309D. **A.** Lithology. **B.** Bulk density of core samples. **C.** *P*-wave velocity of core samples. **D.** Bulk density measured by logging. **E.** *P*-wave velocity measured by logging. **F.** Electrical resistivity measured by the Dual Laterolog borehole tool.

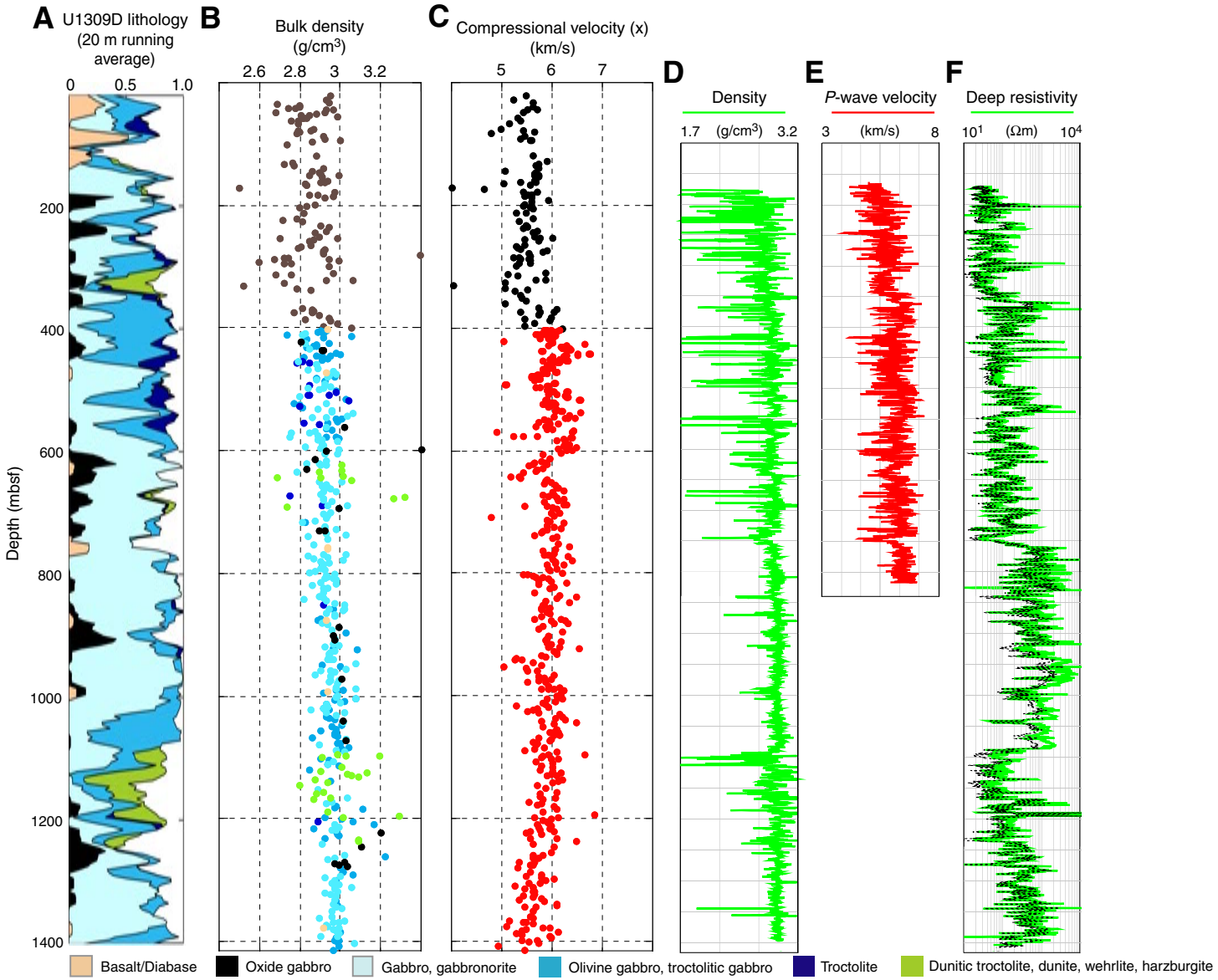

Figure F35. Synthetic seismogram model derived from Hole U1309D logging measurements and comparison to a section of multichannel seismic (MCS) reflection line Meg-4. **A.** Two-way traveltime-to-depth based on VSP shot data to 750 mbsf and an assumed value at 1415 mbsf. **B.** Conversion of logging *P*-wave velocity to traveltime at depth. **C.** Logging bulk density. **D.** Time-depth scales. **E.** Reflectivity model derived from data B and C, bottom velocity value assumed. RC = reflectivity coefficient, which indicates impedance contrast. **F.** Wavelet convolved with reflectivity model. **G.** Resulting synthetic seismogram. **H.** Synthetic seismogram trace overlain on section of MCS Line Meg-4 at projected location of Hole U1309D.

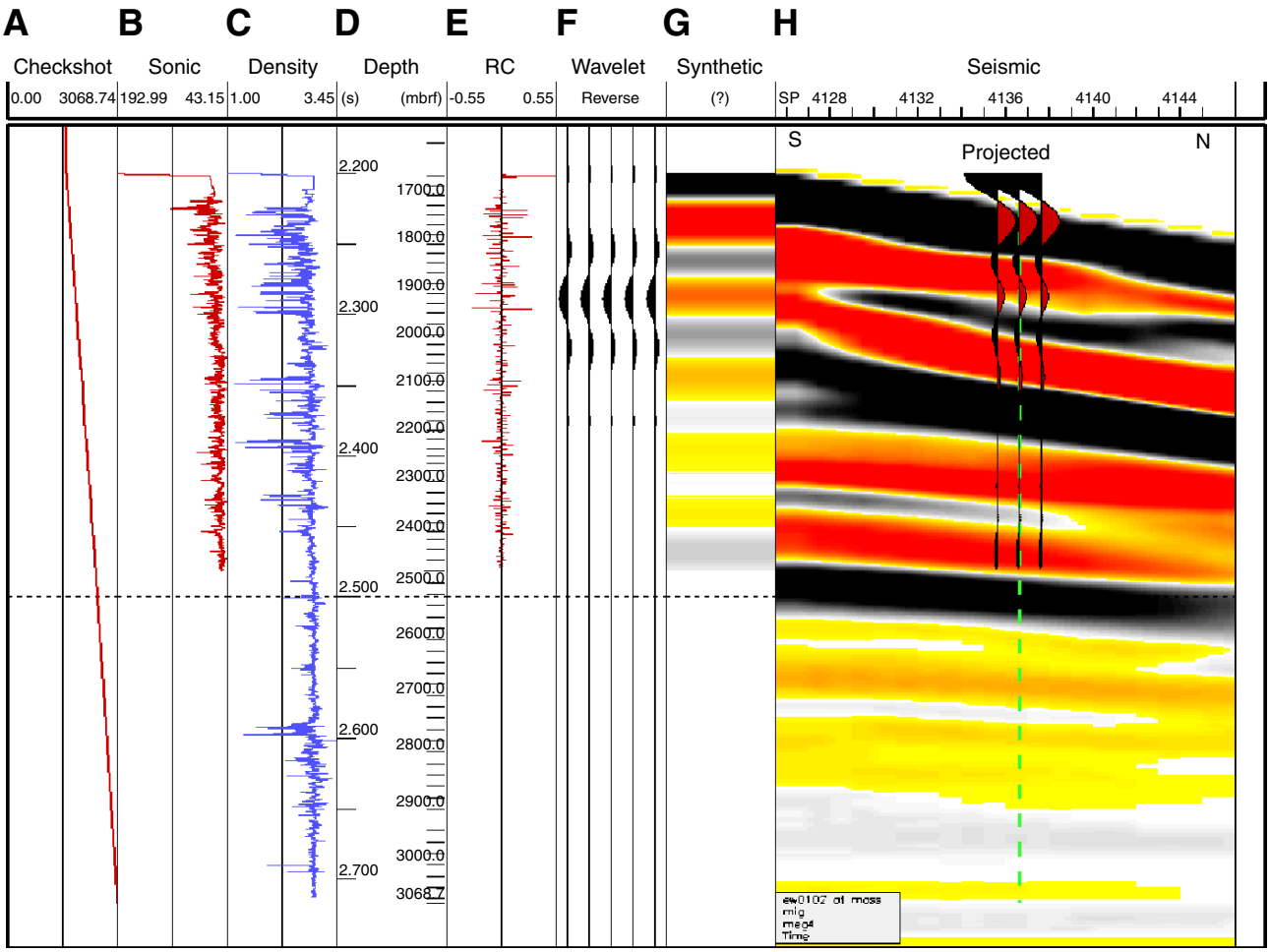

Figure F36. Temperature recorded by the TAP tool. Increase in borehole temperature with time can be seen in downhole versus uphole logging runs and between the main and repeat logging pass, respectively. Dashed lines indicate the location of consistent dips in temperature, the lower two of which are located where a fault zone is inferred to occur.